Catalytic pervaporation membranes for close integration of reaction and separation

Catalytic pervaporation membranes for close integration of reaction and separation

PROEFSCHRIFT

ter verkrijging van de graad van doctor aan de
Technische Universiteit Eindhoven, op gezag van de
Rector Magnificus, prof.dr.ir. C.J. van Duijn, voor een
commissie aangewezen door het College voor
Promoties in het openbaar te verdedigen
op woensdag 29 maart 2006 om 16.00 uur

door

Thijs Andries Peters

geboren te Breda

Dit proefschrift is goedgekeurd door de promotor:

prof.dr.ir. J.T.F. Keurentjes

Copromotor:

dr.ir. N.E. Benes

A catalogue record is available from the Library Eindhoven University of Technology

Peters, Thijs A.

Catalytic pervaporation membranes for close integration of reaction and separation / door Thijs Andries Peters. – Eindhoven: Technische Universiteit Eindhoven, 2006.

ISBN-10: 90-386-3057-3
ISBN-13: 978-90-386-3057-1

Subject headings: esterification / pervaporation / catalytic membrane / dehydration / membrane technology / catalysis / modelling / structured catalyst / condensation reaction.

Trefwoorden: verestering / pervaporatie / katalytisch membraan / ontwatering / membraantechnologie / katalyse / modelleren / gestructureerde katalysator / kondenseringsreactie.

An electronic copy of this thesis is available from the site of the Eindhoven University Library in PDF format (http://www.tue.nl/bib).

Summary

Esterifications represent a significant group of reactions commonly found in industry. These are typical examples of reactions controlled by thermodynamic equilibrium and are commonly catalysed using liquid mineral acids. As a result, conventional esterification processes are faced with problems in product purification.

Pervaporation is an ideal candidate to enhance conversion in reversible condensation reactions in which water is generated as a by-product. In pervaporation-esterification coupling, one side of a membrane is exposed to the reaction mixture, while at the other side of the membrane vacuum is applied. Water permeates preferentially through the membrane, evaporates, and is then removed on the low pressure permeate side. The removal of water drives the esterification reaction to the ester-side. Compared to distillation, pervaporation offers a number of advantages, *e.g.*, the energy consumption is low, the reaction temperature is independent from the reflux temperature, and the separation efficiency is not solely determined by the relative volatility.

Liquid mineral acid catalysts, generally used for esterification reactions, suffer from several drawbacks such as a corrosive nature, the occurence of side reactions, and the fact that the catalyst can not easily be separated from the reaction mixture. Heterogenous acid catalysts offer an alternative since they are not corrosive and, coated onto a support, they can easily be reused.

The present study aims to develop pervaporation membranes showing catalytic activity. These membranes enable close and efficient integration of reaction and separation, while allowing independent optimisation of the catalytic and separation functions. Using reaction kinetics and membrane parameters, model simulations show the potential added value of a composite membrane system and indicate the existence of an optimum catalytic layer thickness, within practically reachable dimensions. At the optimum catalytic layer thickness, the performance of a catalytic membrane reactor can exceed the performance of a membrane reactor in which the same amount of catalyst is dispersed in the bulk liquid.

Amorphous silica and cross-linked PVA water selective membrane layers have been prepared on the outer surface of hollow fibre ceramic substrates. These substrates consist of an α-Al_2O_3 hollow fibre coated with an intermediate γ-Al_2O_3 layer. This intermediate layer provides a sufficiently smooth surface for the deposition of the ultra-thin water selective layers.

High helium permeance ($1.1\text{-}2.9 \cdot 10^{-6}$ mol·m^{-2}·s^{-1}·Pa^{-1}), high He/N_2 permselectivity (~ 100-1000), and Arrhenius type temperature dependence of gas permeance indicate that the silica membranes are microporous and possess a low number of defects. In the dehydration of *1*-butanol (80°C, 5 wt.% water), initially a high water flux and selectivity (2.9 kg·m^{-2}·h^{-1} and 1200, respectively) are observed.

The composite ceramic/PVA membranes have been characterised in the dehydration of different alcohol/water mixtures. In the dehydration of *2*-propanol and *1*-butanol, a simultaneous increase in both water flux and separation factor is observed with increasing temperature or water concentration. This remarkable behaviour is in contrast to the trade-off generally observed for polymer membranes, *i.e.*, an increase in flux is typically combined with a decrease in separation factor. A possible explanation for this behaviour is a low degree of three dimensional swelling in the vicinity of the γ-Al_2O_3 – PVA interface due to an enhanced structural stability. In other words, the expansion of the polymer chains and the increase in free volume, permits an increase in water transport with an increase in temperature, whereas the transport of the larger *2*-propanol and *1*-butanol molecules is still severely hindered. For the dehydration of smaller alcohols, *i.e.*, ethanol and *1*-propanol, the traditional trade-off between an increase in flux and a decrease in selectivity is observed with an increase in temperature.

Catalytic pervaporation membranes have been developed by deposition of H-USY zeolite and Amberlyst 15 layers on silica and PVA membranes, respectively. Membrane pre-treatment and the addition of binder to the dip-coat suspension appear to be crucial in the process. Tuning of the catalytic layer thickness is possible by varying the number of dip-coat steps. This procedure avoids failure of the coating due to the high stresses, which can occur in thicker coatings during firing. In the pervaporation-assisted esterification reaction the catalyst-coated pervaporation

membranes are able to couple catalytic activity and selective water removal. Mass transfer resistances in the catalytic later are found to be negligible. For both coated catalysts the catalytic activity is comparable to the activity of the bulk catalyst. The performance of H-USY-coated membranes is mainly limited by reaction kinetics. This in contrast to Amberlyst-coated membranes, for which the performance is limited by the water removal rate due to their higher activity. It is conceivable that a further improvement in reactor performance can be realised by optimisation of the catalytic layer in terms of thickness and, for example, porosity.

A preliminary large scale composite membrane reactor evaluation is carried out based on the obtained experimental data, *e.g.*, membrane permeability and catalyst activity. The process evaluation suggests that membranes coated with a thin Amberlyst layer can be interesting candidates to be applied in pervaporation-assisted esterifications. A more efficient coupling between water production and removal can be obtained by varying the catalytic layer thickness over the length of the module. To achieve the same effect, a sequence of modules having a different catalytic layer thickness can also be used.

In this thesis two new membrane concepts are introduced; ceramic supported polymer membranes that show an improved performance compared to existing membranes, and catalytic membranes for which close integration of reaction and molecular separation offers advantages over conventional processes. Academic studies of these new concepts can be extended towards future applications, such as ceramic-supported hydrophobic polymers for organic removal, and other equilibrium reaction systems such as the direct formation of DMC from methanol and carbon dioxide. At this point, the challenge is to design and demonstrate reliable pilot scale membrane processes, based on the new concepts presented in this thesis.

Samenvatting

Veresteringen zijn reacties waarbij een organisch zuur en een alcohol met elkaar reageren tot een ester. Veresteringsreacties behoren tot de belangrijkste types reacties in de chemische industrie. Er worden meer dan 500 verschillende esters gemaakt, die bijvoorbeeld worden gebruikt in geur- en smaakstoffen, pesticiden, oplosmiddelen, medicijnen, oppervlakte actieve stoffen, chemische tussenproducten, en monomeren voor hoogmoleculaire polymeren. In het algemeen worden veresteringen homogeen gekatalyseerd, waarbij de conversie gelimiteerd wordt door het thermodynamisch evenwicht. Voor conventionele productieprocessen is daarom het verkrijgen van de gewenste uiteindelijke productzuiverheid dan ook niet eenvoudig.

De evenwichtsligging van een verestering kan naar de productzijde worden verschoven door water aan het reactiemengsel te onttrekken. Pervaporatie is een geschikte methode om dit te verwezenlijken. In pervaporatie-gekoppelde veresteringen wordt water selectief door een membraan verwijderd en aan de permeaatzijde verdampt. Vergeleken met andere scheidingsprocessen, zoals destillatie, biedt pervaporatie een aantal voordelen. Zo is het energieverbruik laag, de reactietemperatuur onafhankelijk van het kookpunt, en wordt de scheiding niet enkel bepaald door het verschil in relatieve vluchtigheden van de te scheiden componenten.

In het algemeen worden voor veresteringen zure homogene katalysatoren gebruikt. Het gebruik van deze katalysatoren brengt verschillende nadelen met zich mee. Zo zijn ze moeilijk van het reactiemengsel te scheiden en daardoor niet eenvoudig opnieuw te gebruiken. Bovendien zijn de homogene zuren erg corrosief. Heterogene zure katalysatoren daarentegen zijn minder corrosief, en gecoat op een support zijn ze wel eenvoudig te hergebruiken.

Dit proefschrift beschrijft het onderzoek naar pervaporatiemembranen met een katalytische functionaliteit, en de toepassing van deze membranen in veresteringen. Dergelijke membranen zouden een effectieve koppeling van reactie en scheiding mogelijk moeten maken. Door de twee verschillende functies, scheiding en katalytische activiteit, in afzonderlijke lagen onder te brengen kunnen deze onafhankelijk van elkaar worden geoptimaliseerd. Met behulp van modelberekeningen is de toegevoegde

waarde van de te ontwikkelen composietmembranen onderzocht. Deze berekeningen voorspellen een optimum in de dikte van de katalytische laag, welke praktisch realiseerbaar is. Voor lagen die dunner zijn dan de optimum dikte is waterverwijdering erg efficiënt, en is de bereikte conversie hoger dan wanneer eenzelfde hoeveelheid katalysator zou worden gedispergeerd in het reactiemengsel. Voor lagen die dikker zijn dan de optimum dikte worden massatransportlimiteringen belangrijk en neemt de behaalde conversie af.

Waterselectieve lagen van zowel amorf silica als vernet PVA zijn aangebracht op keramische holle vezels. Deze vezels zijn opgebouwd uit een α-Al_2O_3 holle vezelsubstraat, waarop een γ-Al_2O_3 tussenlaag is aangebracht. De aanwezigheid van de tussenlaag zorgt ervoor dat een voldoende glad oppervlak wordt verkregen voor het defectvrij aanbrengen van de uitermate dunne waterselectieve lagen.

In de ontwatering van *1*-butanol (80°C, 5 wt.% water) laten de amorfe silica membranen een hoge waterflux en een hoge selectiviteit (2.9 $kg \cdot m^{-2} \cdot h^{-1}$ and 1200) zien. Daarnaast zijn gaspermeatie metingen indicatief voor een microporeus karakter van deze membranen; een hoge He/N_2 permselectiviteit (~ 100-1000), gecombineerd met een hoge He permeatie ($1.1\text{-}2.9 \cdot 10^{-6}$ $mol \cdot m^{-2} \cdot s^{-1} \cdot Pa^{-1}$), en een Arrhenius type temperatuursafhankelijkheid.

De composiet keramisch/PVA membranen zijn getest in de ontwatering van verschillende alcohol/water mengsels. In de ontwatering van *2*-propanol and *1*-butanol, is een gelijktijdige toename van zowel de waterflux als de selectiviteit gemeten, bij zowel een toename van de temperatuur als een toename van de waterconcentratie in de voeding. Dit uitzonderlijke gedrag is in tegenstelling tot wat normaal wordt geobserveerd voor polymeer membranen; een toename van de flux resulteert dan in een afname van de selectiviteit. Een mogelijke verklaring voor dit onverwachte gedrag is een gelimiteerde zwelling van de selectieve laag, met name in de nabijheid van het γ-Al_2O_3 - PVA grensvlak. Door een dergelijke gelimiteerde zwelling zal vooral de bewegelijkheid van grotere moleculen, zoals *2*-propanol en *1*-butanol, minder toenemen bij een temperatuurstijging of bij een toename in waterconcentratie in de voeding. Voor de kleinere alcoholen, ethanol en *1*-propanol, is wel de traditionele wisselwerking tussen flux en selectiviteit gemeten.

Met behulp van de dip-coat techniek zijn katalysatorlagen van zeoliet H-USY en Amberlyst 15 aangebracht op respectievelijk silica en PVA membranen. Hierbij is een juiste voorbehandeling van het membraanoppervlak en de toevoeging van een binder aan de dip-coat oplossing noodzakelijk. Door het aantal dip-coat stappen te variëren zijn zowel de dikte als de morfologie van de katalytische laag te sturen. Door sequentieel dunne katalysatorlagen aan te brengen wordt de ontwikkeling van spanningen voorkomen die tijdens het drogen van één dikke laag tot materiaalbreuk kunnen leiden.

De composietmembranen zijn in staat om op effectieve wijze katalytische activiteit en waterverwijdering te combineren. Uit pervaporatiemetingen blijkt dat transportlimiteringen in de katalytische laag kunnen worden verwaarloosd. Tevens is de katalytische activiteit voor de gecoate katalysatoren vergelijkbaar met die van de katalysatoren die zijn gedispergeerd in het reactiemengsel. De behaalde conversie van H-USY-gecoat membranen wordt vooral gelimiteerd door de reactiekinetiek vanwege de lage activiteit van de zeolietkatalysator. Bij Amberlyst-gecoate membranen wordt de behaalde conversie juist gelimiteerd door de hoeveelheid water die door het membraan kan worden verwijderd.

Een evaluatie van een industriële membraanreactor is uitgevoerd gebruikmakend van experimentele gegevens, zoals katalytische activiteit en membraanpermeabiliteit. Uit deze evaluatie blijkt dat vooral membranen gecoat met een relatief dunne Amberlyst katalysatorlaag interessant kunnen zijn voor toepassing in pervaporatie-gekoppelde veresteringen. Door de dikte van de katalytische laag te variëren over de lengte van de membraanreactor kan een efficiëntere koppeling tussen productie en verwijdering van water worden bewerkstelligd. Eenzelfde effect kan worden verkregen met behulp van een aaneenschakeling van modules met verschillende katalytische laagdiktes.

Samengevat zijn in dit proefschrift twee nieuwe membraanconcepten geïntroduceerd: composiet keramisch/PVA membranen met uitzonderlijke eigenschappen, en katalytische membranen die een efficiënte integratie van reactie en scheiding mogelijk maken. De resultaten van het onderzoek beschreven in dit proefschrift kunnen mogelijk worden uitgebreid naar andere toepassingen. Hierbij kan bijvoorbeeld worden gedacht aan de

ontwikkeling van hydrofobe keramiek/polymeer membranen voor het scheiden van organische mengsels. De katalytische membranen zouden kunnen worden gebruikt voor andere evenwichtsreacties, zoals de directe vorming van dimethylcarbonaat uit koolstofdioxide en methanol. Voor de acceptatie en toepassing op industriële schaal van dergelijke nieuwe ontwikkelingen zal robuustheid in het bijzonder cruciaal zijn. Het zal daarom noodzakelijk zijn om de betrouwbaarheid en de toegevoegde waarde van de nieuwe ontwikkelingen op pilot-schaal aan te tonen.

Contents

Chapter 1

Introduction

Esterifications represent a significant group of reactions commonly found in the chemical industry. Esterifications are typical examples of reactions controlled by thermodynamic equilibrium and are commonly catalysed using liquid mineral acids. As a result, conventional esterification processes are faced with problems in product purification. In this perspective pervaporation is an alternative. Compared to distillation, the energy consumption is low, the reaction temperature is independent from the reflux temperature, and the separation efficiency is not solely determined by the relative volatility. Liquid mineral acid catalysts suffer from several drawbacks, such as a corrosive nature, the existence of side reactions, and the fact that the catalyst can not easily be separated from the reaction mixture. Solid acid catalysts offer an alternative since they are not corrosive and, coated onto a support, they can easily be reused. The present study aims to develop composite catalytic pervaporation membranes. These membranes enable close, and hence efficient, integration of reaction and separation, while allowing independent optimisation of the catalytic and separation function. The present chapter gives a general introduction on membrane technology, pervaporation processes, and the various types of pervaporation membranes. The beneficial aspects of pervaporation-assisted esterifications using composite catalytic membranes are discussed. Finally, an outline of the contents of this thesis is given.

1.1 Introduction

Membrane technology has received considerable attention in the chemical industry during the last decades [Feng and Huang, 1997]. A membrane is a semi-permeable active or passive barrier, which selectively permits passage of one or more components of a mixture. Membranes are able to separate mixtures due to their ability to influence the transport of one or more components of the mixture to a larger extent, because of differences in physical and/or chemical interaction between the membrane and the permeating components [Ho and Sirkar, 1992]. Transport of a component through a membrane requires a driving force, for instance a pressure or a concentration (activity) difference across the membrane.

Membranes are mainly used in purification processes, *i.e.*, gas and liquid purification. Membranes can, however, also be used to enhance the conversion of a thermodynamically limited reaction by selectively removing one or more product species from the reacting mixture. The application of this principle has been mainly restricted to gas phase applications like dehydrogenations and synthesis gas production [Coronas and Santamaría, 1999]. However, there are many equilibrium limited liquid phase systems where the same principle can be applied. In this respect, pervaporation-esterification coupling has received the most attention [Liu *et al.*, 2001], and will also be the main topic of this thesis.

1.2 Pervaporation

Pervaporation is the separation of liquid mixtures by selective partial vaporization through a membrane. The word pervaporation is derived from the two basic steps of the process; permeation and evaporation. Transport of a specific component through the membrane is induced by the partial vapour pressure difference between the feed solution and the permeate [Baker, 2004]. Commonly, this difference is achieved by employing a sweep gas or using a vacuum at the permeate side. Figure 1.1 gives a schematic representation of pervaporation.

The steps included in the separation are the sorption of the components in the membrane, diffusion across the membrane, and finally desorption into a vapour phase at the permeate side of the membrane. The selectivity

is related to the sorption selectivity of the components in the membrane material and the relative mobility of the components through the membrane [Feng and Huang, 1997].

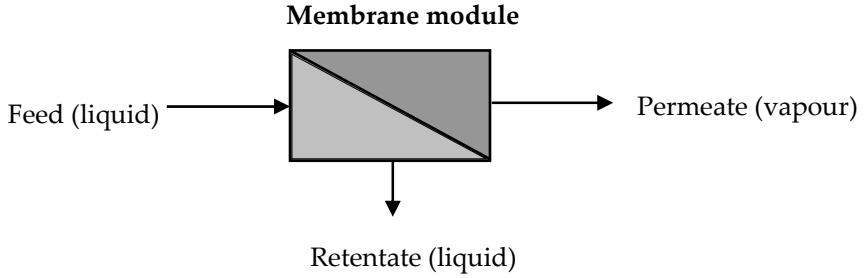

Figure 1.1 Basic schematic diagram of pervaporation.

The applications of pervaporation can be classified into three categories: (i) dehydration of organic solvents, (ii) removal of organic compounds from aqueous solutions, and (iii) separation of anhydrous organic mixtures. Pervaporation has been commercialized for two types of applications: one is the dehydration of alcohols and other solvents, and the other is the removal of small amounts of organic compounds from contaminated waters [Feng and Huang, 1997]. Currently, about one hundred pervaporation units are operating worldwide, most of them dehydrating solvents, such as ethanol and iso-propanol [Wynn, 2001].

In the pervaporation-coupled esterification process, the water removal capability of hydrophilic pervaporation membranes is utilised to selectively remove water from the reaction mixture. Polymeric materials are commonly used for this purpose. However, their temperature and solvent stability is rather limited. Compared to polymer membranes, inorganic membranes generally possess superior chemical and thermal stability [Verkerk *et al.*, 2001]. Nevertheless, only a very few actual industrial processes based on inorganic membranes can be found, *e.g.*, drinking and waste water treatment, separation in organic media, and purification of used oil [Sekulic, 2004a].

1.2.1 Polymer pervaporation membranes

Polymer membranes can be divided into three classes: glassy, rubbery and ionic polymer membranes. Generally, for pervaporative dehydration processes hydrophilic rubbery polymer membranes, like poly(vinyl)alcohol and poly(acrylic)acid, are suitable due to their affinity for water [Feng and Huang, 1997]. The performance of these membranes, however, is greatly affected by changes in process conditions, like temperature, feed water concentration and pressure [Waldburger and Widmer, 1996; Verkerk *et al.*, 2001]. Swelling of the membrane due to sorption of water may cause an increase in solubility and diffusivity of the unwanted component and consequently a decrease in membrane selectivity [Yeom *et al.*, 2001; Guo *et al.*, 2004].

In order to decrease the extent of swelling and improve membrane stability, a common approach proposed in the literature is to utilise cross-linked and/or blended polymeric membrane materials, that are optimised for specific chemical mixtures and operating conditions [Verkerk *et al.*, 2001]. An alternative approach is to use ceramic materials as stable support structures for the polymeric membrane, thereby sufficiently increasing chemical and thermal stability in order to withstand anhydrous solvents and higher temperatures [Yoshida and Cohen, 2003].

1.2.2 Inorganic pervaporation membranes

The majority of inorganic membranes are porous and their selective features are often closely related to their pore size. Ceramic membranes obtained by the combination of a metal with a non-metal in the form of an oxide, nitride, or carbide form the main class of inorganic membranes. At present, ceramic membranes based on amorphous silica and zeolite membranes are mainly investigated for pervaporation purposes.

Amorphous silica membranes for pervaporation purposes are prepared using the sol-gel technique in which a ceramic support is modified by dip-coating with a polymeric silica sol [de Lange *et al.*, 1995]. Generally, membranes based on amorphous silica have an asymmetric structure with the actual selective microporous silica positioned on a macro/mesoporous support structure comprising several α- and γ-alumina layers. Silica membranes were discovered more than a decade ago and are still subject of

extensive study. Especially the replacement of both γ-alumina and silica by a more chemical resistant material, like zirconia and titania is frequently being researched [van Gestel *et al.*, 2002; Sekulic *et al.*, 2004b].

Zeolite membranes, like ZSM-5, A, and T are good candidates for dehydration purposes due to their uniform pore size distribution and high hydrophilicity [Cui *et al.*, 2004]. One of the promising applications of zeolite membranes is the acid-catalyzed esterification in which the membrane acts as both separator and catalyst [Li *et al.*, 2003]. The reproducible preparation of defect-free membranes, however, is still challenging although different synthesis methods, like secondary growth, have been developed to improve membrane quality [Lovallo *et al.*, 1996]. Additionally, zeolite membrane preparation methods are still carried out batch-wise whereas continuous methods are needed in order to scale-up production [Pina *et al.*, 2004].

1.3 Esterification

Esterification reactions are reversible reactions in which a carboxylic acid reacts with an alcohol to form an ester and water. Esterifications are typical examples of reactions controlled by thermodynamic equilibrium and are commonly catalysed using liquid mineral acids. As a result, conventional esterification processes are faced with problems in product purification. A large excess of one of the reactants or reactive distillation to accomplish in-situ removal of one of the products is typically used to drive the equilibrium to the ester side [Reid, 1952]. While employing a large excess of one of the reactants may lead to an inefficient use of the available reactor volume and a higher cost of subsequent separations to recover the unused reactant, reactive distillation is only effective when the difference between the volatility of product species and reactant species is sufficiently large [Feng and Huang, 1996]. Additionally, the preferred reaction temperature range should match the temperature for distillation and energy consumption can be significant due to large reflux ratios. Moreover, if the reaction mixture forms an azeotrope, a simple reactive distillation configuration is inadequate [Feng and Huang, 1996]. In this perspective, pervaporation has attracted attention as an alternative to conventional esterification processes.

1.4 Pervaporation-esterification coupling

Pervaporation is an ideal candidate to enhance conversion in reversible condensation reactions in which water is generated as a by-product. Water permeates preferentially through the membrane and evaporates at the permeate side, which drives the esterification reaction to the ester side. Pervaporation reactors are attractive because their energy consumption is low, since only heat is required for the evaporation of the permeating water. Additionally, the reaction can be carried out at a temperature independent from the reflux temperature, and the separation efficiency in pervaporation is not solely determined by the relative volatility as in reactive distillation [Benedict *et al.*, 2003].

In most pervaporation-coupled esterification studies presented so far, the membranes used are catalytically inactive [Benedict *et al.*, 2003; David *et al.*, 1991; Domingues *et al.*, 1999; Feng and Huang, 1996; Keurentjes *et al.*, 1994; Krupiczka and Koszorz, 1999; Li and Lefu, 2001; Lim *et al.*, 2002; Liu *et al.*, 2001, Liu and Chen, 2002; Tanaka *et al.*, 2001; Waldburger and Widmer, 1996; Zhu *et al.*, 1996]. Several authors have used membranes in which the selective layer itself is catalytically active, and have shown that equilibrium displacement can be enhanced by close integration of production and removal of water [David *et al.*, 1992; Bagnell *et al.*, 1993; Bernal *et al.*, 2002; Nguyen *et al.*, 2003]. Additionally, solid acid catalysts offer an interesting alternative to liquid mineral catalysts since they are not corrosive and, coated onto a support, they can easily be reused. Moreover, this approach does not need an additional catalyst neutralization step, which is normally needed if a homogeneous catalyst is used.

The integration of the selective and catalytic function into one single layer, however, demands contradicting material properties. For example, to achieve a high water selectivity the diffusion of all components except water inside the material should be low, whereas efficient use of the catalytic properties requires the diffusion of the reactants to be high. The conflicting demands on materials properties can be avoided by accommodating the selective and catalytic features in two different distinct layers [Nguyen *et al.*, 2003], which are in close physical contact, as it can be seen in Figure 1.2. This approach allows independent optimisation of the selective and the catalytic properties.

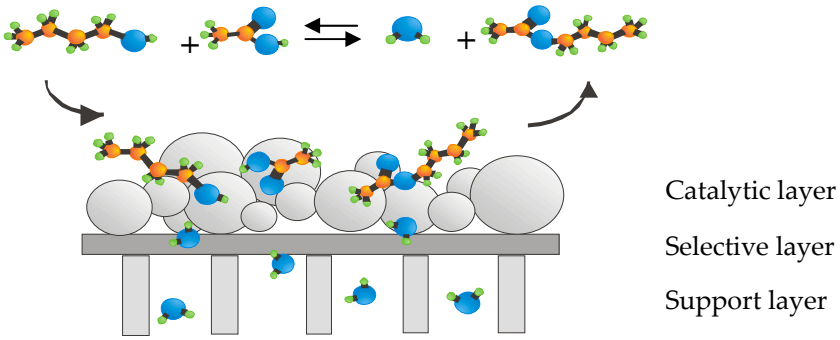

Figure 1.2 Esterification reaction in a composite catalytic membrane reactor.

1.5 Aim and outline of this thesis

The present thesis aims to develop composite catalytic pervaporation membranes as the integration of reaction and separation offers advantages in terms of process efficiency. In **Chapter 2**, the technical viability of composite catalytic hollow fibre membranes for condensation reactions is examined. A parametric pervaporation-esterification model study was carried out to provide a fundamental understanding of the catalytic membrane reactor behaviour as a function of the operating conditions and design parameters. **Chapter 3** deals with the heterogeneous catalysis of esterification reactions. Various acid catalysts are tested for their activity in the esterification between acetic acid and butanol. **Chapter 4** deals with the preparation and separation properties of hollow fibre ceramic silica membranes. In **Chapter 5**, the preparation of composite ceramic/polymer pervaporation membranes and their pervaporation characteristics in the dehydration of various alcohols is described. Subsequently, the preparation of catalyst-coated ceramic silica and composite PVA membranes for the integration of reaction and separation is described in **Chapters 6 and 7**. This approach allows independent optimisation of the selective and the catalytic properties. A preliminary large-scale composite membrane reactor evaluation is carried out in **Chapter 8**, based on the obtained experimental data such as membrane permeability and catalyst activity. Finally, conclusions, recommendations and perspectives are given in **Chapter 9**.

References

Bagnall, L., Cavell, K., Hodges, A.M., Mau, A.W., Seen, A.J., The use of catalytically active pervaporation membranes in esterification reactions to simultaneously increase product yield and permselectivity flux, *J. Membr. Sci.*, 85 (1993) 291-299.

Baker, R.W., *Membrane Technology and Applications*, 2th edition, John Wiley & Sons, Ltd, Chichester, England, 2004.

Benedict, D.J., Parulekar, S.J., Tsai, S-P., Esterification of Lactic Acid and Ethanol with/without pervaporation, *Ind. Eng. Chem. Res.*, 42 (2003) 2282-2291.

Bernal, M.P., Coronas, J., Menéndez, M., Santamaría, J., Coupling of reaction and separation at the microscopic level: esterification processes in a H-ZSM-5 membrane reactor, *Chem. Eng. Sci.*, 57 (2002) 1557-1562.

Coronas, J., Santamaría, J., Catalytic reactors based on porous ceramic membranes, *Catal. Today*, 51 (1999) 377-389.

Cui, Y., Kita, H., Okamoto, K-I., Zeolite T membrane: preparation, characterization, pervaporation of water/organic liquid mixtures and acid stability. *J. Membr. Sci*, 236 (2004) 17-27.

David, M.O., Gref. R., Nguyen, T.Q., Neel, J., Pervaporation-esterification coupling. I. Basic kinetic model. *Trans. IChemE, Part A, Chem. Eng. Res. Des.*, 69 (1991) 335-340.

David, M.O., Nguyen, T.Q., Neel, J., Pervaporation membranes endowed with catalytic properties, based on polymer blends. *J. Membr. Sci*, 73 (1992) 129-141.

Domingues, L., Recasens, F., Larrayoz, M., Studies of a pervaporation reactor: kinetics and equilibrium shift in benzyl alcohol acetylation, *Chem. Eng. Sci.*, 54 (1999) 1461-1465.

Feng, X., Huang, R.Y.M., Studies of a membrane reactor: esterification facilitated by pervaporation, *Chem. Eng. Sci.*, 51 (1996) 4673-4679.

Feng, X., Huang, R.Y.M., Liquid separation by membrane pervaporation: a review, *Ind. Eng. Chem. Res.*, 36 (1997) 1048-1066.

van Gestel, T., Vandecasteele, C., Buekenhoudt, A., Dotremont, C., Luyten, J., Leysen, R., van der Bruggen, B., Maes, G., Alumina and titania multilayer membranes for nanofiltration: preparation, characterization and chemical stability, *J. Membr. Sci.*, 207 (2002) 73-89.

Guo, W.F., Chung, T-S., Matsuura, T., Pervaporation study on the dehydration of aqueous butanol solutions: a comparison of flux vs. permeance, separation factor vs. selectivity, *J. Membr. Sci.*, 245 (2004) 199-210.

Ho, W. S. W., Sirkar, K.K., Membrane Handbook, Chapman & Hall, New York, 1992.

Keurentjes, J.T.F., Janssen, G.H.R., Gorissen, J.J., The esterification of tartaric acid with ethanol: kinetics and shifting the equilibrium by means of pervaporation. *Chem. Eng. Sci.*, 49 (1994) 4681-4689.

Krupiczka, R., Koszorz, Z., Activity-based model of the hybrid process of an esterification reaction coupled with pervaporation, *Sep. Pur. Technol.*, 16 (1999) 55-59.

de Lange, R.S.A., Hekkink, J.H.A., Keizer, K., Burggraaf, A.J, Formation and characterization of supported microporous ceramic membranes by sol-gel modification techniques. *J. Membr. Sci.*, 99 (1995) 57-75.

Li, X., Lefu, W., Kinetic model for an esterification process coupled by pervaporation, *J. Membr. Sci.*, 186 (2001) 19-24.

Lim, S.Y., Park, B., Hung, F., Sahimi, M., Tsotsis, T.T., Design issues of pervaporation membrane reactors for esterification, *Chem. Eng. Sci.*, 57 (2002) 4933-4946.

Li, G., Kikuchi, E., Matsukata, M., Separation of water-acetic acid mixtures by pervaporation using a thin mordenite membrane, *Sep. Pur. Technol.*, 32 (2003) 199-206.

Liu, Q.L., Zhang, Z., Chen, H.F., Study on the coupling of esterification with pervaporation, *J. Membr. Sci.*, 182 (2001) 173-181.

Liu, Q.L., Chen, H.F., Coupling of esterification of acetic acid with *n*-butanol in the presence of $Zr(SO_4)_2.4H_2O$ coupled pervaporation, *J. Membr. Sci.*, 196 (2002) 171-178.

Lovallo, M.C., Tsapatsis, M., Okubo, T., Preparation of an asymmetric zeolite L film, *Chem. Mater.*, 8 (1996) 1579-1583.

Nguyen Q.T., M'Bareck C.O., David, M.O., Métayer, M., Alexandre, S., Ion-exchange membranes made of semi-interpenetrating polymer networks, used for pervaporation-assisted esterification and ion transport, *Mat. Res. Innovat.*, 7 (2003) 212-219.

Pina, M.P., Arruebo, M., Felipe, M., Fleta, F., Bernal, M.P., Coronas, J., Menéndez M., Santamaría J., A semi-continuous method for the synthesis of NaA zeolite membranes on tubular supports, *J. Membr. Sci.*, 244 (2004) 141-150.

Reid, E.E., Esterification, in *Unit Processes in Organic Synthesis*, 4th edition Groggins, P.H. (ed), McGraw Hill, New York, USA, 1952, pp 596-642.

Sekulic, J., Mesoporous and microporous titania membranes, Ph.D. thesis, University of Twente, Fedodruk BV, Enschede, The Netherlands, 2004a.

Sekulić, J., ten Elshof, J. E., Blank, D.H.A., A microporous titania membrane for nanofiltration and pervaporation, *Adv. Mater.*, 16 (2004b) 1546-1550.

Tanaka, K., Yoshikawa, R., Ying, C., Kita, H., Okamota, K., Application of zeolite membranes to esterification reactions, *Cat. Today*, 67 (2001) 121-125.

Verkerk, A.W., van Male, P., Vorstman, M.A.G., Keurentjes, J.T.F., Properties of high flux ceramic pervaporation membranes for dehydration of alcohol/water mixtures, *Sep. Purif. Technol.*, 22 and 23 (2001) 689-695.

Waldburger, R.M., Widmer, F., Membrane reactors in chemical production processes and the application to the pervaporation-assisted esterification, *Chem. Eng. Technol.*, 19 (1996) 117-126.

Wynn, N., Pervaporation comes of age, CEP magazine, 97 (2001) 66-72.

Yeom, C.K., Lee, S.H., Lee, J.M., Pervaporative permeations of homologous series of alcohol aqueous mixtures through a hydrophilic membrane, *J. Appl. Pol. Sci.*, 79 (2001) 703-713.

Yoshida, W., Cohen, Y., Ceramic-supported polymer membranes for pervaporation of binary organic/organic mixtures, *J. Membr. Sci.*, 213 (2003) 145-157.

Zhu, Y., Minet, R.G., Tsotsis, T.T., A continuous pervaporation membrane reactor for the study of esterification reactions using a composite polymeric/ceramic membrane, *Chem. Eng. Sci.*, 51 (1996) 4103-4113.

Chapter 2

Design directions for composite catalytic hollow fibre membranes

A parametric model study was carried out to provide a fundamental understanding of the composite catalytic membrane reactor behavior in pervaporation assisted esterifications. With increasing catalytic layer thickness, the conversion becomes no longer limited by the amount of catalyst present in the reactor but by diffusion in the catalytic layer. An optimum catalytic layer thickness was found to be around 100 μm under the prevailing conditions, which is within practically reachable dimensions. At this optimum catalytic layer thickness, the performance of a catalytic membrane reactor exceeds the performance of an inert membrane reactor due to the close integration of reaction and separation. This shows the potential added value of such a membrane system compared to more usual reactor designs.

This chapter is based on: Peters, T.A., Fontalvo, J., Vorstman, M.A.G., Keurentjes, J.T.F., *Design directions for composite catalytic hollow fibre membranes for condensation reactions*, Trans. IChemE, Part A, Chem. Eng. Res. Des., 82 (2004) 220-228.

2.1 Introduction

The use of membranes in the chemical industry has received considerable attention during the last decades. Membranes can be used to enhance the conversion of a thermodynamically limited reaction by selectively removing one or more product species from the reacting mixture. The application of this principle has, in practice, been mainly restricted to gas phase applications like dehydrogenations and synthesis gas production. However, there are many equilibrium-limited liquid phase systems where the application of the same concept is obvious. In this respect, pervaporation-esterification coupling has received the most attention [Liu *et al.*, 2001]. Esterification reactions are limited by a thermodynamic equilibrium. To drive the equilibrium to the ester side, it is typical to use a large excess of one of the reactants, usually the alcohol, or to use reactive distillation to accomplish in-situ removal of products [Reid, 1952]. While employing a large excess of one of the reactants may lead to an inefficient use of the available reactor volume and a higher cost of subsequent separations to recover the unused reactant, reactive distillation is only effective when the difference between the volatility of product species and reactant species is sufficiently large [Feng and Huang, 1996]. Additionally, the preferred reaction temperature range should match that for the distillation, energy consumption can be significant due to the large reflux ratios and, in the case where the reaction mixture forms an azeotrope, a simple reactive distillation configuration is inadequate [Feng and Huang, 1996]. Pervaporation is an ideal candidate to enhance conversion in reversible condensation reactions, generating water as a by-product. In pervaporation-esterification coupling, one side of a membrane is exposed to the liquid phase, while at the other side of the membrane vacuum is maintained. Water permeates preferentially through the membrane and evaporates. The water is then removed on the low pressure permeate side driving the esterification reaction to the ester-side. Pervaporation reactors are attractive because the energy consumption is low, the reaction can be carried out at the optimal temperature, and the separation efficiency in pervaporation is not determined by the relative volatility as in reactive distillation [Benedict *et al.*, 2003].

In most pervaporation-coupled esterification studies presented so far, the membranes used are catalytically inactive, and are operated batch wise [Li and Lefu, 2001; Tanaka *et al.*, 2001; Liu *et al.*, 2001; Liu and Chen, 2002] or placed in a recycle loop [David *et al.*, 1991; Keurentjes *et al.*, 1994; Feng and Huang, 1996; Domingues *et al.*, 1999; Krupiczka and Koszorz, 1999; Benedict *et al.*, 2003]. Several authors investigated the coupled pervaporation-esterification process in a continuous-flow inert membrane reactor [Zhu *et al.*, 1996; Waldburger and Widmer, 1996; Lim *et al.*, 2002; Bernal *et al.*, 2002] to obtain advantages in terms of compactness and process efficiency by combining the membrane and reactor into the same unit. In inert membrane reactors, the membrane does not participate in the reaction directly: it is used to add reactants to, or to remove products from the reactor. David *et al.*, [1992], Bagnell *et al.*, [1993], Bernal *et al.*, [2002] and Nguyen *et al.* [2003], however, used catalytically active membranes to carry out esterifications of different alcohols. They showed that the equilibrium displacement could be enhanced through reaction coupling if the membrane itself provides the catalytic function. In this case, however, the membranes turn out to be not very selective to water in the esterification mixtures [Nguyen *et al.*, 2003]. Therefore, it was suggested to make use of a composite catalytic membrane to avoid reactant and ester loss. In this way, both the selective layer and the catalytic layer of the composite catalytic membrane can be optimized separately. The principle of an esterification reaction in a composite catalytic membrane reactor is schematically shown in Figure 2.1.

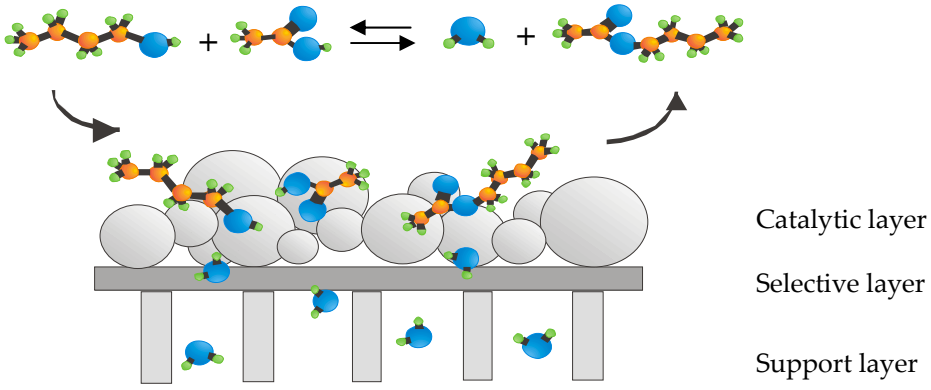

Figure 2.1 Esterification reaction in a catalytic membrane reactor.

The acid and alcohol diffuse into the catalytic layer. In the catalytic layer, the acid and alcohol are converted to the ester and water. The formed ester diffuses back towards the bulk liquid whereas water is removed in-situ through the membrane due to the close integration of reaction and separation. Consequently, the hydrolysis of the formed ester is reduced and the attained conversion will be increased compared to the inert membrane reactor [David *et al.*, 1992; Bagnall *et al.*, 1993; Bernal *et al.*, 2002]. Additionally, heterogeneous catalysts might be used more efficiently due to the thinness of the catalytic layer present on the membrane support [Vergunst *et al.*, 2001]. Other advantages are that no catalyst neutralisation or recovery is needed.

Our research aims to develop a continuous catalytic pervaporation membrane reactor as both integration of reaction and separation and continuous operation may offer advantages in terms of process efficiency and compactness. The present chapter examines the viability of composite catalytic hollow fibre membranes for condensation reactions. The esterification reaction between acetic acid and butanol has been taken as a model reaction, for which a parametric pervaporation-esterification model study was carried out to provide a fundamental understanding of the catalytic membrane reactor behaviour. The presented parametric study helps the identification of critical (process) parameters and aids in an optimal design of the envisioned catalytic membrane. The influence of catalyst position, catalytic layer thickness, reaction kinetics and the membrane permeability on the performance of the catalytic membrane reactor are investigated.

2.2 Pervaporation-coupled esterification model

2.2.1 Reaction kinetics

Esterification is a reversible reaction in which a carboxylic acid (*A*) reacts with an alcohol (*B*) in the presence of an acid catalyst to form an ester (*E*) and water (*W*). This type of reaction can be written as

$$\underset{(A)}{R-COOH} + \underset{(B)}{R'-OH} \longleftrightarrow \underset{(E)}{R-COO-R'} + \underset{(W)}{H_2O} \tag{2.1}$$

Assuming first order reaction kinetics for all the components, the rate of esterification can be represented by k_{fw} [A][B] whereas the rate of hydrolysis can be represented by k_{bw} [E][W], where the quantities between brackets represent the molar concentration of the reacting species. Thus, for concentrations at chemical equilibrium, then

$$\frac{k_{fw}}{k_{bw}} = K_i = \frac{[E]\cdot[W]}{[A]\cdot[B]} \tag{2.2}$$

The constant K is called the equilibrium constant of the reaction. The rate of ester production can be written as

$$R_E = k_{fw}\cdot\left([A]\cdot[B] - \frac{[E]\cdot[W]}{K}\right) \tag{2.3}$$

2.2.2 Reactor model

The hollow fibre module considered in the modelling in this paper is a single-pass reactor without recirculation of reactants. The reactor consists of tubular catalytic hollow fibres mounted in a module. The structure of the modules is depicted in Figure 2.2 and the geometric properties are summarized in Table 2.2.

Table 2.2 Geometric parameters for the catalytic membrane reactor.

hydraulic diameter	d_h	[m]	$d_h = \frac{d^2_{m,i} - N_f \cdot d^2_{f,o}}{d_{m,i} + N_f \cdot d_{f,o}}$	(2.4)
module void fraction	ε_m	[-]	$\varepsilon_m = 1 - N_f \cdot \left(\frac{d_{f,o} + 2 \cdot \delta_{cat}}{d_{m,i}} \right)^2$	(2.5)
initial module void fraction	$\varepsilon_{m,in}$	[-]	$\varepsilon_{m,in} = 1 - N_f \cdot \left(\frac{d_{f,o}}{d_{m,i}} \right)^2$	(2.6)
geometric surface area	a_m	[m^{-1}]	$a_m = \frac{4 \cdot d_{f,o} \cdot N_f}{L \cdot (d^2_{m,i} - N_f \cdot (d_{f,o} + 2 \cdot \delta_{cat})^2)}$	(2.7)
volume fraction of catalyst	ϕ_{cat}	[-]	$\phi_{cat} = \frac{Nf \cdot \left[(d_{f,o} + 2 \cdot \delta_{cat})^2 - d^2_{f,o} \right]}{(d^2_{m,i} - Nf \cdot d^2_{f,o})}$	(2.8)

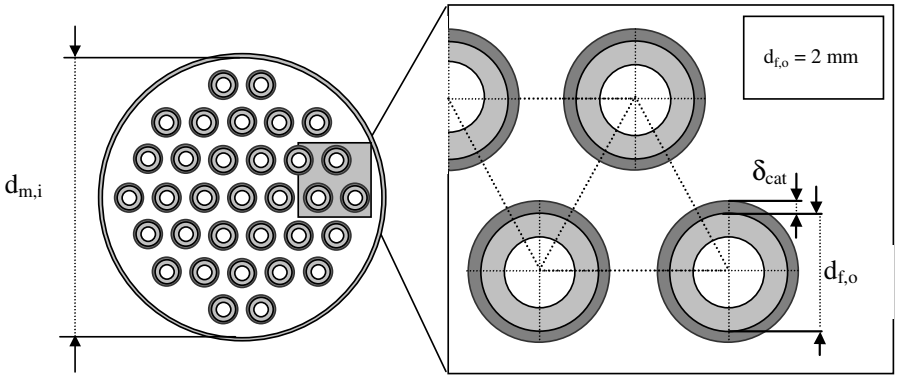

Figure 2.2 Definition of geometric properties for a composite catalytic membrane module.

One of the important issues in the development of membrane reactors is to obtain a sufficient high ratio of membrane surface over reactor volume. In the modelling in this paper, hollow fibres are used, leading to a high membrane area over volume ratio. Since ceramic hollow fibre membranes are commercially available with the water selective layer on the outside of the support we have chosen to have the reacting liquid at the shell-side of the membrane. The composite catalytic membranes consist of a support

coated with a water selective layer and on top of that a porous catalytic layer. In the development of the pervaporation-coupled esterification model, several simplifying assumptions have been made.

I. The membrane reactor behaves as an ideal isothermal plug-flow reactor; axial diffusion in the catalytic layer and in the liquid is not taken into account;

II. External transport limitations on the permeate-side are negligible under the pressure conditions at the permeate side. Concentration polarization effects in the shell-side, however, are taken into account;

III. The membrane is completely water selective, so no other species than water will permeate through the membrane;

IV. The catalyst particles are assumed to be non-porous and the catalytic activity is uniformly distributed over the catalyst coating layer.

The catalytic membrane reactor is modelled using a one-dimensional catalyst model with mass transfer to and from the catalytic layer and diffusion and reaction occurring in the catalytic layer. The mathematical description of the catalytic membrane reactor is depicted in Figure 2.3 and the governing equations are summarized in Table 2.3.

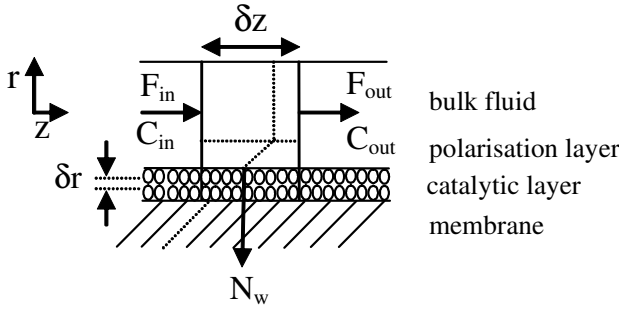

Figure 2.3 Coordinate system for the modelling of a catalytic membrane reactor and proposed concentration profiles.

Table 2.3 Model equations for the catalytic membrane reactor.

Mass balances

- Liquid bulk

$$\frac{d\,(F \cdot C_i)}{dz} = -2 \cdot \pi \cdot r_{cat} \cdot N_f \cdot D_{e,i} \cdot \left(\frac{\partial C_i}{\partial r} \right)\Big|_{r_{cat}} + R_{b,i} \cdot \varepsilon_m \cdot \pi \cdot r_m{}^2 \qquad (2.9)$$

$$with\ D_{e,i} = \frac{\varepsilon_{cat}}{\zeta_{cat}} \cdot D_i \qquad (2.10)$$

- Catalytic layer

$$\frac{\partial^2 C_i}{\partial r^2} + \frac{1}{r} \cdot \frac{\partial C_i}{\partial r} + \frac{\varepsilon_{cat} \cdot R_{cat,i}}{D_{e,i}} = 0 \qquad (2.11)$$

$$with\ R_{cat,i} = k_r \cdot \frac{(1-\varepsilon_{cat}) \cdot \rho_{cat}}{\varepsilon_{cat}} \cdot (a_A \cdot a_B - \frac{a_E \cdot a_W}{K}) \qquad (2.12)$$

Boundary conditions

- Membrane-catalytic layer

$$P_i \cdot \left[(\gamma_i \cdot x_i \cdot p_i^{\,*}) - (y_i \cdot p_p) \right] = D_{e,i} \cdot \left(\frac{\partial C_i}{\partial r} \right)\Big|_{r_{mem}} \qquad (2.13)$$

- Catalytic layer-bulk interface

$$D_{e,i} \cdot \left(\frac{\partial C_i}{\partial r} \right)\Big|_{r_{cat}} = k_{F,i} \cdot (C_{b,i} - C_{mem,i}) \qquad (2.14)$$

Mass transfer polarisation layer

$$Sh = \frac{k_{F,i} \cdot d_h}{D_i} = 3.66 + 1.2 \cdot \left(\sqrt{(1-\varepsilon_m)} \right)^{-0.8} \qquad (2.15)$$

The change in bulk concentration of the reactants and products is calculated as the sum of the mass transfer from the bulk liquid to the catalytic layer and the reaction rate in the bulk liquid (equation 2.9). The catalytic layer surface concentration is required for this calculation. This concentration is calculated from a mass balance over a slice of the catalytic layer at axial position, *z*, and a mass balance across the catalytic layer surface. Under steady state conditions, the net rate of water diffusion through a concentric slice of width *d*r into the water selective membrane at the radial position r_{mem} must equal the water flux through the membrane water selective layer (equation 2.13). The water flux through the membrane has been calculated using the partial water vapour pressure difference between the retentate and the permeate side of the membrane multiplied by the permeance of the membrane [Verkerk *et al.*, 2001]. Verkerk *et al.* [2001] calculated a water permeance value, P_w, of $2 \cdot 10^{-6}$ mol·m^{-2}·s^{-1}·Pa^{-1} for a typical ceramic pervaporation membrane for the dehydration of *1*-butanol

water mixtures. In pervaporation-assisted esterification reactions, however, water fluxes are strongly reduced [Verkerk, 2003]. This reduction in water flux is most likely a result of the adsorption of the alcohol onto the selective silica layer and the supporting layers whereby the alcohol imparts hydrophobic characteristics to the membrane surface [Font *et al.*, 1996; Dafinov *et al.*, 2002]. Therefore, a water permeance value, P_w, of $2 \cdot 10^{-7}$ mol·m^{-2}·s^{-1}·Pa^{-1} is used in the simulations. Equation 2.14 defines the requirement that the transport from the bulk liquid to the catalytic surface by mass transfer equals the transport into the catalytic layer. The mass transfer coefficient in the concentration polarisation layer is calculated using general empirical Sherwood correlations. For laminar flow in direction parallel to the fibres, for a fully developed hydrodynamic and concentration profile, the Sherwood number is expressed by equation 2.15 [Lipnizki and Field, 2001].

The model is solved in Matlab using a Runge-Kutta procedure in the axial direction coupled with a differential element method for the mass transfer and reaction in the radial direction. During each iteration, all activity coefficients, calculated by means of the UNIFAC method [Fredenslund *et al.*, 1975], all diffusion coefficients [Wilke and Chang, 1955; Leffler and Cullinan, 1970], and the viscosity [Poling *et al.*, 2001] and density [Perry *et al.*, 1997] of the mixture are calculated. Table 2.4 shows the feed composition and operating conditions used in the calculations of the catalytic membrane reactor for condensation reactions.

Table 2.4 Feed composition and operating conditions used in the modelling of the catalytic membrane reactor.

Operating conditions			**Membrane properties**		
T	348	K	P_W	$2 \cdot 10^{-7}$	mol·m^{-2}·s^{-1}·Pa^{-1}
p	100	kPa	ε_{cat}	0.5	-
T_P	348	K	ζ_{cat}	2	-
p_P	6	kPa	**Catalytic properties**		
τ	1	hr	ρ_{cat}	0.9	g·cm^{-3}
Feed composition			k_{obs}	$1.8 \cdot 10^{-8}$	m^3·mol^{-1}·g$_{cat}^{-1}$·s^{-1}
initial equimolar concentration					

The initial module void fraction, $\varepsilon_{m,in}$ (equation 2.6), and the catalytic layer thickness, δ_{cat}, were varied. The coating thickness 2was varied between 1 and 400 μm, whereas the initial module void fraction was varied between 0.2 and 0.5. For the performance of a pervaporation-coupled esterification process, the ratio of water removal to water production is found to be the key factor, for which the ratio of membrane area to reactor volume, amount of available catalyst and residence time in the membrane reactor are the major influencing parameters [Liu *et al*. 2001]. In this modelling, the ratio of feed flow rate to membrane surface area and the amount of catalyst present in the reactor are used to represent the ratio of water removal to water production.

2.3 Results and Discussion

2.3.1 Geometric properties

The geometric properties of the catalytic membrane reactor will change if the catalytic layer thickness and the initial module void fraction are changed during the modelling. To minimise the influence of this effect on the modelling results, the required diameter of the membrane module is chosen to increase with increasing catalytic layer thickness to maintain a constant residence time in the module. This implies that the module void fraction decreases and thus, the mass transfer coefficient in the concentration polarisation layer will change according to equation 2.15. However, this proves to have a minor influence on the attained performance compared to the influence of the ratio of feed flow rate to membrane surface area and the amount of catalyst present in the reactor.

2.3.2 Effect of catalyst position and catalytic layer thickness

The viability of a composite catalytic membrane reactor can be examined by comparing the performance of the composite catalytic membrane reactor with the performance of an inert membrane reactor. Figure 2.4 shows the effect of catalyst position on the performance of the catalytic membrane reactor. Two simulations are performed with the parameters shown in Table 2.4, the first with the composite catalytic membrane reactor (CMR) and the second one with an inert membrane reactor (IMR) with the same amount of catalyst but now dispersed in the liquid bulk of the reactor.

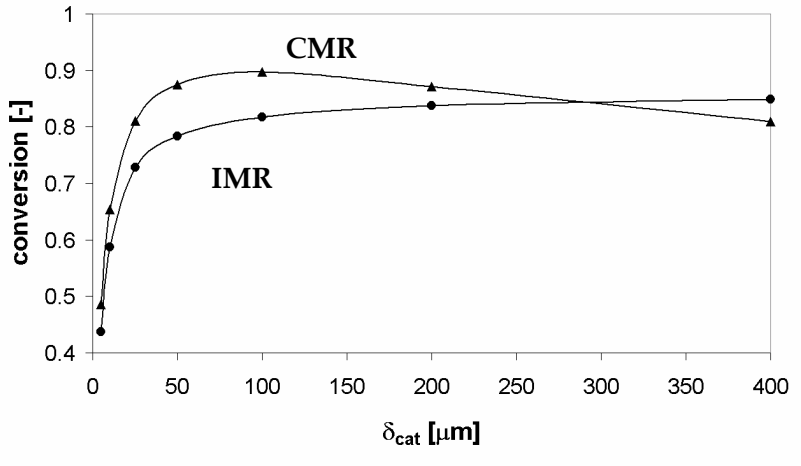

Figure 2.4 Effect of catalyst position and catalytic layer thickness on module performance; $F/A_{mem} = 3.5*10^{-4}$ m s^{-1}.

For the inert membrane reactor, the conversion increases monotonically with an increase in the amount of heterogeneous catalyst, since complete catalyst effectiveness is assumed. For the catalytic membrane reactor, however, a maximum in reached conversion is observed. It can also be seen that the performance of the catalytic membrane reactor exceeds the performance of the inert membrane reactor at relatively thin catalytic layers. This shows the potential added value of a composite catalytic membrane reactor compared to more usual reactor designs. This is similar to the results obtained by Bernal *et al.* [2002]. Based on experiments, it was concluded that an integration of reaction and separation at the microscopic level has numerous potential applications. The esterification reaction between acetic acid and ethanol was studied, for which the performance of a catalytic membrane reactor exceeded the performance of an inert membrane reactor with the same amount of heterogeneous catalyst located in the bulk liquid.

In a heterogeneous catalytic reaction employing porous catalysts, the reaction rate of an individual reaction is influenced by the following processes occurring in series and parallel: external transport from the bulk liquid to the catalyst surface, intraparticle transport (porous diffusion) and

the kinetics of the reactions at the catalyst surface (adsorption/desorption and surface reaction steps). Two parameters that are used to indicate if mass transfer limitations are pronounced are the internal and external effectiveness factor. These are shown in Figure 2.5a and b, respectively. Figure 2.5a shows the external effectiveness factor, defined as the concentration of component *i* on the surface of the porous catalytic layer divided by that in the bulk liquid, over the length of the membrane reactor.

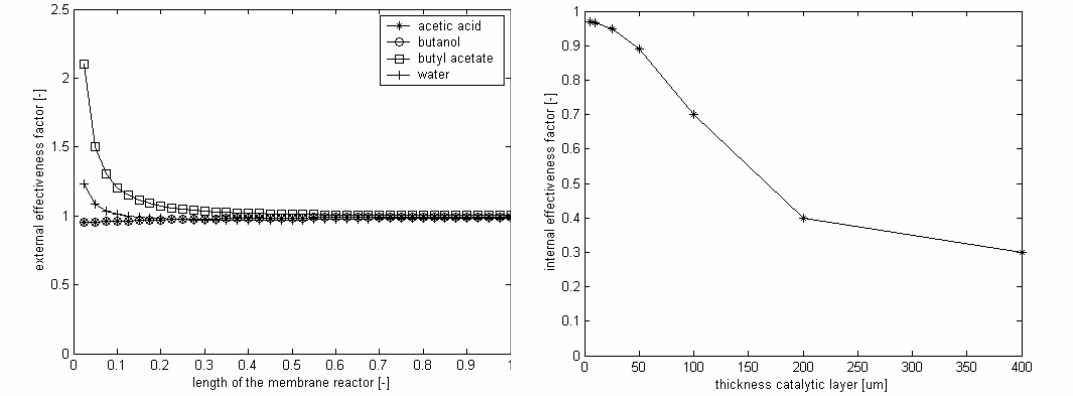

Figure 2.5 (a) External effectiveness factor over the length of the membrane reactor; δ_{cat} = 100 μm, F/A_{mem} = $3.5*10^{-4}$ m s^{-1}; (b) Internal effectiveness factor as a function of the catalytic layer thickness.

The external effectiveness factor indicates that external mass transfer limitations can be neglected. The internal effectiveness factor is defined as the actual rate of reaction in the whole catalytic layer divided by the reaction rate evaluated at outer surface conditions [Xu and Chuang, 1997]. For this, the concentration profile within the catalytic layer is needed. This concentration profile is calculated using equation 2.11. Figure 2.5b demonstrates that the internal effectiveness factor of the catalytic layer decreases with increasing catalytic layer thickness, indicating substantial internal mass transfer limitations at increasing catalytic layer thickness. At catalytic layers thicker than 50 μm, the diffusion of reactants inside the catalytic layer cannot keep up with the reaction rate and mass transfer limitations become pronounced, whereas at a thin catalytic layer, the amount of available catalyst limits the conversion rate. Additionally, the

water removal capacity of the catalytic membrane becomes lower with increasing catalytic layer thickness, as water has to diffuse through a longer path before it is removed through the membrane. Figures 2.6a and b show typical two-dimensional water concentration profiles in the catalytic layer for a relatively thin and a thick catalytic layer, respectively.

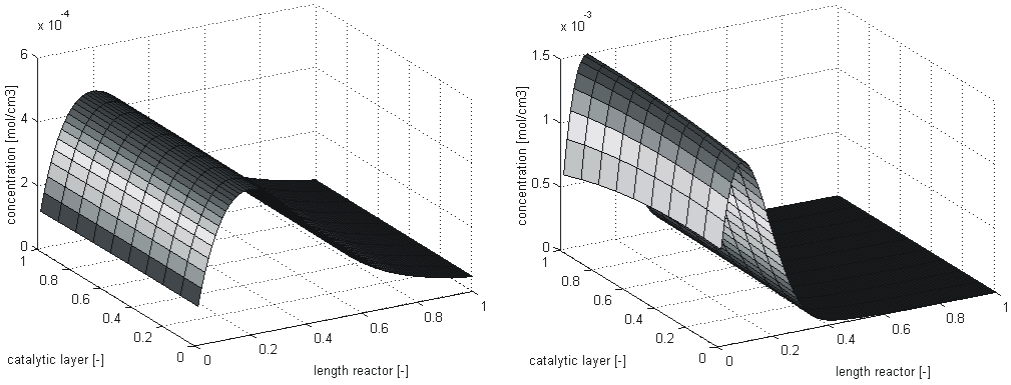

Figure 2.6 Water concentration profiles in the catalytic layer for different catalytic layer thickness; (a) δ_{cat} = 25 µm; (b) δ_{cat} = 200 µm; F/A_{mem} = $3.5*10^{-4}$ m s^{-1}.

It can be seen that the water concentration in the radial direction of the catalytic layer becomes higher with increasing catalytic layer thickness. Due to the higher catalyst loading, water production is higher as reaction rates are enhanced and consequently, water build-up in the bulk liquid is increased since not all the water formed is removed through the membrane but instead diffuses towards the bulk liquid.

The internal mass transfer limitations at thicker catalytic layers and deficiency of catalyst at thin catalytic layers lead to an optimum catalytic layer thickness. From Figure 2.4 it can be seen that this optimum in catalytic layer thickness is observed at a thickness of 100 µm under the prevailing conditions. The concentration profiles along the length of the reactor for an initial module void fraction of 0.2 and a catalytic layer thickness of 100 µm are presented in Figure 2.7.

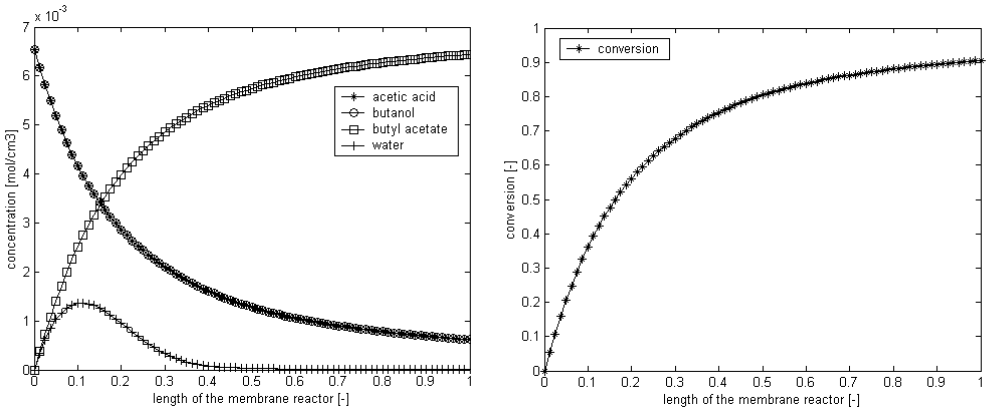

Figure 2.7 Bulk concentration of the components and reached conversion in the membrane reactor; δ_{cat} = 100 μm, $F/A_{mem} = 3.5*10^{-4}$ m s^{-1}

It can be seen that acetic acid and butanol are converted rapidly in the beginning of the reactor, whereas the reaction rate is lower at the end of the reactor. At the entrance of the membrane reactor, water concentration in the bulk liquid increases as a part of the water formed in the catalytic layer diffuses towards the bulk liquid. Gradually, water concentration in the bulk liquid decreases as more water is removed at the low pressure permeate side of the membrane than is formed by reaction. Consequently, the water concentration in the membrane reactor is reduced because water is removed in-situ after formation. Thus, hydrolysis of the formed ester can be neglected and, compared to the inert membrane reactor, reaction rates will be enhanced.

2.3.3 Effect of kinetic and membrane parameters

The optimum catalytic layer thickness is a function of the reaction rate constant and the membrane permeability. From Figures 2.8 and 2.9 it can be seen that an increase in catalyst activity, which may be realised by increasing the temperature, suggests a lower optimum catalytic layer thickness whereas an increase in membrane permeability gives a thicker optimum catalytic layer thickness.

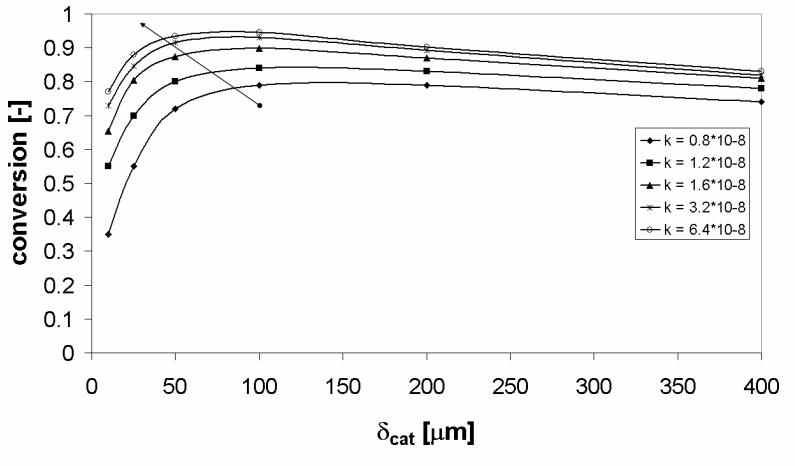

Figure 2.8 Effect of catalyst activity on module performance; δ_{cat} = 100 μm, $F/A_{mem} = 3.5*10^{-4}$ m s^{-1}.

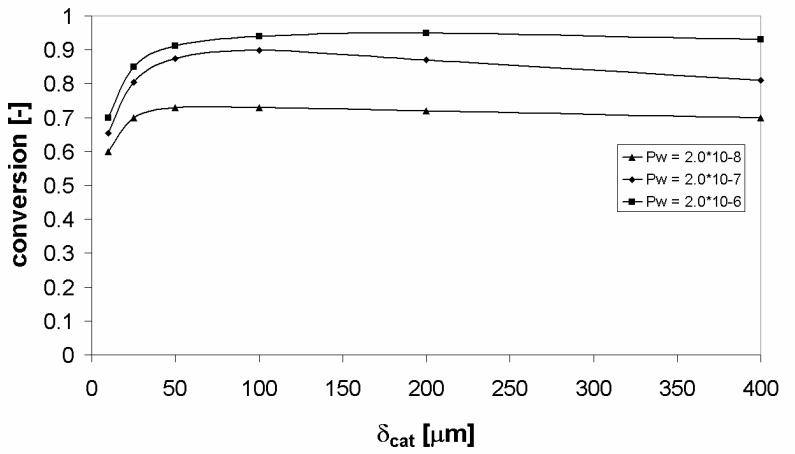

Figure 2.9 Effect of membrane permeability on module performance; δ_{cat} = 100 μm, $F/A_{mem} = 3.5*10^{-4}$ m s^{-1}.

Due to the higher reaction rates with increasing catalyst activity, the diffusion of reactants inside the catalytic layer cannot keep up with the reaction rate and mass transfer limitations become pronounced. Additionally, a faster water build-up in the reactor due to the higher reaction rates causes the optimum catalytic layer thickness to decrease as

the water removal from the membrane reactor is increased if the catalytic layer thickness decreases. The attained conversion increases with an increased catalyst activity. This occurs only up to a certain level, as shown in Figure 2.8 since at a certain catalyst activity mass transfer limitations become pronounced. A higher membrane permeability, however, increases the water removal capacity resulting in a thicker optimum catalytic layer as can be seen by Figure 2.9. It is shown that the reactor performance is hardly affected by the membrane if the membrane permeability is really low. On the other hand, no clear optimum in catalytic layer thickness is observed if the membrane permeability has a value of $2 \cdot 10^{-6}$ mol·m^{-2}·s^{-1}·Pa^{-1}.

2.4 Conclusions

The developed mathematical model can be used to provide design rules for composite catalytic hollow fibre membranes for condensation reactions. The composite catalytic membranes used in the model consist of a support coated with a water selective layer and on top of that a porous catalytic layer. Equilibrium displacement can be enhanced through integration of reaction and separation by means of composite catalytic membranes. An optimum catalytic layer thickness was found to be around 100 μm under the prevailing conditions, which is within practically reachable dimensions. The exact position of this optimum is a function of the reaction rate constant and the permeability of the membrane used. At this optimum catalytic layer thickness, the performance of a catalytic membrane reactor exceeds the performance of an inert membrane reactor due to the close integration of reaction and separation, which shows the potential added value of such a membrane system compared to more usual reactor designs. With increasing catalytic layer thickness, the conversion becomes no longer limited by the amount of catalyst present in the reactor but by diffusion in the catalytic layer. External mass transfer was never found to be rate-limiting. Based on the solution method developed, catalytic membrane modules can be designed conveniently if both the reaction kinetic parameters and the membrane parameters are known.

Acknowledgements

This work was performed in a cooperative project of the Centre for Separation Technology and was financially supported by TNO and NOVEM.

Nomenclature

C_i	concentration	[mol·m $_{liq}^{-3}$]
d	diameter	[m]
$D_{e,i}$	effective diffusion coefficient	[$m_{liq}^2 \cdot s^{-1}$]
D_i	diffusion coefficient	[$m_{liq}^2 \cdot s^{-1}$]
F	flow rate	[$m_{liq}^3 \cdot s^{-1}$]
k	reaction rate constant	[$m_{liq}^3 \cdot mol^{-1} \cdot s^{-1}$]
k_r	reaction rate constant per catalyst concentration	[$m_{liq}^6 \cdot mol^{-1} \cdot g_{cat}^{-1} \cdot s^{-1}$]
$k_{F,i}$	mass transfer coefficient	[$m_{liq} \cdot s^{-1}$]
K	equilibrium constant	[-]
N	number	[-]
p	pressure	[Pa]
p_i^*	vapor pressure	[Pa]
P_i	permeance	[$mol \cdot m^{-2} \cdot s^{-1} \cdot Pa^{-1}$]
r	radius	[m]
R_i	reaction rate	[$mol \cdot m_{liq}^{-3} \cdot s^{-1}$]
Sh	Sherwood	[-]
x_i	molar fraction retentate	[-]
y_i	molar fraction permeate	[-]
z	axial coordinate	[m]

	Greek letters	
δ	thickness	[m]
ε	void fraction	[-]
γ_i	activity coefficient	[-]
ρ	density	[kg·m^{-3}]
ζ	tortuosity	[-]
	Subscripts	
b	bulk liquid	
cat	catalyst	
f	fibre	
h	hydrodynamic	
i	component *i*	
in	in	
int	internal	
liq	liquid	
m	module	
mem	membrane surface	
o	outside	
obs	observed	
out	out	
p	permeate	

References

Bagnall, L., Cavell, K., Hodges, A.M., Mau, A.W., Seen, A.J., The use of catalytically active pervaporation membranes in esterification reactions to simultaneously increase product yield and permselectivity flux, *J. Membr. Sci.,* 85 (1993) 291-299.

Benedict, D.J., Parulekar, S.J., Tsai, S-P., Esterification of Lactic Acid and Ethanol with/without pervaporation, *Ind. Eng. Chem. Res.,* 42 (2003) 2282-2291.

Bernal, M.P., Coronas, J., Menéndez, M., Santamaría, J., Coupling of reaction and separation at the microscopic level: esterification processes in a H-ZSM-5 membrane reactor, *Chem. Eng. Sci.,* 57 (2002) 1557-1562.

Dafinov, A., Garcia-Valls, R., Font J., Modification of ceramic membranes by alcohol adsorption, *J. Membr. Sci.,* 196 (2002) 69-77.

David, M.O., Gref. R., Nguyen, T.Q., Neel, J., Pervaporation-esterification coupling. I. Basic kinetic model, *Chem. Eng. Res. Des.*, 69 (1991) 335-340.

David, M.O., Nguyen, T.Q., Neel, J., Pervaporation membranes endowed with catalytic properties, based on polymer blends, *J. Membr. Sci.*, 73 (1992) 129-141.

Domingues, L., Recasens, F., Larrayoz, M., Studies of a pervaporation reactor: kinetics and equilibrium shift in benzyl alcohol acetylation, *Chem. Eng. Sci.*, 54 (1999) 1461-1465.

Feng, X., Huang, R.Y.M., Studies of a membrane reactor: esterification facilitated by pervaporation, *Chem. Eng. Sci.*, 51 (1996) 4673-4679.

Font, J., Castro, R.P., Cohen, Y., On the loss of hydraulic permeability in ceramic membranes, *J. Col. Int. Sci.*, 181 (1996) 347-350.

Fredenslund, A., Jones, R.L., Prausnitz, J.M., Group-contribution estimation of activity coefficients in nonideal liquid mixtures, *AIChE J.,* 21 (1975) 1086-1099.

Keurentjes, J.T.F., Janssen, G.H.R., Gorissen, J.J., The esterification of tartaric acid with ethanol: kinetics and shifting the equilibrium by means of pervaporation, *Chem. Eng. Sci.*, 49 (1994) 4681-4689.

Krupiczka, R., Koszorz, Z., Activity-based model of the hybrid process of an esterification reaction coupled with pervaporation, *Sep. Pur. Technol.,* 16 (1999) 55-59.

Leffler, J., Cullinan, Jr. H.T., 1970, Variation of Liquid Diffusion Coefficients with Composition, *Ind. Eng. Chem. Fund.*, 9 (1970) 88-93.

Li, X., Lefu, W., Kinetic model for an esterification process coupled by pervaporation, *J. Membr. Sci.*, 186 (2001) 19-24.

Lim, S.Y., Park, B., Hung, F., Sahimi, M., Tsotsis, T.T., Design issues of pervaporation membrane reactors for esterification, *Chem. Eng. Sci.*, 57 (2002) 4933-4946.

Lipnizki, F., Field, R.W., Mass transfer performance for hollow fibre modules with shell-side axial feed flow: using an engineering approach to develop a framework, *J. Membr. Sci.*, 193 (2001) 195-208.

Liu, Q.L., Zhang, Z., Chen, H.F., Study on the coupling of esterification with pervaporation, *J. Membr. Sci.*, 182 (2001) 173-181.

Liu, Q.L., Chen, H.F., Coupling of esterification of acetic acid with *n*-butanol in the presence of $Zr(SO_4)_2.4H_2O$ coupled pervaporation, *J. Membr. Sci.*, 196 (2002) 171-178.

Nguyen Q.T., M'Bareck C.O., David, M.O., Métayer, M., Alexandre, S., Ion-exchange membranes made of semi-interpenetrating polymer networks, used for pervaporation-assisted esterification and ion transport, *Mat. Res. Innovat.*, 7 (2003) 212-219.

Perry, R.H., Green, D.W., Maloney, J.O., 1997, *Perry's Chemical Engineering Handbook*, 7th edition (McGraw-Hill, New York, USA)

Poling, B.E., Prausnitz, J.M., O'Connel, J.P., 2001, *The Properties of Gases and Liquids*, 5th edition (McGraw-Hill, London).

Reid, E.E., 1952, Esterification, in *Unit Processes in Organic Synthesis*, 4th edition Groggins, P.H. (ed) (McGraw Hill, New York, USA) pp 596-642.

Tanaka, K., Yoshikawa, R., Ying, C., Kita, H., Okamota, K., Application of zeolite membranes to esterification reactions, *Cat. Today*, 67 (2001) 121-125.

Verkerk, A.W., Male van, P., Vorstman, M.A.G., Keurentjes, J.T.F., Properties of high flux ceramic pervaporation membranes for dehydration of alcohol/water mixtures, *Sep. Pur. Technol.*, 22-23 (2001) 689-695.

Verkerk, A.W., *Application of silica membranes in separations and hybrid reactor systems*, PhD thesis, Eindhoven University of Technology, Universiteitsdrukkerij, Technische Universiteit Eindhoven, Eindhoven, the Netherlands, 2003.

Vergunst, T., Kapteijn, F., Moulijn, J.A., Optimization of geometric properties of a monolithic catalyst for the selective hydrogenation of phenylacetylene, *Ind. Eng. Chem. Res.*, 40 (2001) 2801-2809.

Waldburger, R.M., Widmer, F., Membrane reactors in chemical production processes and the application to the pervaporation-assisted esterification, *Chem. Eng. Technol.*, 19 (1996) 117-126.

Wilke, C.R., Chang, P., Correlation of Diffusion Coefficients in Dilute Solutions, *AIChE J.*, 1 (1955) 264-270.

Xu, Z.P., Chuang, X.T., Effect of internal diffusion on heterogeneous catalytic esterification of acetic acid, *Chem. Eng. Sci.*, 52 (1997) 3011-3017.

Zhu, Y., Minet, R.G., Tsotsis, T.T., A continuous pervaporation membrane reactor for the study of esterification reactions using a composite polymeric/ceramic membrane, *Chem. Eng. Sci.*, 51 (1996) 4103-4113.

Chapter 3

Comparison of solid acid catalysts for the esterification of acetic acid with butanol

Esterification of acetic acid with butanol has been studied in a heterogeneous reaction system, using a variety of solid acid catalysts. Comparative esterification experiments have been carried out using the homogeneous catalysts sulphuric acid, *p*-toluenesulphuric acid, and a heteropolyacid. The weight based activity of the heterogeneous catalysts decreases in the following order: Smopex 101 > Amberlyst 15 > sulphated ZrO_2 > H-USY-20 > H-BETA-12.5 > H-MOR-45 > Nb_2O_5 > H-ZSM-5-12.5. The low activity of ZSM 5 is a result of internal diffusion limitations in the medium sized pores of this zeolite type material. For the H USY type zeolites, the influence of the Si/Al ratio on catalytic activity has been examined. Although the amount of acid sites decreases with an increase in the Si/Al ratio, an optimum Si/Al ratio of 20 has been found. The activity of sulphated zirconia shows an optimum calcination temperature, although both the amount and acidity of the acid sites increase monotonically with calcination temperature. For Amberlyst 15, the influence of catalyst particle size, catalyst loading, and reaction temperature have been investigated.

This chapter is based on: Peters, T.A., Benes, N.E., Holmen, A., Keurentjes, J.T.F., *Comparison of commercial solid acid catalysts for the esterification of acetic acid with butanol*, Appl. Catal. A: General, 297 (2006) 182-188.

3.1 Introduction

Industrially widely applied esterification reactions are commonly catalysed using mineral liquid acids, such as sulphuric acid and *p*-toluenesulphonic acid. The catalytic activity of homogeneous catalysts is high. They suffer, however, from several drawbacks, such as their corrosive nature, the existence of side reactions, and the fact that the catalyst can not easily be separated from the reaction mixture [Altiokka and Citak, 2003; Chen *et al.*, 1999; Liu and Tan, 2001; Yadav and Thathagar, 2002]. The use of solid acid catalysts offers an alternative and has received a lot of attention in the past years [Liu and Tan, 2001]. Solid acid catalysts are not corrosive and, coated onto a support, they can easily be reused. Examples of solid acid catalysts used in esterification reactions include ion-exchange resins, zeolites, and superacids like sulphated zirconia and niobium acid.

Ion-exchange resins are the most common heterogeneous catalysts used and have proven to be effective in liquid phase esterification and etherification reactions [Altiokka and Citak, 2003; Bart *et al.*, 1996; Chen *et al.*, 1999; Lee *et al.*, 2002; Mazzotti *et al.*, 1997; Liu and Tan, 2001; Yadav and Mehta, 1994; Yadav and Thathagar, 2002; Xu and Chuang, 1996]. Because of their selective adsorption of reactants and swelling nature, these resins not only catalyse the esterification reaction but also affect the equilibrium conversion [Liu and Tan, 2001; Mazzotti *et al.*, 1997]. Shortcomings include insufficient thermal resistance, which limits the reaction temperature to 120°C, preventing widespread use in industry.

Zeolites, like Y, X, BEA, ZSM-5 and MCM-41 offer an interesting alternative and have proven to be efficient catalysts for esterification reactions [Corma, *et al.*, 1989; Hoek *et al.*, 2004; Kirumakki *et al.*, 2003, 2004; Ma *et al.*, 1996; Namba *et al.*, 1985; Zhang *et al.*, 1997, 1998]. Zeolites have found wide application in oil refining, petrochemistry, and in the production of fine chemicals. Their success is based on the possibility to prepare zeolites with strong Brønsted acidity that can be controlled within a certain range, combined with a good resistance to high reaction temperatures [Corma *et al.*, 1989].

Among the many superacids, sulphated zirconia has gained the most importance due to its catalytic activity, selectivity, thermal resistance and

reusability. Sulphated zirconia has been tested for a number of esterification reactions, including the esterification of acetic acid with butanol [Ardizzone *et al.*, 1999; Hino and Arata, 1981, 1985; Manohar *et al.*, 1998; Thorat *et al.*, 1992; Yadav and Mehta, 1994; Yadav and Nair, 1999]. In addition, niobium acid has received some attention, because when heat-treated at relative low temperatures it exhibits excellent catalytic activity [Chen *et al.*, 1984; Guo and Qian, 1993; Hiyoshi *et al.*, 2004; Iizuka *et al.*, 1986]. Especially for esterification reactions niobium acid seems to be the most promising superacid, because even when hydrated it maintains a fairly high acid strength [Hiyoshi *et al.*, 2004; Nowak and Ziolek, 1999].

In this study, the activity of various solid acid catalysts is assessed with respect to the esterification of acetic acid with butanol. The ion-exchange resin Amberlyst 15, Smopex-101, the acid zeolites H-ZSM-5, H-MOR, H-BETA and H-USY, and the solid superacids sulphated zirconia and niobium acid are used. Comparative esterification experiments have been carried out using the homogeneous catalysts sulphuric acid, *p*-toluenesulphuric acid and a heteropolyacid (HPA). The catalysts have been characterised using gas adsorption analysis (BET), X-ray diffraction (XRD), scanning electron microscopy (SEM) and temperature-programmed decomposition (TPD) techniques. Additionally, for Amberlyst 15, a more elaborate kinetic study for the esterification reaction between acetic acid and butanol is performed.

3.2 Theory

3.2.1 Esterification reactions

Esterification is a reversible reaction in which a carboxylic acid (A) reacts with an alcohol (B) in the presence of an acid catalyst to form an ester (E) and water (W):

$$\underset{(A)}{R-COOH} + \underset{(B)}{R'-OH} \longleftrightarrow \underset{(E)}{R-COO-R'} + \underset{(W)}{H_2O} \tag{3.1}$$

Although more elaborate models concerning the heterogeneous catalysis of esterification reactions exist [Mazzotti *et al.*, 1997; Lee *et al.*, 2002], the quasi-homogeneous model allows for a comparison between the various

catalysts tested [Lilja *et al.*, 2002]. Assuming first order reaction kinetics in all the components, the rate of esterification is k_{fw}·[A][B] and the rate of hydrolysis is k_{bw}·[E][W], where the quantities between brackets represent the molar concentration of the reacting species. Thus, for a composition corresponding to chemical equilibrium the following relation holds

$$\frac{k_{fw}}{k_{bw}} = K = \frac{[E][W]}{[A][B]} \tag{3.2}$$

where K is the equilibrium constant of the reaction. The overall rate of ester production can be written as

$$R_E = \frac{d[E]}{dt} = k_{fw} \cdot \left([A][B] - \frac{[E][W]}{K} \right) \tag{3.3}$$

3.3 Experimental

3.3.1 Catalysts

The heterogeneous catalysts studied were Amberlyst 15, Smopex-101, various zeolites, sulphated zirconia, and niobium acid. For comparison, sulphuric acid, *p*-toluenesulphuric acid, and a heteropolyacid (HPA) molybdatophosphoric acid hydrate were used.

Amberlyst 15 was obtained from Sigma (Steinheim, Germany), whereas a Smopex-101 research sample was obtained from Johnson Matthey Catalysts (Royston, UK). These catalysts were dried for 24 hours at 90°C prior to use. Amberlyst 15 are highly cross-linked styrene-divinyl benzene copolymer beads functionalised with sulfonic groups. Smopex-101 is a poly(ethylene) based fibre that is grafted with styrene, which is sulphonated with chloro-sulfonic acid. As in Amberlyst 15, the active group in Smopex-101 is sulfonic acid. H-BETA, H-MOR and H-USY are obtained from Zeolyst Int. (Valley Forge, USA). The average particle size was 1 μm, measured by SEM. Zeolite H-ZSM-5 was obtained from TriCat zeolites (Bitterfeld, Germany). Zeolite H-ZSM5-x, H-BETA-x, H-MOR-x and H-USY-x, where x represents the silica to alumina ratio, were used after calcination in an air stream for 8 hours at 500°C. Sulphated zirconia was prepared from a commercially available mesoporous precursor

(MEL XZO999/01) acquired from Mel Chemicals (Manchester, UK) by calcination at the desired temperature in an air stream for 6 hours. The SO_3 loading of the uncalcined zirconia pre-cursor was 5 wt.%. SEM micrographs indicated an average particle size of 5-10 μm. Niobium oxide (HY 340) was acquired from CBMM ltd (Araxá, Brazil) and was used after calcination at 300°C in a nitrogen stream for 3 hours. Sulphuric acid, *p*-toluenesulphuric acid and molybdatophosphoric acid hydrate were obtained from Merck. The chemo-physical properties of all heterogeneous catalysts are given in Table 3.1a-d.

3.3.2 Characterisation techniques

BET analysis

The specific surface area (BET) and average pore size of sulphated zirconia were determined on a Micromeretics ASAP 2010 instrument. The catalyst was first pre-treated at 200°C under vacuum for over 8 hours to desorb contaminating molecules (mainly water) from the catalyst surface. For the determination of BET surface area, the value of p/p_0 in the range $0 < p/p_0 \leq 0.3$ was used. For the pore size measurements, the value of p/p_0 was further increased to 1 and subsequently reduced to 0.14.

X-Ray diffraction

XRD analysis was performed using a Riguka Geigerflex B-max system. The catalyst surface was scanned by monochromatic Cu-$K_{\alpha 1}$ radiation (λ = 1.54056 Å) at 40kV and 25mA. The angle (2θ) was measured in steps of 0.02° with a dwell time of 1 second, between 15° and 85°.

Scanning electron microscopy

SEM pictures were taken using a JEOL JSM-5600 with an acceleration voltage of 15 kV. Catalyst samples were gold-coated prior to scanning.

Temperature-programmed decomposition

Temperature-programmed decomposition of adsorbed isopropylamine (TPD IPAm) was used to determine the total amount of acidic sites. In a typical experiment, 100 mg of catalyst was dried in a helium flow of 100 NmL·min^{-1} while heating at a rate of 2°C·min^{-1} to 300°C or 500°C for zirconia and the zeolites, respectively. The sample was kept at this temperature for 1 hour and subsequently cooled to 125°C. A helium flow saturated with IPAm at 125°C was led over the catalyst bed until no further adsorption was observed by online mass spectrometry. Subsequently, the

larger part of physisorbed IPAm was removed by purging in a helium flow for 16 h at 125°C. Temperature-programmed decomposition of IPAm was started by heating the sample at a rate of 5°C·min^{-1} to 400°C. The total number of acidic sites was calculated from the number of propene molecules originated from IPAm decomposition. A correction was made for the desorption of residual IPAm, which also yields a propene fragment in the mass spectrometric analysis.

Table 3.1 Properties of the catalysts used.

physical property		catalyst	
		Amberlyst 15	Smopex-101
shape	-	beads	fibres
size*	µm	500	10·4000
surface area*	$m^2 \cdot g^{-1}$	45	-
porosity*	%	36	-
acid content*	mmol $H^+ \cdot g_{cat}^{-1}$	4.7	3.4

physical property		H-USY-x				
Si/Al ratio	-	2.6	6	15	20	40
surface area*	$m^2 \cdot g^{-1}$	750	730	780	750	780
acid content	mmol $H^+ \cdot g_{cat}^{-1}$	1.09	0.74	0.47	0.27	0.20

physical property		HBETA-x		H-ZSM-5-x		H-MOR-x
Si/Al ratio	-	12.5	37.5	12.5	32.5	45
surface area*	$m^2 \cdot g^{-1}$	680	650	> 400	> 400	500
acid content	mmol $H^+ \cdot g_{cat}^{-1}$	1.27	0.47	1.26	0.55	0.38

physical property		sulphated ZrO_2					Nb_2O_5
calcination temp.	°C	300	400	500	600	700	300
BET surface area	$m^2 \cdot g^{-1}$	342	287	194	153	90	193
pore diameter	nm	3.0	2.9	3.3	4.0	5.6	4.3
acid content	mmol $H^+ \cdot g_{cat}^{-1}$	0.34	0.32	0.41	0.39	0.52	0.19

* data obtained from supplier

3.3.3 Esterification procedure

The catalyst activity in the esterification reaction between acetic acid and butanol was studied in a stirred batch reflux system at a temperature of 75°C. Acetic acid (>99.8 %) and butanol (>99.5 %) were obtained from Merck. A three-necked flask equipped with a condenser and stirrer was charged with a certain amount of acetic acid (0.66 mol) and pre-activated catalyst. The pre-activation was performed at the desired temperature and according the conditions given in paragraph 3.3.1. Then, the system was heated up to the reaction temperature after which the pre-heated butanol (0.66 mol) was added. Sufficient stirring of the mixture was used to avoid external mass or heat transport limitations. A further increase in stirrer speed did not alter the catalyst performance. The reaction temperature was maintained by means of a thermostatic water bath in which the reactor was immersed. For kinetic measurements, samples were taken periodically and analysed by a gas chromatograph equipped with a flame ionisation detector and a thermal conductivity detector. All catalysts were employed under similar reaction conditions. GC analysis confirmed that no by-products were formed. The reaction rate constants were evaluated by fitting Equation 3.3 to the measured time-dependent concentration curves, using a differential method combined with a non-linear least-squares regression technique. The activity of the catalysts is expressed in terms of a second-order reaction rate constant normalised for the catalyst weight. As the reaction also proceeds without adding a catalyst, the first-order reaction rate constant of this reaction is also given. The rate of esterification catalysed by the catalyst is obtained as the difference between them.

3.4 Results and discussion

3.4.1 Catalyst performance

For the esterification reaction between acetic acid and butanol all catalysts studied showed the assumed first-order behaviour in the reactant concentrations. The obtained time-dependant conversion curves are shown in Figures 3.1-3.3. The reaction rate constants obtained from the time-dependent concentration curves are shown in Table 3.2.

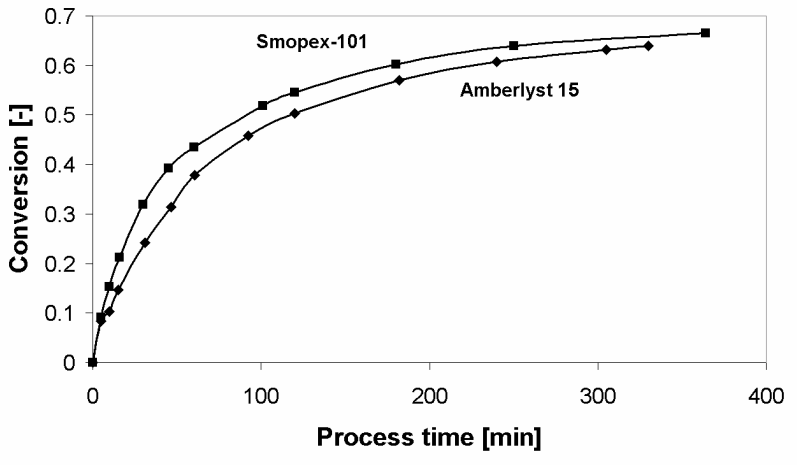

Figure 3.1 Conversion of acetic acid as a function of process time in the esterification between acetic acid and butanol, ion-exchange resins as catalyst, m_c ~ 1.9 gram, 75°C.

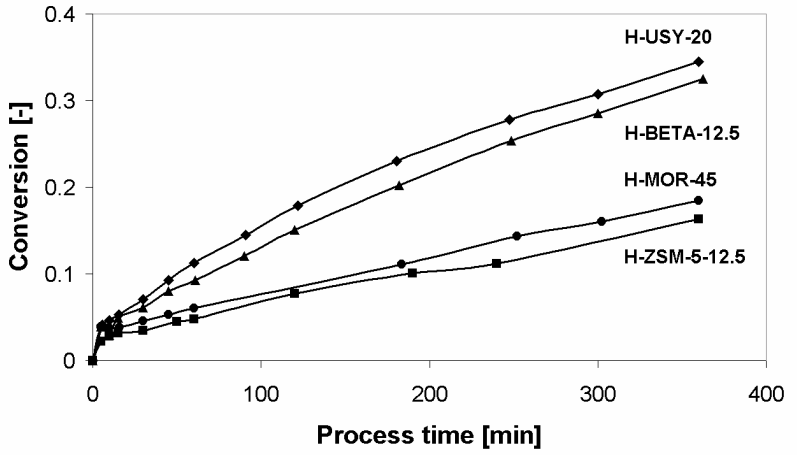

Figure 3.2 Conversion of acetic acid as a function of process time in the esterification between acetic acid and butanol, various zeolites as catalyst, m_c ~ 2.8 gram, 75°C.

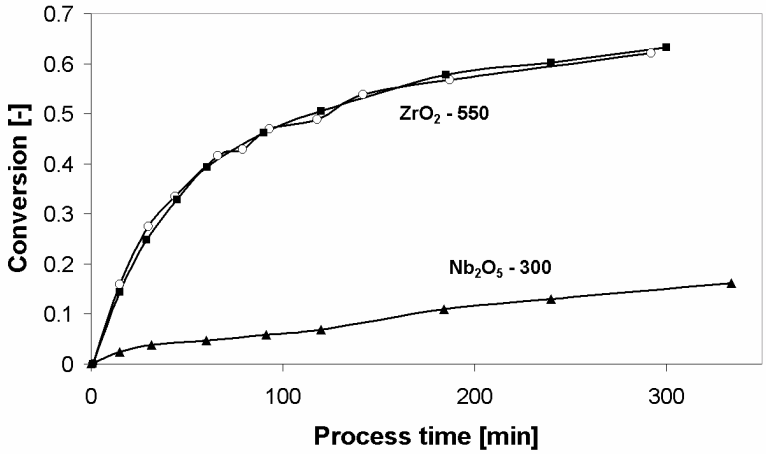

Figure 3.3 Conversion of acetic acid as a function of process time in the esterification between acetic acid and butanol, solid superacids as catalyst, closed symbols: fresh catalyst; open symbols: reused catalyst, m_c ~ 5 gram, 75°C.

Table 3.2 Activity of the different catalysts in the esterification reaction between acetic acid and butanol, 75°C.

	catalyst	amount [gram]	k [$m^3 \cdot mol^{-1} \cdot s^{-1}$]	k [$m^3 \cdot mol^{-1} \cdot g_{cat}^{-1} \cdot s^{-1}$]
	no catalyst	-	$1.30 \cdot 10^{-9}$	-
homogeneous	sulphuric acid	0.90	$1.7 \cdot 10^{-7}$	$1.9 \cdot 10^{-7}$
	p-tol sulf acid	1.77	$1.7 \cdot 10^{-7}$	$9.4 \cdot 10^{-8}$
	HPA	5.55	$1.2 \cdot 10^{-7}$	$2.1 \cdot 10^{-8}$
ion-exchange	Amberlyst 15	1.90	$3.0 \cdot 10^{-8}$	$1.6 \cdot 10^{-8}$
	Smopex-101	1.85	$4.4 \cdot 10^{-8}$	$2.4 \cdot 10^{-8}$
zeolite	H-ZSM-5-12.5	2.82	$1.7 \cdot 10^{-10}$	$5.9 \cdot 10^{-11}$
	H-BETA-12.5	2.81	$2.2 \cdot 10^{-9}$	$7.7 \cdot 10^{-10}$
	H-USY-20	2.88	$2.8 \cdot 10^{-9}$	$9.8 \cdot 10^{-10}$
	H-MOR-45	2.79	$2.9 \cdot 10^{-10}$	$1.0 \cdot 10^{-10}$
superacid	ZrO_2*	5.00	$4.4 \cdot 10^{-8}$	$8.8 \cdot 10^{-9}$
	Nb_2O_5**	5.17	$1.5 \cdot 10^{-9}$	$9.8 \cdot 10^{-11}$

* calcined at 550°C, ** calcined at 300°C

The acidic ion-exchange resins Amberlyst and Smopex-101 appear to be effective catalysts for the selected esterification reaction, as can be seen from Table 3.2. Compared to the ion-exchange resins, the weight-based activity of the zeolites and superacids is lower under these reaction conditions. However, for these catalysts also the acid site density is much lower as can be seen in Table 3.1. Additionally, the catalytic activity of the acid site may depend on the environment of the acid sites such as hydrophobicity. Furthermore, the diffusion of molecules to the active sites can become a limiting process in porous solid acids such as zeolites [Chen *et al.*, 1999].

From Table 3.2 it can be seen that the H-BETA-12.5 zeolite, having similar channel sizes (0.56 x 0.65 nm, 0.57 x 0.75 nm) as the H-USY zeolite (0.74 x 0.74 nm), shows an activity similar to H-USY-20. H-ZSM-5-12.5 has the lowest activity of the zeolites, although the amount of acid sites on this zeolite is similar that of H-BETA-12.5. The low activity of H-ZSM-5 can be explained by internal diffusion limitations in the medium sized pores (0.56 x 0.56 nm). Although H-MOR zeolite has a channel size (0.65 x 0.70 nm) similar to that of H-USY and H-BETA, the catalytic activity of H-MOR is only slightly higher compared to that of H-ZSM-5. For H-MOR-45 the low activity can be explained by diffusion limitations imposed by the one-dimensional channels of the zeolite (0.65 x 0.70 nm) [Machado *et al.*, 2000]. Srinivas *et al.* report an acidity for H-MOR-10, H-MOR-45 and H-BETA-12.5 of 1.30, 0.56 and 1.03 $mmol \cdot g^{-1}$, respectively, measured by the temperature-programmed desorption of ammonia [Srinivas *et al.*, 2002]. This is in accordance with the values found in this study using TPD IPAm, and is comparable to the amount of tetrahedral aluminum in the zeolite framework.

The weight-based activity of sulphated zirconia exceeds the activity of the zeolites tested as can be seen from Table 3.2. However, due to water adsorption on the active sites or loss of sulphur surface species, the activity of sulphated zirconia gradually decreases. Although the highest initial activity is found for the sulphated zirconia sample calcined at a temperature of 525°C, the sulphated zirconia calcined at 550°C is the most stable. After the reaction, the catalyst has been filtrated, calcined and subsequently used as catalyst in a second esterification reaction to investigate the reusability of sulphated zirconia. In the second esterification

experiment, the activity of the sulphated zirconia is similar to the activity of the fresh catalyst as can be seen in Figure 3.3. Thus, it can be concluded that sulphated zirconia can be regenerated and reused after calcination. The amount of acid sites on the commercial zirconia sample calcined at 500°C measured using TPD IPAm (0.41 $mmol \cdot g^{-1}$) is lower compared to the value obtained by Kuriakose and Nagaraju (0.98 $mmol \cdot g^{-1}$) from the temperature-programmed desorption of ammonia for a home-made sulphated zirconia sample [Kuriakose and Nagaraju, 2004].

The data in Table 3.2 also show that the activity of niobium acid towards the esterification reaction between acetic acid and butanol is very low. The amount of acid sites on niobium acid, determined using TPD IPAm, is lower compared to the value of 0.58 $mmol \cdot g^{-1}$ obtained by Chen *et al.*, using the titration of *n*-butylamine [Chen *et al.*, 1984]. The majority of the acid sites on niobium acid are expected to be Lewis acid sites [Tanabe, 1987]. Hence, the low activity might be linked largely to the absence of Brønsted acid sites that are essential for the esterification reaction.

Effect of Si/Al ratio on zeolite activity

Zeolite properties like pore size, acid strength distribution and hydrophobicity can be tuned by preparing zeolites with different crystalline structure, acid exchange level and framework Si/Al ratio [Corma *et al.*, 1989]. With increasing Si/Al ratio the zeolite surface becomes more hydrophobic, *i.e.*, has more affinity for the reactants, whereas the number of acid sites decreases. Additionally, the intrinsic acidity of the acid sites increases with an increase in the Si/Al ratio [Machado *et al.*, 2000]. Hence, an optimum Si/Al ratio may exist. Figure 3.4 shows the influence of the zeolite Si/Al ratio for the H-USY-type materials on the zeolite activity in the esterification reaction between acetic acid and butanol, and on the total amount of acid sites as probed by IPAm TPD.

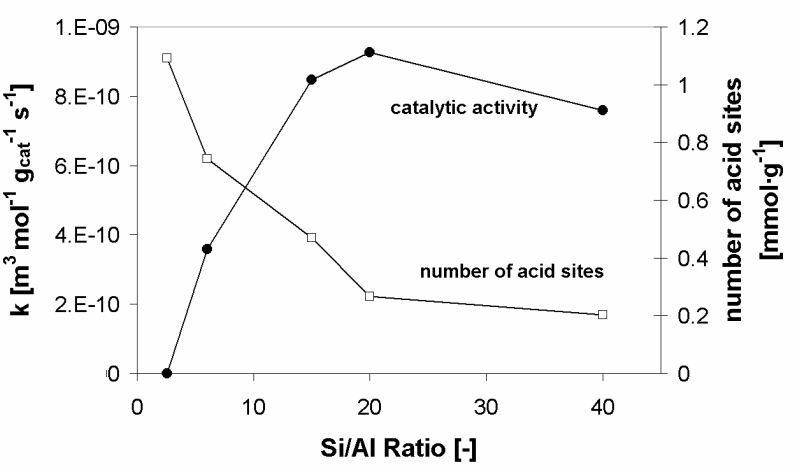

Figure 3.4 Effect of the H-USY Si/Al ratio on the amount of acid sites and on the reaction rate constant in the esterification reaction between acetic acid and butanol, 75°C.

From Figure 3.4 it can be seen that the H-USY zeolite activity indeed shows a maximum at a Si/Al ratio of 20. This agrees well with the results of Corma *et al.* [Corma *et al.*, 1989], from which it was concluded that the zeolite catalyst must have framework Si/Al ratio larger than 15. The total amount of acid sites measured using TPD IPAm decreases monotonically with increasing Si/Al ratio (Figure 3.4). Although TPD IPAm does not differentiate between Brønsted acid and Lewis acid sites, it is known that an increase in Si/Al ratio results in a decrease of the ratio of the number of Brønsted acid to Lewis acid sites [Wang *et al.*, 2001]. The total amount of acid sites is the largest for the H-USY zeolite with a Si/Al ratio of 2.6. However, this catalyst is inactive towards the esterification reaction, most likely due to the hydrophilic nature of this H-USY zeolite causing facile adsorption of water and poisoning of the acid sites [Namba *et al.*, 1985]. Srinivas *et al.* [Srinivas *et al.*, 2002] report an acidity for H-USY-15 of 0.56 mmol·g^{-1} measured by temperature-programmed desorption of ammonia, which is higher compared to the value in Table 3.1. This discrepancy is due to the fact that isopropylamine does not interact with the Brønsted acid sites located in the sodalite cages of the H-USY zeolite. Hence, these sites are not measured using TPD IPAm.

Effect of calcination temperature on sulphated zirconia activity

The properties of sulphated zirconia highly depend on the catalyst pre-treatment. For example, at increasing calcination temperature the crystallinity of the sulphated zirconia increases, whereas the surface area and the amount of surface sulphur species decreases [Hu *et al.*, 2000]. Hence, an optimum in activity as a function of the calcination temperature can be expected at which the best Brønsted to Lewis acid site ratio is obtained. The XRD spectra of sulphated zirconia calcined at different temperatures are collected in Figure 3.5. It can be seen that the material has remained amorphous up to calcination temperatures of 400°C. At higher calcination temperatures, cubic and tetragonal zirconia phases are present. After calcination at 700°C, an additional monoclinic zirconia phase appears. Figure 3.6 shows the influence of calcination temperature on the catalytic activity, and the total amount of acid sites measured by IPAm TPD.

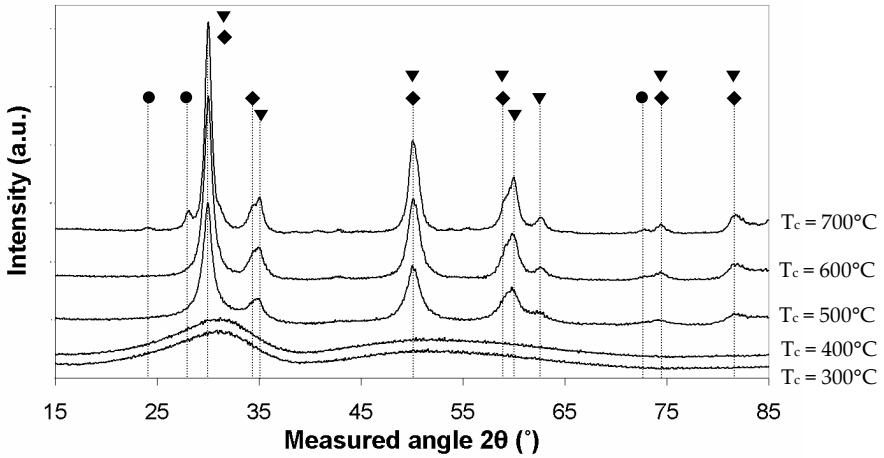

Figure 3.5 X-ray diffraction patterns of sulphated ZrO_2 catalysts as a function of the calcination temperature; (●) monoclinic phase; (◆) tetragonal phase; (▼) cubic phase.

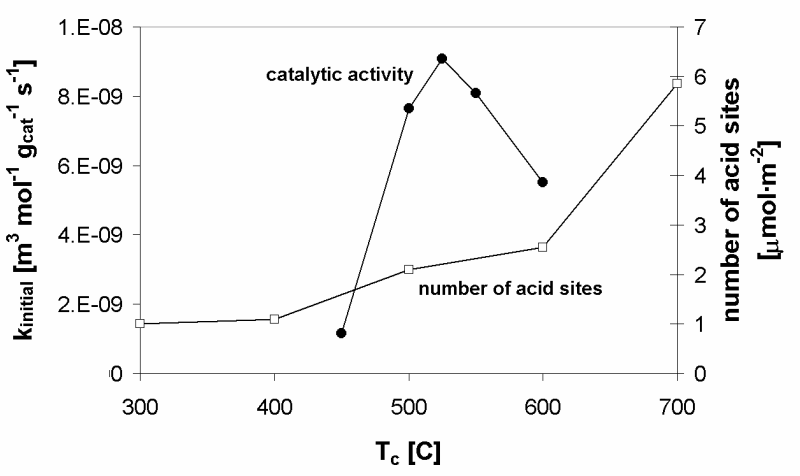

Figure 3.6 Effect of the calcination temperature of sulphated zirconia on the amount of acid sites and on the initial reaction rate constant in the esterification reaction between acetic acid and butanol, 75°C.

Figure 3.6 shows that for the catalytic activity of sulphated zirconia an optimum intermediate calcination temperature exists, although the amount of acid sites as a function of the calcination temperature shows a monotone increase. Figure 3.7 shows the temperature TPD IPAm profiles as a function of the calcination temperature. It can be seen that the isopropylamine peak shifts towards a lower decomposition temperature with an increasing calcination temperature. Additionally, the area beneath the decomposition peak increases with an increase in calcination temperature. Thus, both the total amount and the acidity of the acid sites on the sulphated zirconia increase at a higher calcination temperature. Most likely, at higher calcination temperatures Lewis acid sites are formed and Brønsted acid sites are removed. As Brønsted acid sites are essential for catalysis of esterification reactions this explains the decrease in activity.

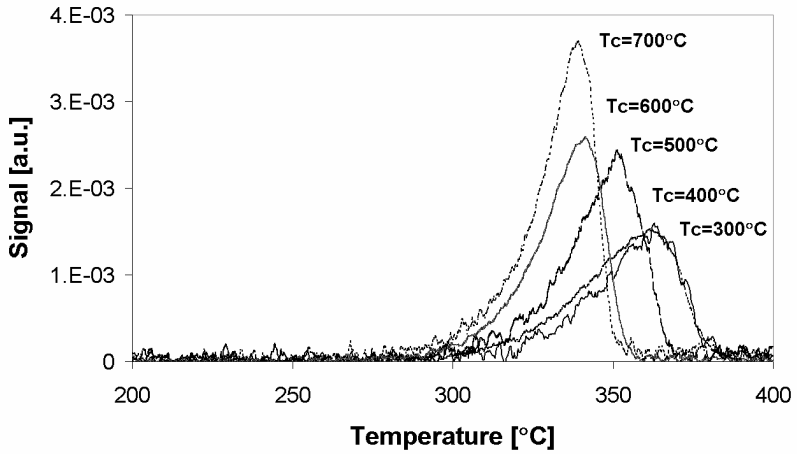

Figure 3.7 Temperature-programmed decomposition profiles of isopropylamine on sulphated zirconia as a function of the calcination temperature.

The optimum calcination temperature for sulphated zirconia is found at a temperature of 525°C (Figure 3.6). This agrees with the optimum calcination temperature of 575°C obtained by Hino *et al.* [Hino *et al.*, 1981] for the esterification reaction of acetic acid and ethanol in the presence of sulphated zirconia. However, the value is relatively low as compared to the value (620°C) obtained by Bianchi *et al*. [Bianchi *et al.*, 2004] for the esterification of benzoic acid to methyl benzoate.

3.4.2 Amberlyst 15

For the ion-exchange resin, Amberlyst 15, a more elaborate kinetic study has been performed, because of the high activity and stability of this catalyst. The influence of catalyst loading, catalyst particle size, and reaction temperature has been investigated.

3.4.2.1 Catalyst loading and particle size

The catalyst loading has been varied between 8.75 and 35.5 kg·m^{-3}, based on the total reactants volume at a temperature of 75°C. The results can be seen in Figure 3.8. The Figure shows a linear increase in reaction rate with catalyst loading, indicating that the reaction is catalytically activated.

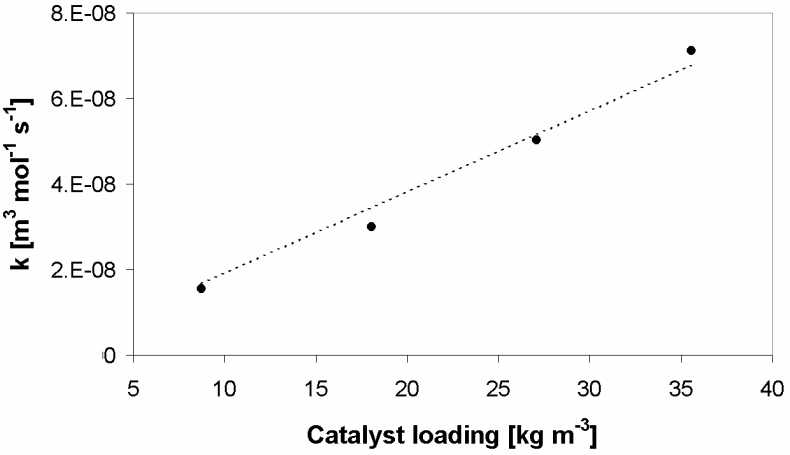

Figure 3.8 Effect of the Amberlyst 15 loading on the reaction rate constant in the esterification reaction between acetic acid and butanol.

For the reactions catalysed by the Amberlyst 15 resin, internal mass transport limitations are usually negligible [Bart *et al.*, 1996; Liu and Tan, 2001; Xu and Chuang, 1996, 1997]. The extent of internal mass transport can be estimated from the Weisz modulus:

$$W_{\mathrm{m}} = -\frac{r_{\mathrm{A}} \cdot L^2}{D_{\mathrm{eff}} \cdot C_{\mathrm{A}}{}^{0}} \tag{3.4}$$

where r_A is the reaction rate, L the characteristic length and C_A^0 is the initial acetic acid concentration. The diffusion coefficient of acetic acid, D_{AB}, in butanol has been evaluated by the Wilke-Chang equation [Wilke and Chang, 1955], and is corrected for the morphology of the porous catalyst by multiplying it with the porosity ε, and dividing it by the tortuousity τ:

$$D_{\text{eff}} = \frac{\varepsilon}{\tau} D_{\text{AB}} \tag{3.5}$$

Generally, the mass transport limitations in a porous particle are considered insignificant when $W_m < 0.15$. For all experiments carried out with Amberlyst 15 in this study the estimated values of W_M were less than 0.1, indicating negligible internal mass transport limitations. The absence of significant internal mass transport limitations in the bead-shaped Amberlyst 15 particles has been evaluated experimentally at a temperature of 75°C. Figure 3.9 shows the alcohol conversion for four different Amberlyst 15 particle sizes. For an average particle size less than 700 μm, hardly any effect of particle size on the conversion is observed. This indicates that the catalytic process is kinetically controlled, because external and intraparticle mass transport limitations are negligible [Yadav *et al*., 2002].

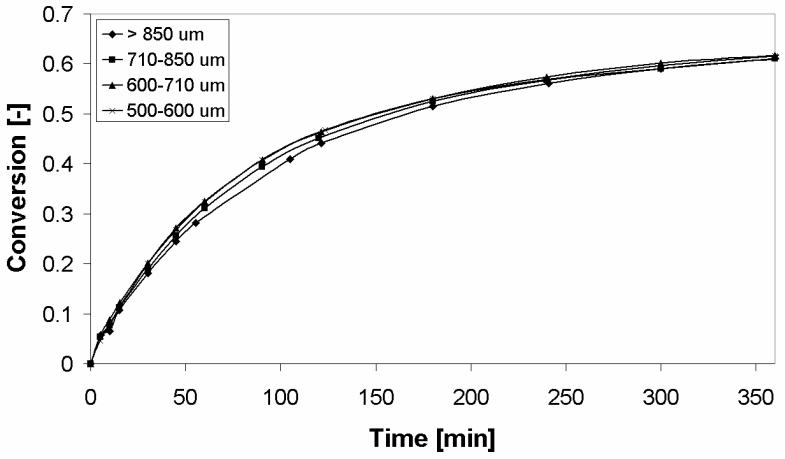

Figure 3.9 Effect of the particle size of Amberlyst 15 on the reaction rate constant in the esterification reaction between acetic acid and butanol.

3.4.2.2 Temperature

The effect of the temperature on the conversion has been studied in the temperature range between 65 and 80°C, under otherwise similar conditions. The results can be seen in Figure 3.10, from which it can be concluded that the conversion increases with an increase in temperature.

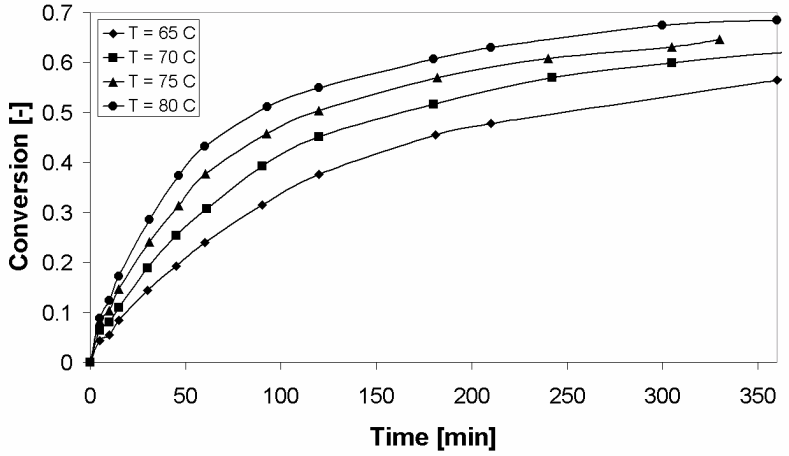

Figure 3.10 Effect of the reaction temperature on the reached conversion in the esterification reaction between acetic acid and butanol.

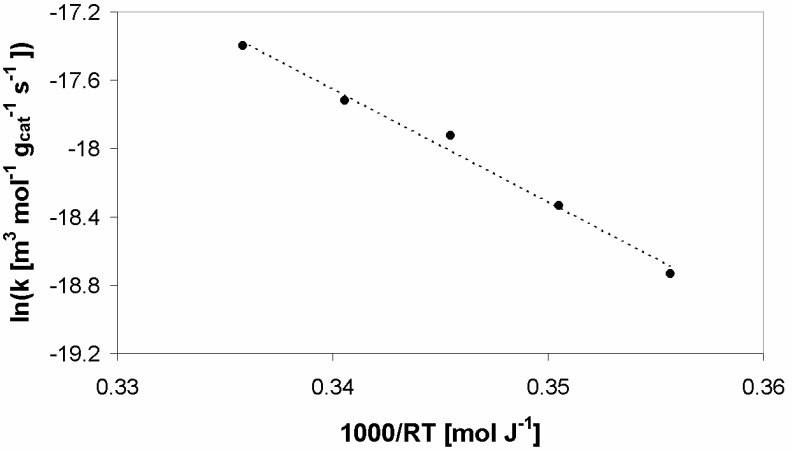

Figure 3.11 Arrhenius plot for the esterification between acetic acid and butanol.

From the reaction rate constants at different temperatures, the frequency factor, A_f, and activation energy, E_A, could be evaluated according to the Arrhenius equation:

$$k = A_f \cdot e^{-\left(E_A / R \cdot T\right)} \tag{3.6}$$

A fairly linear dependence of ln(k) on 1/T is observed, as shown in Figure 3.11. The frequency factor has been evaluated as 5.8 $m^{-3} \cdot mol^{-1} \cdot s^{-1}$ and the activation energy equals 69 $kJ \cdot mol^{-1}$. This value is in good agreement with the activation energy, 70.6 $kJ \cdot mol^{-1}$, obtained by Gangadwala *et al.* [Gangadwala *et al.*, 2003]. The relative high value for the activation energy further confirms that the process is kinetically controlled [Xu and Chuang, 1996].

3.5 Conclusions

The activity of various heterogeneous and homogeneous catalysts has been examined for the esterification reaction between acetic acid and butanol. Heterogeneous catalysis is very effective from the viewpoint of activity and reusability compared with homogeneous catalysts. For the various solid acid catalysts the activity per proton of significantly different, because the specific reaction rate depends on the environment of the acid sites, such as hydrophobicity. Furthermore, the diffusion of molecules to the active sites becomes important in the case of porous solid acids such as zeolites.

The weight-based activity of the heterogeneous catalysts tested decreases in the following order: Smopex-101 > Amberlyst 15 > sulphated ZrO_2 > H-USY-20 > H-BETA-12.5 > H-MOR-45 > Nb_2O_5 > H-ZSM-5-12.5.

For the H-USY-type materials, the influence of the zeolite Si/Al ratio on the zeolite activity in the esterification reaction between acetic acid and butanol has been examined. An optimum Si/Al ratio of 20 is found. No clear relationship, however, has been observed between the total amount of acid sites, measured with the temperature-programmed decomposition of isopropylamine, and the catalytic activity.

The activity and stability of sulphated zirconia towards the esterification reaction depends highly on the catalyst pre-treatment. The zirconia activity in the esterification reaction of acetic acid and butanol shows an optimum calcination temperature, although both the amount and acidity of the acid sites as a function of the calcination temperature shows a monotone increase.

The effect of various parameters on the reaction rate demonstrate that the reaction catalysed by Amberlyst 15 is kinetically controlled, with overall second order reaction kinetics. Moreover, there are no intraparticle and interparticle mass transport limitations. The activation energy has been found to be 69 kJ·mol^{-1}.

Acknowledgements

This work has been performed in a cooperative project of the Centre for Separation Technology and is financially supported by TNO and NOVEM. We would like to thank MelChem, Tricat and CBMM ltd for supplying the catalysts. Furthermore, we would like to thank Emiel Hensen and Rene Vermerris for their help during the TPD experiments and Marco Hendrix for performing the XRD analysis.

Nomenclature

A	acid	[-]
A_f	frequency factor	[m^3·mol^{-1}·s^{-1}]
B	alcohol	[-]
Ci	concentration	[mol·m^{-3}]
D_{AB}	infinite diluted diffusion coefficient	[m^2·s^{-1}]
$D_{eff,i}$	effective diffusion coefficient	[m^2·s^{-1}]
E	ester	[-]
E_A	activation energy	[J·mol^{-1}]
k_{obs}	observed reaction rate constant	[m^3·mol^{-1}·g$_{cat}^{-1}$·s^{-1}]
K	equilibrium constant	[-]

R	gas constant	[J·mol^{-1}·K^{-1}]
R_i	reaction rate	[mol·m^{-3}·s^{-1}]
t	time	[s]
T	temperature	[°C]
X	conversion	[-]
W	water	[-]
	Greek letters	
ε	catalyst porosity	[-]
τ	catalyst tortuosity	[-]
	Subscripts	
bw	backward	
eff	effective	
fw	forward	

References

Altiokka, M.R., Citak, A., Kinetics study of esterification of acetic acid with isobutanol in the presence of amberlite catalyst, *Appl. Catal. A: General*, 239 (2003) 141-148.

Ardizzone, S., Bianchi, C.L., Ragaini, V., Vercelli, B., SO_4–ZrO_2 catalysts for the esterification of benzoic acid to methylbenzoate, *Catal. Lett.*, 62 (1999) 59-65.

Bart, H.J., Kaltenbrunner, W., Landschuetzer, H., Kinetics of esterification of acetic acid with propyl alcohol by heterogeneous catalysis, *Int. J. Chem. Kinet.*, 28 (1996) 649-656.

Bianchi, C.L., Ardizonne, S., Cappelletti, G., Surface state of sulfated zirconia: the role of the sol-gel reaction parameters, Surf. Interface Anal. 36 (2004) 745-748.

Chen, Z., Iizuka, T., Tanabe, K., Niobic acid as an efficient catalyst for vapor phase esterification of ethyl alcohol with acetic acid, *Chem. Lett.*, (1984) 1085-1088.

Chen, X., Xu, Z., Okuhara, T., Liquid phase esterification of acrylic acid with 1-butanol catalyzed by solid acid catalysts, *Appl. Catal. A: General*, 180 (1999) 261-269.

Corma, A., Garcia, H., Iborra, S., Primo, J., Modified faujasite zeolites as catalysts in organic reactions: esterification of carboxylic acids in the presence of HY zeolites, *J. Catal.*, 120 (1989) 78-87.

Gangadwala, L., Mankar, S., Mahajani, S., Esterification of acetic acid with butanol in the presence of ion-exchange resins as catalysts, *Ind. Eng. Chem. Res.*, 42 (2003) 2146-2155.

Guo, C., Qian, Z., Acidic and catalytic properties of niobic acid crystallized at low temperature, *Catal. Today*, 16 (1993) 379-385.

Hino, M., Arata, K., Synthesis of esters from acetic acid with methanol, ethanol, propanol, butanol, and isobutyl alcohol catalyzed by solid superacid, *Chem. Lett.*, (1981) 1671-1672.

Hino, M., Arata, K., Solid catalysts treated with anions. 13. Synthesis of esters from terephthalic and phthalic acids with n-octyl and 2-ethylhexyl alcohol, acrylic acid with ethanol and salicylic acid with methanol catalyzed by solid superacid, *Appl. Catal.*, 18 (1985) 401-404.

Hiyoshi, M., Lee, B., Lu, D., Hara, M., Kondo, J.N., Domen, K., Supermicroporous niobium oxide as an acid catalyst, *Catal. Lett.*, 98 (2004) 181-186.

Hoek, I., Nijhuis, T.A., Stankiewicz, A.I., Moulijn, J.A., Kinetics of solid acid catalyzed etherification of symmetrical primary alcohols: Zeolite BEA catalyzed etherification of 1-octanol, *Appl. Catal. A: General*, 266 (2004) 109-116.

Hu, J., Wei, C., Qiu, F., Xu, Z., Chen, Q., Preparation of a new type solid acid SO_4^{2-}/Fe_2O_3-ZrO_2-SiO_2 and its application in the esterification of acetic acid and butanol, *J. Nat. Gas Chem.*, 9 (2000) 212-216.

Iizuka, T., Fujie, S., Ushikubo, T., Chen, Z.H., Tanabe, K., Esterification of acrylic acid with methanol over niobic acid catalyst, *Appl. Catal.*, 28 (1986) 1-5.

Kirumakki, S.R., Nagaraju, N., Chary, K.V.R., Narayanan, S., Kinetics of esterification of aromatic carboxylic acids over zeolites Hb and HZSM5 using dimethyl carbonate, *Appl. Catal. A: General*, 248 (2003) 161-167.

Kirumakki, S.R., Nagaraju, N., Narayanan, S., Kinetics study of esterification of acetic acid with isobutanol in the presence of amberlite catalyst, *Appl. Catal. A: General*, 273 (2004) 1-9.

Kuriakose, G., Nagaraju, N., Selective synthesis of phenyl salicylate (salol) by esterification reaction over solid acid catalysts, *J. Mol. Cat. A: Chem.*, 223 (2004) 155-159.

Lee, M.J., Chiu, J.Y., Lin, H.M., Kinetics of catalytic esterification of propionic acid and n-butanol over Amberlyst 35, *Ind. Eng. Chem. Res.*, 41 (2002) 2882-2887.

Lilja, J., Murzin, D. Yu, Salmi, T., Aumo, J., Mäki-Arvela, P., Sundell, M., Esterification of different acids over heteregenous and homogeneous catalysts and correlation with the Taft equation, *J. Mol. Cat. A: Chem.*, 182-183 (2002) 555-563.

Liu, W.T., Tan, C.S., Liquid-Phase Esterification of propionic acid with n-butanol, *Ind. Eng. Chem. Res.*, 40 (2001) 3281-3286.

Ma, Y., Wang, Q.L., Yan, H., Ji, X., Qiu, Q., Zeolite-catalyzed esterification. I. Synthesis of acetates, benzoates and phthalates, *Appl. Catal. A: General* , 139 (1996) 51-57.

Machado, M. da S., Pérez-Pariente, J., Sastre, E., Cardoso, D., de Guereñu, A.M., Selective synthesis of glycerol monolaurate with zeolitic molecular sieves, *Appl. Catal. A: General* , 203 (2000) 321-328.

Manohar, B., Reddy, V.R., Reddy, B.M., Esterification by ZrO_2 and Mo-ZrO_2 eco-friendly solid acid catalysts, *Synth. Commun.*, 28 (1998) 3183-3187.

Mazzotti, M., Neri, B., Gelosa, D., Kruglov, A., Morbidelli, M., Kinetics of liquid-phase esterification catalyzed by acidic resins, *Ind. Eng. Chem. Res.*, 36 (1997) 3-10.

Namba, S., Wakushima, Y., Shimizu, T., Yashima, T., Catalytic application of hydrophobic properties of high-silica zeolites. II. Esterification of acetic acid with butanols, *Stud. Surf. Sci. Cat.*, 20 (1985) 205-211.

Nowak, I., Ziolek, M., Niobium compounds: preparation, characterization, and application in heterogeneous catalysis, *Chem. Rev.*, 99 (1999) 3603-3624.

Srinivas, N., Singh, A.P., Ramaswamy, A.V., Finiels, A., Moreau, P., Shape-selective aklylation of 2-methoxynaphtalene with *tert*-butanol over large-pore zeolites, *Cat. Letters*, 80 (2002) 181-186.

Tanabe, K., Niobic acid as an unusual acidic solid material, *Mat. Chem. and Phys.*, 17 (1987) 217-225.

Thorat, T.S., Yadav, V.M., Yadav, G.D., Esterification of phthalic anhydride with 2-ethylhexanol by solid superacidic catalysts, *Appl. Catal. A: General*, 90 (1992) 73-96.

Wang B., Lee, C.W., Cai, T-X., Park, S-E., Identification and influence of acidity on alkylation of phenol with propylene over ZSM-5, *Cat. Letters*, 76 (2001) 219-224.

Wilke, C.R., Chang, P., Correlation of Diffusion Coefficients in Dilute Solutions, *AIChE J.*, 1 (1955) 264-270.

Xu, Z.P., Chuang, K.T., Kinetics of acetic acid esterification over ion exchange catalysts, *Can. J. Chem. Eng.*, 74 (1996) 493-500.

Xu, Z.P., Chuang, X.T., Effect of internal diffusion on heterogeneous catalytic esterification of acetic acid, *Chem. Eng. Sci.*, 52 (1997) 3011-3017.

Yadav, G.D., Mehta, P.H., Heterogeneous catalysis in esterification reactions: preparation of phenethyl acetate and cyclohexyl acetate by using a variety of solid acidic catalysts, *Ind. Eng. Chem. Res.*, 33 (1994) 2198-2208.

Yadav, G.D., Nair, J.J., Sulfated zirconia and its modified versions as promising catalysts for industrial processes, *Micr. Meso. Mater.*, 33 (1999) 1-48.

Yadav, G.D., Thathagar, M.B., Esterification of maleic acid with ethanol over cation-exchange resin catalysts, *React. Funct. Polym.*, 52 (2002) 99-100.

Zhang, H.B., Zhang, K., Yuan, Z.Y., Zhao, W., Li, H.X., Surface acidity of zeolite HZSM-5 and its catalytic properties in esterification of acetic acid with alcohols, *J. Nat. Gas Chem.*, 6 (1997) 228-236.

Zhang, H.B., Zhang, K., Yuan, Z.Y., Zhao, W., Li, H.X., Esterification of acetic acid with n-amyl alcohol over zeolite beta, *J. Nat. Gas Chem.*, 7 (1998) 336-345.

Chapter 4

Synthesis of hollow fibre microporous silica membranes

Thin microporous silica membranes were prepared on the outer surface of hollow fibre ceramic substrates. In principle this enables relatively fast and inexpensive production of large membrane surface area, combined with a low support resistance and a high membrane surface area / module volume ratio (> 1000 $m^2 \cdot m^{-3}$) compared to tubular membranes. Membranes were analyzed using SEM, SNMS, single gas permeance and pervaporation. High He permeance (1.1-2.9·10^{-6} $mol \cdot m^{-2} \cdot s^{-1} \cdot Pa^{-1}$), high He/$N_2$ permselectivity (~ 100-1000) and Arrhenius type temperature dependence of gas permeance indicate that the membranes are microporous and possess a low number of defects. The contribution of the hollow fibre substrate to the overall mass transport resistance is found to be small, even for fast permeating gases like helium. In the dehydration of *1*-butanol (80°C, 5 wt.% water) initially a high flux and selectivity were observed (2.9 $kg \cdot m^{-2} \cdot h^{-1}$ and 1200, respectively).

This chapter is based on: Peters, T.A., Fontalvo, J., Vorstman, M.A.G., Benes, N.E., van Dam, R.A., Vroon, Z.A.E.P., van Soest-Vercammen E.L.J., Keurentjes, J.T.F., *Hollow fibre microporous silica membranes for gas separation and pervaporation; synthesis, performance and stability*, J. Membr. Sci., 248 (2005) 73-80.

4.1 Introduction

Compared to their organic counterparts inorganic membrane materials generally possess superior structural stability, *e.g.*, no swelling and compaction, even in harsh chemical environments and at high temperatures [van Gemert and Petrus-Cuperus, 1995; Verkerk *et al.*, 2001; Wynn, 2001]. The majority of inorganic membranes are porous and their selective features are often closely related to their pore size. Amorphous silica is an inorganic material containing exceptionally small pores. Membranes based on this material have an asymmetric structure with the actual selective microporous silica positioned on a support structure comprising several α- and γ- alumina layers. Silica membranes were discovered more than a decade ago [de Lange *et al.*, 1995; Uhlhorn *et al.*, 1992] and are still subject of extensive study.

Silica membranes reported in literature have either a flat plate or tubular geometry. The flat plate geometry is advantageous from an academic point of view, but it usually has a small surface area (typically ~ 10^{-2} m^2) due to limitations imposed on the dimensions by the dip-coating technique. The surface area of tubular silica membranes is larger and their geometry is also more compatible with the technology developed in organic membrane science. Consequently, commercially available membranes for pervaporation have a tubular geometry [Wynn, 2001]. Drawbacks of this geometry include a relatively low surface area-to-volume ratio (typically < 500 $m^2 \cdot m^{-3}$) and high costs associated with tubular ceramic membrane supports.

In this work silica layers are positioned on top of ceramic hollow fibres. In principle this enables the relatively rapid and inexpensive preparation of a large membrane surface area, combined with a high membrane surface-area-to-volume ratio (> 1000 $m^2 \cdot m^{-3}$). Additionally, pervaporation modules built with externally coated hollow fibres allow for high mass and heat transfer coefficients combined with low liquid pressure drops. The membranes were characterised using SEM, SNMS, single gas permeance and pervaporation.

4.2 Theory

4.2.1 Gas permeation

Numerous theories for describing transport in microporous media have been presented in literature [Barrer, 1939; van den Broeke *et al.*, 1999; Kaerger and Ruthven, 1992]. These theories become increasingly complex when the microporous medium is less uniform and when more mobile species are present. For our purpose, *i.e.*, the assessment of membrane quality, a simple phenomenological approach is sufficient.

For single gas permeation of permanent gases through amorphous microporous silica membranes, at sufficiently high temperatures and low pressures, transport is activated and permeance is independent of pressure [de Lange *et al.*, 1995; Uhlhorn *et al.*, 1992; de Vos and Verweij, 1998a]. Hence, permeance is described by:

$$P \equiv \frac{N}{\Delta p} = (H_0 D_0)\exp((Q - E_D)/RT) \tag{4.1}$$

where N is the molar flux, H_0 and D_0 are pre-exponential factors related to the Henry and diffusion coefficients, respectively, and R and T have their usual meaning. The overall thermally activated nature of transport arises from the simultaneous occurrence of diffusion (E_D) and sorption (Q).

4.2.2 Pervaporation

For dehydration of solvents by pervaporation the performance of a membrane is usually expressed in terms of water flux, or permeance, and separation factor α. The latter is defined as:

$$\alpha = \frac{y_{H2O}/x_{H2O}}{y_j/x_j} \tag{4.2}$$

where y and x are the molar fractions in the permeate and retentate, respectively. Permeance is defined as the flux divided by the partial pressure difference over the membrane. The equilibrium vapour pressure of component i at the retentate side is related to the mole fraction x and activity coefficient γin the liquid mixture

$$p_i^* = \gamma_i \cdot x_i \cdot p_i^0 \tag{4.3}$$

where and p_i^0 is the vapour pressure of the pure component *i*. When the pressure at the permeate side is small compared to the equilibrium vapour pressure at the retentate side, permeance can be expressed as [Verkerk *et al.*, 2001]:

$$P_i = \frac{N_i}{\gamma_i \cdot x_i \cdot p_i^{\,0}} \tag{4.4}$$

4.3 Experimental

4.3.1 Membrane preparation

Support

The ceramic hollow fibres membrane supports (CEPAration, The Netherlands) have a porosity of ~30%, a pore diameter of either 150 or 300 nm, a length in the range of 20-30 cm, and an inner and outer diameter of 2.0 and 3.0 mm, respectively.

γ-Al_2O_3 intermediate support preparation

On the outer side of the hollow fibre substrates intermediate mesoporous γ-Al_2O_3 layers were prepared by sequential dip-coating with a boehmite coating solution. The boehmite solution was made by adding aluminium-tri-sec-butoxide (Aldrich) dropwise to water at 90°C under vigorous stirring, and subsequent boiling for 90 minutes to remove the 2-butanol produced during the hydrolysis. A white solution was obtained, which was peptised with 1 mol·l^{-1} HNO_3 (water/alkoxide/acid ratio: 70/1/0.07). The peptisation was accompanied by a change in colour from white to "nano" blue. After refluxing for 16 hours the resulting solution had a pH of 3.8. Finally, 120 ml polyvinyl alcohol (PVA) solution was added to 180 ml boehmite solution, followed by stirring at room temperature for 30 minutes and subsequently stirring at 90°C for 150 minutes. The PVA solution was prepared by dissolving 8.75 gram PVA (Aldrich, PVA Powder, average M_w 89-98 kD, hydrolysis grade 98%) in 250 ml of 0.05 M HNO_3. The dip-coat process was performed at room temperature in a laminar flow cupboard (Interflow, quality class 100) to minimize dust contamination. The substrate speed was 10 mm·s^{-1} and the dip-time was 25 seconds. The membranes were dried in a climate chamber

(Espec 100) at 40ºC and 60 RH% for at least 120 minutes. After drying, the membranes were sintered at 600ºC for 180 minutes (heating rate 1ºC·min^{-1}). The procedure for dipping, drying and sintering was repeated three times in order to obtain defect-free intermediate γ-Al_2O_3 membranes.

Silica separation layer preparation

The intermediate γ-Al_2O_3 layers were modified by dip-coating with a polymeric silica sol, prepared via acid catalysed hydrolysis and subsequent polycondensation of tetraethylorthosilicate (TEOS) (Aldrich, >99 %). The polymeric silica solution was prepared by drop-wise addition of water and HNO_3 to a TEOS/ethanol solution under vigorous stirring (water/TEOS/acid/ethanol: 6.4/1/0.085/3.8) and refluxing at 60°C for 180 minutes. The resulting solution was diluted 18-fold with ethanol. Dip-coating was performed in a laminar flow cupboard (Interflow, quality class 100). After dip-coating (substrate speed 10 mm·s^{-1}, dip-time 5 seconds) the membranes were dried for 30 minutes at 40°C and 60 RH%. After drying, the membranes were sintered at 350-600°C for 180 minutes (heating rate 0.5ºC·min^{-1}).

4.3.2 Membrane characterisation

The thickness and morphology of the different layers were studied by Scanning Electron Microscopy (SEM) using a JEOL 840 microscope. Samples were sputtered with a thin layer of gold. Independently, the thickness of the silica layers was determined by Secondary Neutral Mass Spectrometry (SNMS).

4.3.3 Gas permeation

Single gas permeance of one single fibre was measured in a pressure controlled dead-end set-up. Viton O-rings were used for sealing, limiting the temperature to 210°C. The effective membrane length was 17 cm leading to an effective membrane area of 0.0017 m^2. Prior to measurements, the membranes were pre-treated by permeating He at 180°C for two days. Measurements were performed with He and N_2 (>99% pure) at temperatures from 25°C to 200°C. The pressure at the permeate side was kept slightly above ambient pressure, while the pressure at the feed side was varied in the range 150 - 350 kPa. The flow required to maintain the pressure drop over the membrane was measured by a mass flow indicator.

4.3.4 Pervaporation

The organic solvent used in dehydration experiments was *1*-butanol (pro-analyse, Merck). Activity coefficients of water and *1*-butanol were approximated using the Wilson equation [Gmehling and Onken, 1977]. Vapour pressures were calculated using the Antoine equation [Gmehling and Onken, 1977]. The recommended values from the Dechema Data Series were used.

A common set-up was used for pervaporation [Verkerk *et al.*, 2001]. On the permeate side a vacuum was maintained (10 mbar) by a cascade of a liquid nitrogen cold trap and a vacuum pump. In the dehydration of *1*-butanol the feed was supplied to the membrane by simply submerging the membrane in a large vessel of *1*-butanol/water. Vigorous stirring (3 pitched-blade stirrers mounted on a single axis, Ø=5 cm, 1300 rpm) of the bulk mixture was used to avoid polarisation effects on the outside of the membrane. Due to safety regulations the experiments were stopped overnight, during which time the membranes remained in the feed liquid without vacuum applied on the permeate side (*1*-butanol at room temperature). Subsequent start of an experiment was preceded by a stabilisation period of one hour, during which vacuum was applied on the permeate side. The retentate was analysed using Karl-Fischer (Mettler Toledo DL50 Graphix), while the permeate composition was analysed using gas chromatography.

4.4 Results

4.4.1 Membrane characterisation

The SNMS depth profile of the silica membrane (Figure 4.1) shows a monotonous decrease in Si concentration from the membrane surface (0 nm) towards the intermediate γ-Al_2O_3 layer. Correspondingly, the Al concentration increases with depth and at approximately 20 nm reaches a practically constant value. The crossover point is at 5 nm. The SNMS profiles indicate that the silica layer on top of the γ-Al_2O_3 layer has a thickness of at least 20 nm, which is in reasonable agreement with the thickness determined by SEM (20-60 nm). The gradual decrease in Si concentration with depth may be due to the surface roughness of the γ-Al_2O_3 and partial penetration of silica into this layer. In Figure 4.2 SEM pictures of a hollow fibre substrate (Figure 4.2a), coated with intermediate γ-Al_2O_3 layers (Figure 4.2b), and coated with silica (Figure 4.2c) are shown. Figure 4.2b clearly shows that the four γ-Al_2O_3 layers form a single 3-4 μm thick homogeneous layer on the substrate, providing a sufficiently smooth surface for silica to be deposited on. For thinner intermediate layers the preparation of defect free silica layer appeared unsuccessful. The particle size in the intermediate layer is in the range 30-80 nm (Figure 4.2c), which is comparable to the thickness of the silica layer (20-60 nm).

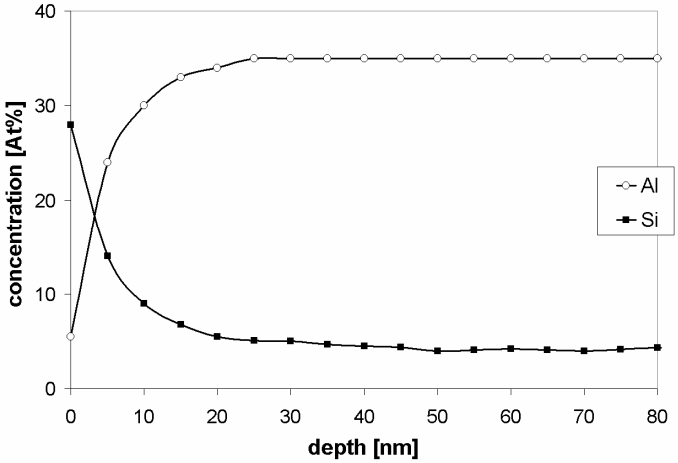

Figure 4.1 SNMS depth profile of a silica membrane from batch TNO-3.

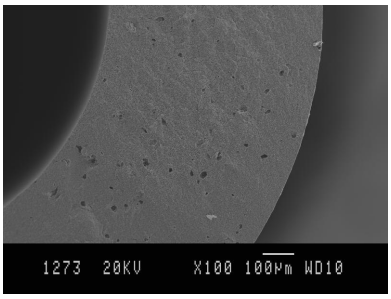

a) Substrate cross-sections (magnification 100x).

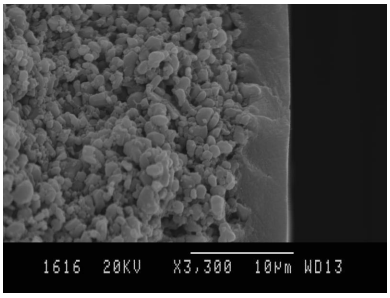

b) Cross-section intermediate γ-Al_2O_3 layers on top of substrate (magnification 3.300x).

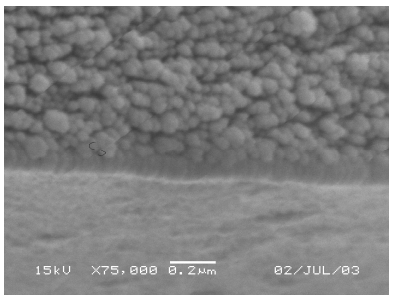

γ-Al_2O_3 intermediate layer

SiO_2 layer

c) Cross-section silica membrane on the intermediate γ-Al_2O_3 layers (magnification 75.000x)

Figure 4.2 SEM micrographs of the various layers constituting the membrane.

4.4.2 Gas permeation

Single gas permeation has been performed using helium and nitrogen at different trans-membrane pressure and temperatures. For both gases the permeance appears to be independent of pressure. At a temperature of 200°C the helium and nitrogen flux are $2.2 \cdot 10^{-6}$ mol·m^{-2}·s^{-1}·Pa^{-1} and $4.0 \cdot 10^{-9}$ mol·m^{-2}·s^{-1}·Pa^{-1}, respectively. The high helium permeance and the high permselectivity of this gas with respect to the larger nitrogen are typical for microporous silica membranes. The low permeance of nitrogen suggests that the pore size of the silica is similar to the molecular dimensions of N_2 (kinetic diameter 3.64 Å). Under the conditions applied, the contribution of the hollow fibre support to the total resistance for mass transport is smaller than 5%. Hence, the small dimensions of the substrate enable further improvement of the silica layer without the support resistance becoming significant [de Vos and Verweij, 1998b].

For both helium and nitrogen excellent linear fits of the Arrhenius plots are obtained (Figure 4.3), confirming that transport is thermally activated. The increase in helium permeance with temperature (apparent energy of activation -6.6 kJ·mol^{-1}) indicates that for this inert gas the temperature dependence of diffusion predominates that of sorption. For nitrogen a decrease in permeance is observed with temperature (apparent energy of activation 3.3 kJ·mol^{-1}). The less pronounced change with temperature indicates that for nitrogen the temperature dependence of sorption predominates that of diffusion, albeit only slightly.

Table 4.1 contains permeance data for several batches silica membranes. Every batch of membranes consists of 20 membranes from which at least 5 membranes were tested. In total 42 membranes were tested out of which 35 show a helium/nitrogen permselectivity exceeding 150. High values are observed for the permeance of helium (1.1 - $2.9 \cdot 10^{-6}$ mol·m^{-2}·s^{-1}·Pa^{-1}, 200°C). Differences in helium/nitrogen permselectivity have both been found between the 7 batches likely due to differences in silica dip-coat solution and in one batch probably due to differences in substrate quality. The performance of the hollow fibres prepared in our study is comparable to that of the flat plate membranes described by De Vos and Verweij [1998b]. Nair *et al.* [2000] measured a helium permeance of approximately one order of magnitude lower ($2 \cdot 10^{-7}$ mol m^{-2} s^{-1} Pa^{-1}, 135°C), with a permselectivity of

1230, comparable to our results. The high permeance value can partly be attributed to the small contribution of support resistance.

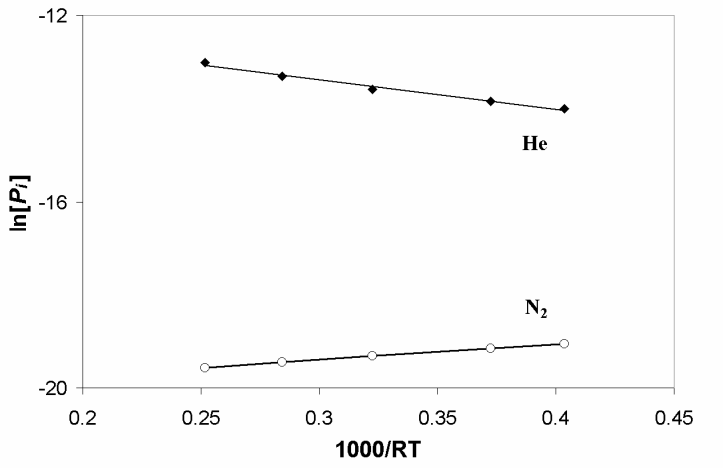

Figure 4.3 Arrhenius plots of helium and nitrogen permeance, trans-membrane pressure difference 100 kPa, membrane TNO-8a.

Table 4.1 Helium single gas permeance and He/N_2 permselectivities for several silica membranes, 200°C.

Membrane series code	P(He) [10^{-6} mol·m^{-2}·s^{-1}·Pa^{-1}]	P(N_2) [10^{-6} mol·m^{-2}·s^{-1}·Pa^{-1}]	Permselectivity He/N_2
TNO-3	0.85	0.003	290
TNO-4	1.51	0.002	760
TNO-5	2.07	0.022	100
TNO-6	1.51	0.003	510
TNO-7	1.86	0.002	940
TNO-8	2.20	0.004	560
TNO-9	1.86	0.010	190

4.4.3 Pervaporation

Dehydration of *1*-butanol

Dehydration of *1*-butanol has been carried out using several silica membranes and their performance is summarized in Table 4.2. Typical values for the initial water flux and selectivity are in the range of 2-3 $kg \cdot m^{-2} \cdot h^{-1}$ and 500-1200, respectively.

Table 4.2 Pervaporation performance of various membranes in the dehydration of *1*-butanol, 80°C, 5 wt.% water.

Membrane code	N_0	N_t	P_0	P_t	α_0	α_t	t_{pr}
	[$kg \cdot m^{-2} \cdot h^{-1}$]		[$kg \cdot m^{-2} \cdot h^{-1} \cdot bar^{-1}$]		[-]		[h]
TNO-3a	2.92	1.31	11.1	5.28	1200	900	55
TNO-3b	2.53	1.82	9.94	7.32	500	500	14
TNO-5a	2.05	0.82	8.20	3.22	200	150	70
TNO-5b	3.04	1.11	12.1	4.54	1000	500	30
TNO-7a	2.23	0.76	9.17	3.03	900	300	40

Figure 4.4 shows typical data for the water permeance and selectivity as a function of time (80ºC, 5 wt.% water). Clearly, the water permeance decreases with time. The selectivity also appears to decrease with time, although this effect is less apparent and notably influenced by the overnight stops of the measurement.

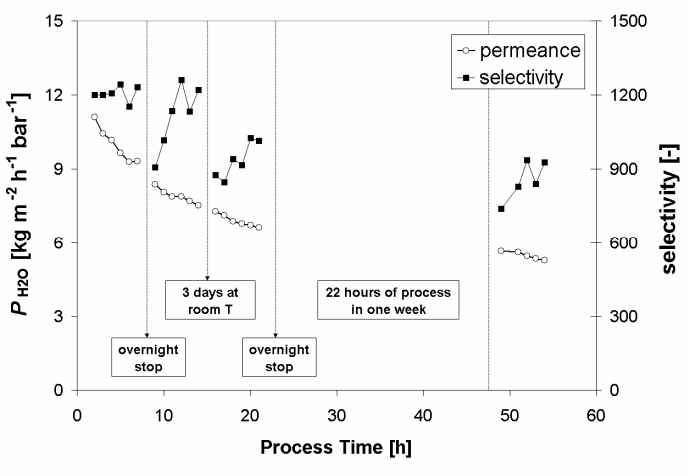

Figure 4.4 Water permeance and selectivity in the dehydration of *1*-butanol as a function of time, T = 80°C, 5 wt.% water, membrane TNO-3a.

The observed decline in permeance with time is likely due to interactions of water and alcohol with the silica material, *i.e.*, adsorption on and reaction with hydroxyl groups on the silica surface. Reaction of the *1*-butanol with these hydroxyl groups would render the silica more hydrophobic. This would be advantageous for the solvent flux, while it would induce a decrease in water flux. Reactions of *1*-butanol with the supporting alumina layers may enhance this effect [Dafinov *et al.*, 2002]. Possibly, reactions between water and silica could lead to a reduction in the surface energy associated with the excess surface area of the pores, resulting in a densification of the material accompanied by an increase of the pore size. Again, the result would be a decrease in performance.

A decline in flux with time has also been observed by others. Van Veen *et al.* [van Veen *et al.*, 2001] measured the performance of a silica membrane in the dehydration of IPA over a period of 73 days (80°C, 4.5 wt.% water). They found that after an initial decrease of both the water and the alcohol flux the process stabilized (water flux 1.9 $kg \cdot m^{-2} \cdot h^{-1}$, selectivity 1100). Similar behaviour was found by Sommer [Sommer, 2003]. Asaeda *et al.* [Asaeda *et al.*, 2002] investigated the performance of a SiO_2-ZrO_2 membrane in the dehydration of isopropyl alcohol (75°C, 10 wt.% water) and observed

a constant water permeance in time, accompanied by an increase in selectivity. They claim that the inherent hydrothermal stability of their composite material circumvents a substantial decline in the water flux and attribute the increase in selectivity to pore blocking by the alcohol.

Comparison with literature data

Table 4.3 gives an overview of pervaporation data presented in open literature, including the results of our study. Clearly, the performance of our hollow fibre silica ceramic membranes is comparable to that of tubular ceramic silica membranes. For the dehydration of *1*-butanol system the selectivity of the hollow fibre membranes is significantly higher compared to commercially available membranes [Gallego-Lizon *et al.*, 2002a; Gallego-Lizon *et al.*, 2002b; Sommer *et al.*, 2002] and comparable to that of membranes prepared by ECN [van Veen *et al.*, 2001; Verkerk *et al.*, 2001].

Table 4.3 Literature data for pervaporation performance of various silica membranes in the dehydration of various solvents.

Organic compound	Permeate pressure [mbar]	Water concentration [wt.%]	Feed temperature [°C]	Water flux [kg·m^{-2}·h^{-1}]	Process selectivity [-]	Type	Ref.
Ethanol		2	70	0.15	400	Home	Van Gemert, 1995
2-propanol		2	70	0.16	600	"	"
1-Butanol	10	5	70	2.3	680	ECN	Verkerk, 2001
IPA	10	5	70	2.1	600	"	"
1-Butanol	10	5	75	4.5	600	ECN	Van Veen, 2001
IPA	25	4.5	80	1.9	1150	"	"
Methanol	8-10	5	80	1.85*	20	PervaTech	ten Elshof, 2003
t-Butanol	8-10	10	60	3.5	144	SMS	Gallego-Lizon, 2002a
IPA	8-10	10	70	4	50-100	SMS	Gallego-Lizon, 2002b
IPA	20	5	80	1.4		SMS	Sommer, 2002
Butanol	<2	5	75	3.0	250	Home	Petrus-cuperus, 2002
2-Butanol		5	80	0.76	360	Home	Sekulic, 2002
1-Butanol	10	5	80	2.92-1.31	1200-900	TNO	This study

* total flux [kg·m^{-2}·h^{-1}]

4.5 Conclusions

Thin microporous silica membranes have been prepared on the outer surface of hollow fibre ceramic membrane substrates. The membranes were characterized using SEM, SNMS, single gas permeance and dehydration of *1*-butanol via pervaporation. The thickness of the silica on top of the intermediate γ-alumina layers is in the order of 20-60 nm. Gas permeance data suggest that the membranes are microporous, with a pore size close to the molecular dimensions of small molecules, and possess a small number of defects. Pervaporation performance in the dehydration of *1*-butanol was better compared to that of commercially availably tubular membranes, and comparable to that of membranes prepared by ECN.

Compared to tubular supports, ceramic hollow fibres are inexpensive and enable a high membrane surface area / module volume (> 1000 $m^2 \cdot m^{-3}$). Combined with the good performance of the hollow fibre membranes and the low support resistance this makes them interesting candidates for a variety of applications.

Nomenclature

C_i	concentration	[$mol \cdot m^{-3}$]
N	total flux	[$kg \cdot m^{-2} \cdot h^{-1}$]
N_i	flux of component *i*	[$kg \cdot m^{-2} \cdot h^{-1}$]
p	pressure	[Pa]
p_i^*	partial equilibrium vapour pressure	[Pa]
p_i^0	vapour pressure of pure component *i*	[Pa]
P_i	permeance	[$mol \cdot m^{-2} \cdot s^{-1} \cdot Pa^{-1}$] or [$kg \cdot m^{-2} \cdot h^{-1} \cdot bar^{-1}$]
T	temperature	[K]
*TNO-Y*x	membrane x from membrane series Y	[-]
x_i	molar fraction retentate	[$mol \cdot mol^{-1}$]
y_i	molar fraction permeate	[$mol \cdot mol^{-1}$]

	Greek letters	
α	separation factor	[-]
γ_i	activity coefficient	[-]
	Subscripts	
c	calcination	
i	component *i*	
j	component *j*	
0	initial	
p	permeate	
pr	process	
r	retentate	
t	final	

References

Asaeda, M., Sakou, Y., Yang, J., Shimasaki, K., Stability and performance of porous silica-zirconia composite membranes for pervaporation of aqueous organic solutions, *J. Membr. Sci.*, 209 (2002) 163-175.

Barrer, R.M., Activated diffusion in membranes, *Trans. Faraday Soc.*, 35 (1939) 644-656.

van den Broeke, L.J.P., Bakker, W.J.W., Kapteijn, F., Moulijn, J.A., Binary permeation through a silicalite-1 membrane, *AIChE J.*, 45 (1999) 976-985.

Dafinov, A., Garcia-Valls, R., Font, J., Modification of ceramic membranes by alcohol adsorption, *J. Membr. Sci.*, 196 (2002) 69-77.

ten Elshof, J.E., Abadal, C.R., Sekulic, J., Chowdhury, S.R., Blank, D.H.A., Transport mechanisms of water and organic solvents through microporous silica in the pervaporation of binary liquids, *Micr. Meso. Mater.*, 65 (2003) 197-208.

Gallego-Lizon, T., Edwards, E., Lobiundo, G., Freitas dos Santos, L., Dehydration of water/t-butanol mixtures by pervaporation: comparative study of commercially available polymeric, microporous silica and zeolite membranes, *J. Membr. Sci.*, 197 (2002) 309-319.

Gallego-Lizon, T., Ho, Y.S., Freitas dos Santos, L., Comparative study of commercially available polymeric and microporous silica membranes for the dehydration of IPA/water mixtures by pervaporation/vapour permeation, *Desalination*, 149 (2002) 3-8.

van Gemert, R.W., Petrus-Cuperus, F., Newly developed ceramic membranes for dehydration and separation of organic mixtures by pervaporation, *J. Membr. Sci.*, 105 (1995) 287-291.

Gmehling, J., Onken, U., DeChema Chemistry Data Series. Vapor-Liquid Equilibrium Data Collection, Vol. 1, Pt. 1: Aqueous-Organic Systems, 1977.

Kaerger, J., Ruthven, D.M., Editors., Diffusion in zeolites and other microporous solids, Wiley, New York, 1992.

de Lange, R.S.A., Hekkink, J.H.A., Keizer, K., Burggraaf, A.J., Formation and characterization of supported microporous ceramic membranes prepared by sol-gel modification techniques, *J. Membr. Sci.*, 99 (1995) 57-75.

Nair, B.N., Keizer, K., Suematsu, H., Suma, Y., Kaneko, N., Ono, S., Okubo, T., Nakao, S.I., Synthesis of gas and vapor molecular sieving silica membranes and analysis of pore size and connectivity, *Langmuir*, 16 (2000) 4558-4562.

Petrus-Cuperus, F., van Gemert, R.W., Dehydration using ceramic silica pervaporation membranes - the influence of hydrodynamic conditions, *Sep. Purif. Technol.*, 27 (2002) 225-229.

Sekulic, J., Luiten, M.W.J., ten Elshof, J.E., Benes, N.E., Keizer, K., Microporous silica and doped silica membrane for alcohol dehydration by pervaporation, *Desalination*, 148 (2002) 19-23.

Sommer, S., Klinkhammer, B., Melin, T., Integrated system design for dewatering of solvents with microporous silica membranes, *Desalination*, 149 (2002) 15-21.

Sommer, S., Pervaporation and vapor permeation with microporous inorganic membranes, Thesis, RWTH, Aachen, 2003.

Uhlhorn, R.J.R., Keizer, K., Burggraaf, A.J., Gas transport and separation with ceramic membranes. Part II. Synthesis and separation properties of microporous membranes, *J. Membr. Sci.*, 66 (1992) 271-287.

van Veen, H.M., van Delft, Y.C., Engelen, C.W.R., Pex, P.P.A.C., Dewatering of organics by pervaporation with silica membranes, *Sep. Purif. Technol.*, 22 and 23 (2001) 361-366.

Verkerk, A.W., van Male, P., Vorstman, M.A.G., Keurentjes, J.T.F., Properties of high flux ceramic pervaporation membranes for dehydration of alcohol/water mixtures, *Sep. Purif. Technol.*, 22 and 23 (2001) 689-695.

de Vos, R.M., Verweij, H., Improved performance of silica membranes for gas separation, *J. Membr. Sci.*, 143 (1998) 37-51.

de Vos, R.M., Verweij, H., High-selectivity, high-flux silica membranes for gas separation, *Science*, 279 (1998) 1710-1711.

Wynn, N., Dehydration with silica pervaporation membranes, *Mem. Techn.*, 2001 (2001) 10-11.

Chapter 5

Thin high flux ceramic-supported PVA membranes

Thin, high-flux and highly selective cross-linked poly(vinyl)alcohol water selective layers have been prepared on top of hollow fibre ceramic supports. The supports consist of an α-Al_2O_3 hollow fibre substrate and an intermediate γ-Al_2O_3 layer, which provides a sufficiently smooth surface for the deposition of ultra-thin PVA layers. Membranes have been characterised by SEM and pervaporation experiments. The thickness of the PVA layer formed on top of the γ-Al_2O_3 intermediate layer is in the order of 0.3-0.8 μm. In the dehydration of *1*-butanol (80°C, 5 wt.% water) the membranes exhibit a high water flux (0.8 - 2.6 $kg \cdot m^{-2} \cdot h^{-1}$), combined with a high separation factor (500 - 10.000). In the dehydration of *2*-propanol and *1*-butanol, a simultaneous increase in both water flux and separation factor is observed with increasing temperature or water concentration. This remarkable behaviour is in contrast to the trade-off generally observed for polymer membranes, *i.e.*, an increase in flux is typically combined with a decrease in separation factor. A possible explanation for this behaviour is a low degree of three dimensional swelling in the vicinity of the γ-Al_2O_3 - PVA interface due to an enhanced structural stability.

This chapter is partially based on: Peters, T.A., Poeth, C.H.S., Benes, N.E., Buijs, H.C.W.M., Vercauteren F.F., Keurentjes, J.T.F., *Ceramic-supported thin PVA pervaporation membranes combining high flux and high selectivity; contradicting the flux-selectivity paradigm*, J. Membr. Sci., (2006) accepted.

5.1 Introduction

Pervaporation is a promising process for separating azeotropic mixtures, close-boiling mixtures, and for the dehydration of temperature-sensitive products. In the development of high-flux membranes, much effort has been made to change the membrane structure from a dense thick film to an asymmetric or composite structure, in order to reduce the effective thickness of the membrane. However, the reduction in thickness is typically accompanied by a decrease in selectivity, due to a higher number of defects. Hence, to what extent the layer thickness can be decreased is limited by various aspects, including the pore size, porosity and surface roughness of the membrane support [Rezac and Koros, 1992].

In this article we report the synthesis of thin high-flux and highly selective cross-linked poly(vinyl)alcohol (PVA) water selective layers on top of an α-Al_2O_3 hollow fibre substrate. Intermediate γ-Al_2O_3 layers have been prepared on top of the substrates in order to provide a sufficiently smooth surface for the ultra-thin PVA layer. Compared to polymeric supports, ceramic supports exhibit a high surface porosity, and superior structural stability, *e.g.*, no swelling and compaction, while introducing negligible transport resistance [Rezac and Koros, 1992; Song and Hong, 1997; Yoshida and Cohen, 1997]. In principle the preparation method described in this paper enables relatively fast and inexpensive production of large membrane surface areas, combined with a high membrane surface area / module volume ratio (> 1000 $m^2 \cdot m^{-3}$). The membranes have been analysed by SEM and the pervaporation performance has been determined for the dehydration of various aqueous alcohol mixtures as a function of both temperature and feed water concentration.

5.2 Experimental

5.2.1 Membrane preparation

Ceramic hollow fibre membrane supports (α-Al_2O_3) were used (CEPAration, the Netherlands) with a porosity of ~30%, a pore diameter of 300 nm, a length in the range of 20-30 cm, and an inner and outer diameter of 2.0 and 3.0 mm, respectively. On the outside of these fibres, mesoporous γ-Al_2O_3 layers were prepared by four times sequential dip-coating with a

boehmite coating solution [Peters *et al.*, 2005]. In order to minimise the amount of imperfections in the intermediate γ-Al_2O_3 layer, the layer is prepared in a clean-room environment. The intermediate γ-Al_2O_3 layers were modified by dip-coating in a 0.75 wt.% PVA (Mowiol 56/98, Clariant) solution. The weight average molar mass of the PVA used is 195 kg·mol^{-1}, corresponding to a weight average degree of polymerisation of 4300. The degree of hydrolysis is 98.4%. Maleic anhydride (MA) was used as cross-linking agent in a concentration of 0.05 mol MA per mol of PVA. The membranes were dried at 55°C for 30 min and cured at 130°C for 1 hour.

5.2.2 Membrane characterisation

Scanning Electron Microscopy (SEM)

The thickness of the various layers and the nature of the surface were determined by Scanning Electron Microscopy (SEM) using a JEOL 5600 apparatus. The samples were sputtered with a thin layer of gold prior to analysis. Post-process analysis was performed with a SEM (Philips XL30 FEG-ESEM) equipped with an Energy Dispersive X-ray Analysis device. The EDX-samples were sputtered with a thin layer of carbon (Emitech K575X).

Pervaporation

Dehydration experiments of ethanol, *1*-propanol, *2*-propanol and *1*-butanol (pro-analyse, Merck, Darmstadt, Germany) were carried out in a common pervaporation set-up [Verkerk *et al.*, 2001] at temperatures between 50 and 90°C, and a feed water concentration between 2.5 and 19 wt.%. At the permeate side a vacuum was maintained (10 mbar) by a cascade of a liquid nitrogen cold trap and a vacuum pump. The feed was supplied to the membrane by simply submerging the membrane in a large vessel containing an alcohol/water mixture. Sufficient stirring (3 pitched-blade stirrers mounted on a single axis, 1300 rpm) of the bulk mixture was used to avoid polarisation effects at the outside of the membrane. A further increase in stirrer speed did not result in an altered membrane performance. The retentate composition was analysed using Karl-Fischer titration, while the permeate composition was analysed using gas chromatography. The performance of a membrane is usually expressed in terms of the water flux and separation factor α. The latter is defined as:

$$\alpha = \frac{y_{H2O} / x_{H2O}}{y_j / x_j} \tag{5.1}$$

where y and x are the molar fractions in the permeate and retentate, respectively. Permeance is defined as the flux divided by the partial pressure difference over the membrane. The equilibrium vapour pressure of component i at the retentate side is related to the mole fraction x and activity coefficient γ in the liquid mixture

$$p_i^* = \gamma_i \cdot x_i \cdot p_i^0 \tag{5.2}$$

where p_i^0 is the vapour pressure of the pure component i. When the pressure at the permeate side is small compared to the equilibrium vapour pressure at the retentate side, permeance can be expressed as [Verkerk *et al.*, 2001]:

$$P_i = \frac{N_i}{\gamma_i \cdot x_i \cdot p_i^0} \tag{5.3}$$

Activity coefficients of water and alcohol were approximated using the Wilson equation. Vapour pressures were calculated using the Antoine equation. Recommended values from the Dechema Data Series were used [Gmehling and Onken, 1977].

5.3 Results

5.3.1 Membrane characterisation

A cross-section of the composite ceramic-supported PVA membrane is shown in Figure 5.1. The membrane consists of three layers; the hydrophilic PVA layer, intermediate γ-Al_2O_3 layers and an α-Al_2O_3 hollow fibre substrate.

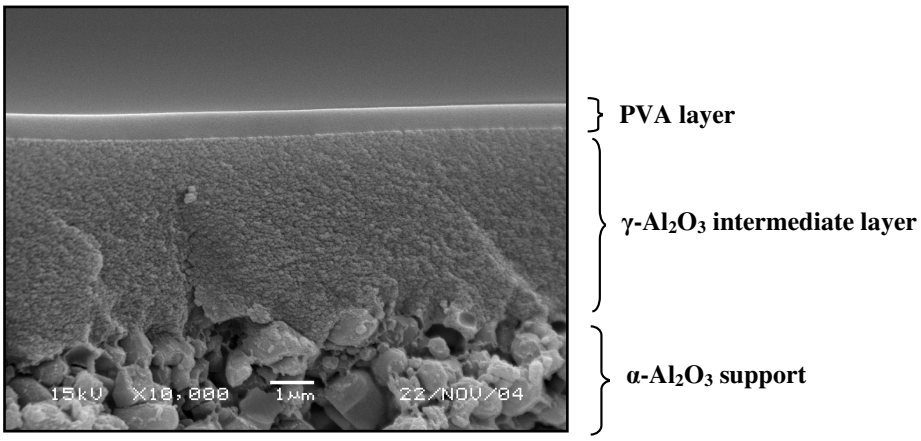

Figure 5.1 SEM-picture of cross-section of the PVA water selective layer on the intermediate γ-Al_2O_3 layers (magnification 10.000x).

From Figure 5.1 it can be seen that the four γ-Al_2O_3 intermediate layers form a single 3-4 μm thick layer on the substrate providing a smooth surface for the PVA layer. A 0.3 - 0.8 μm thick PVA layer is formed on top of the γ-Al_2O_3 intermediate layer. Clearly, the presence of the intermediate layer enables the formation of a defect-free thin selective layer. Furthermore, the small pore-size of the intermediate layer circumvents significant infiltration of PVA into the ceramic support, as can be expected from the large hydrodynamic radius of the PVA. An estimation of the hydrodynamic radius of polymer coils is given by the Flory radius, $R_F = N^{0.6} \cdot a$ [Yoshida and Cohen, 1997], where N is the number of monomer units per chain, and a is the monomer size. Using an estimated monomer size of 0.37 nm, the Flory radius of the PVA used is calculated to be 56 nm, which is clearly larger than the 4 nm intermediate layer pore size.

5.3.2 Pervaporation

5.3.2.1 Membrane separation capability

The pervaporation performance of the membranes has been determined for the dehydration of *1*-butanol. Figure 5.2 shows a typical behaviour of the water flux and selectivity in time observed for a fresh membrane. From this figure it is apparent that after a period of three days, in which the water flux decreases, both water flux and selectivity are stable.

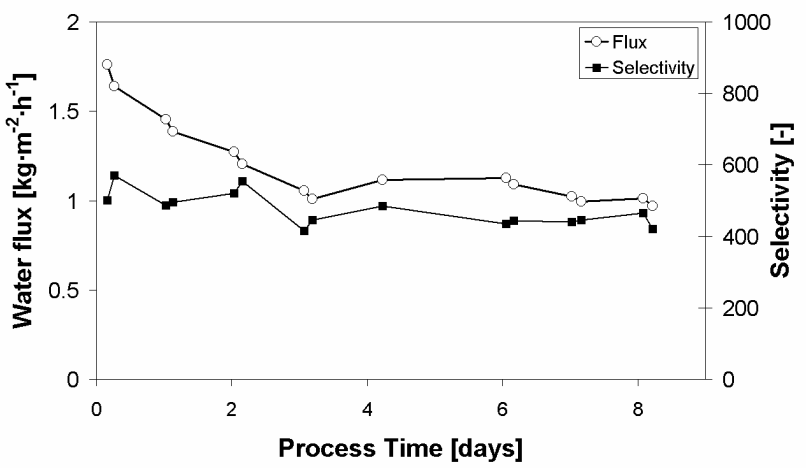

Figure 5.2 Dehydration of 94.5 (± 0.5) wt.% *1*-butanol, influence of process time, T = 80°C, Membrane TNO-PVA-4a.

The performance of various membranes prepared using the same procedure is summarized in Table 5.1. The data given in Table 5.1 indicate that all composite membranes prepared show a high flux and a high separation factor indicating that the preparation method is reproducible. The best performance was observed for membrane TNO-PVA-3, having a water flux and separation factor of 2.39 $kg \cdot m^{-2} \cdot h^{-1}$ and 6300, respectively (80°C, 5 wt.% water).

Table 5.1 Separation performance of various membranes measured. Dehydration of 95 (± 0.5) wt.% *1*-butanol, T = 80°C.

Membrane code	N_0	N_t	α_0	α_t	t_{pr}
	[kg·m^{-2}·h^{-1}]		[-]		[h]
PVA-1a	1.78	1.4	1050	1040	40
PVA-2a	1.43	1.29	>10.000	>10.000	20
PVA-2b	0.79	0.74	1500	1400	10
PVA-2c	1.92	1.29	4000	3700	35
PVA-3a	2.66	2.39	8600	6300	25
PVA-4a	1.76	0.97	500	460	200

The flux values obtained in this study for the dehydration of *1*-butanol are substantially higher compared with values presented in literature in the dehydration of similar compounds by polymer-supported PVA membranes, see Table 5.2. It should be noted that comparison of the various selectivity data is complicated by the fact that different alcohols are used. However, for the dehydration of alcohols using cross-linked PVA membranes, generally an increase in separation factor in the following order is found: MeOH << EtOH < PrOH < BuOH << *i*-PrOH < *t*-BuOH [Burshe *et al.*, 1997]. Hence, from comparison of the data presented in Table 5.2 it is apparent that, in the dehydration of alcohols, the performance of our ceramic-supported PVA membranes is superior compared to the performance of polymer-supported PVA membranes. The ceramic-supported PVA membranes prepared in this study, show a similar performance as "state-of-the-art" silica [Peters *et al.*, 2005; Cuperus and van Gemert, 2002; van Veen *et al.*, 2001; Verkerk *et al.*, 2001] and zeolite membranes [Gallego-Lizon *et al.*, 2002; Morigami *et al.*, 2001], see Table 5.3. However, the relatively simple fabrication method for the ceramic-supported PVA membranes described in this article, as compared to ceramic silica and zeolite membranes enables relatively rapid and inexpensive preparation of a large membrane surface area. An additional advantage of the ceramic-supported PVA membranes is the possible regeneration of the expensive ceramic support, *i.e.*, the organic layer can be

removed either by washing the membrane with an appropriate solvent, or by thermal treatment [Song and Hong, 1997]. In contrast, full ceramic membranes have to be replaced and disposed of after contamination or damage.

The combination of high fluxes and high selectivities, obtained in this study, requires a defect-free thin selective layer. However, the reduction in selective layer thickness is accompanied by an increase in the possibility of selective layer defects that lead to a decrease in selectivity. In contrast to polymer supports, the intermediate γ-Al_2O_3 layer provides evidently a very smooth and rigid surface for deposition of an ultra-thin PVA layer for which a high selectivity is maintained. Additionally, the porosity of the alumina support is very high as compared to the porosity of conventional polymer support materials like PES, leading to a small contribution of the support to the overall transport resistance. Assuming Knudsen diffusion to be the pre-dominant transport mechanism in the support given the low pressure, the support contribution to the total resistance was calculated to be less than 20 %.

Additional dehydration experiments were performed to study the performance of the membranes as a function of temperature and feed water concentration using various alcohol/water mixtures. The membrane showing significant alcohol permeation (membrane TNO-PVA-4a) was selected for these experiments to be able to observe variations in permeate composition generated from the change in either temperature or feed water concentration.

Table 5.2 Literature data of pervaporation performance of various cross-linked PVA membranes in the dehydration of various solvents.

Organic compound	Support	Selective layer [µm]	Water concentration [wt.%]	Temperature [°C]	Water flux [kg·m^{-2}·h^{-1}]	Process selectivity [-]	Ref.
1-propanol	PAN	0.1*	5	60	0.15	90	Wesslein, 1990
2-propanol	PES	20	5	80	0.25	3800	Nam, 1999
1-butanol	PAN	0.1*	5	60	0.25	350	Schehlmann, 1995
t-butanol	PAN	0.1*	4.9	80	0.4	342	Gallego-Lizon, 2002
Ethylene -glycol	PES	2-5	17.5	80	0.38	231	Chen, 1996
1-butanol	PAN	0.1	5	80	0.7	180	Guo, 2004
1-butanol	inorganic	0.3-0.8	5	80	0.8-2.6	500->10.000	This study

* prepared by GFT/Sulzer, 0.1 µm thick PVA selective layer [Ho and Sirkar, 1992]

Table 5.3 Literature data of pervaporation performance of various silica and zeolite membranes in the dehydration of alcohols.

Organic compound	Permeate pressure [mbar]	Water concentration [wt.%]	Feed temperature [°C]	Water flux [$kg \cdot m^{-2} \cdot h^{-1}$]	Process selectivity [-]	Type	Ref.
1-butanol	10	5	80	2.92-1.31	1200-900	silica	Peters, 2005
1-butanol	10	5	70	2.3	680	silica	Verkerk, 2001
1-butanol	10	5	75	4.5	600	silica	Van Veen, 2001
1-butanol	< 2	5	75	3.0	250	silica	Cuperus, 2001
t-butanol	8-10	5.2	60	1.3	22.000	NaA	Gallego-Lizon, 2002
2-propanol	1.33	10	75	1.76	10.000	NaA	Morigami, 2001
1-butanol	10	5	80	0.8-2.6	500 ->10.000	PVA	This study

5.3.2.2 Effect of feed temperature on pervaporation

The temperature dependence of the pervaporation performance of membrane TNO-PVA-4a in the dehydration of ethanol, *1*-propanol, 2-propanol and *1*-butanol is investigated in the range 60 - 90°C. In Figure 5.3a-d, water flux and separation factor are depicted as a function of the feed temperature.

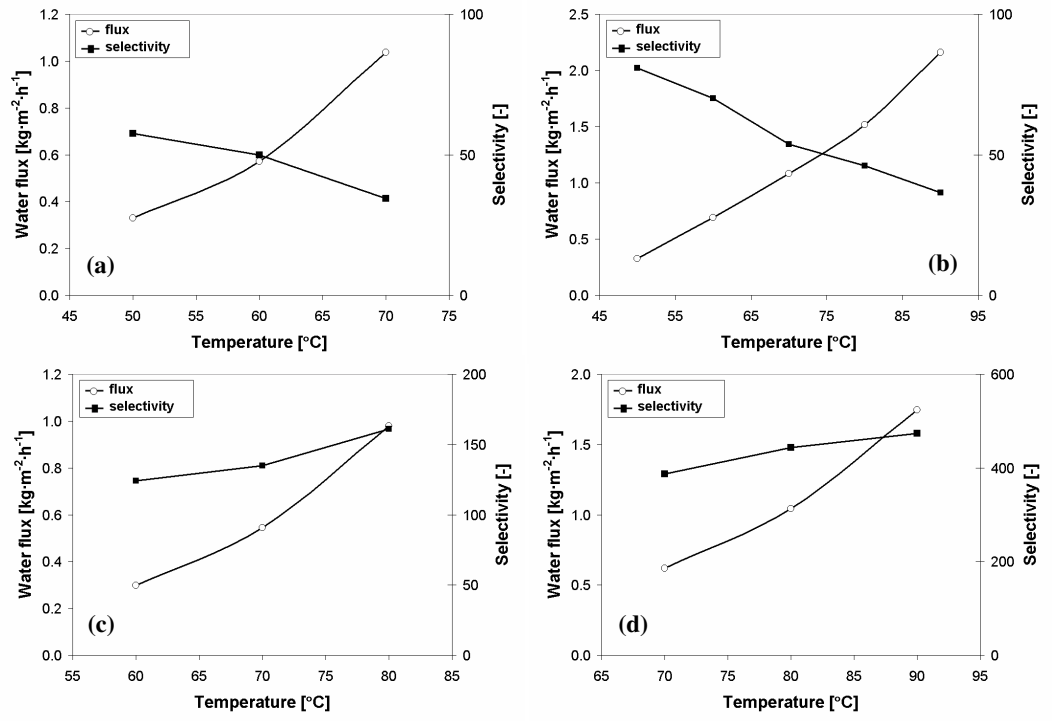

Figure 5.3 Water flux and selectivity in the dehydration of aqueous alcohol mixtures, influence of temperature, membrane TNO-PVA-4a. (a) ethanol, 10 wt.% water; (b) *1*-propanol, 5 wt.% water; (c) 2-propanol, 5 wt.% water; (d) *1*-butanol, 5 wt.% water.

Remarkably, both the water flux and the separation factor increase with increasing feed temperature in the case of *2*-propanol and *1*-butanol. Although this simultaneous increase has once been observed for a composite PAN/chitosan membrane [Wang *et al.*, 2000], it is opposite to the typical behaviour of polymer membranes [Guo *et al.*, 2004; Morigami *et al.*, 2001; Cuperus and van Gemert, 2002; Yoshida and Cohen, 1997]. Above the glass transition temperature of polymer membranes, an increase in flux with temperature is generally at the expense of selectivity due to swelling and plasticization of the membrane material [Yeom *et al.*, 2001]. From Figure 5.3a and b it is clear that in contrast to the dehydration of *2*-propanol and *1*-butanol, the traditional trade-off between an increase in flux and decrease in selectivity is observed for the dehydration of ethanol and *1*-propanol. To explain this behaviour, it is likely to assume that in our ceramic/polymer composites swelling and plasticization effects are less pronounced: an increase in temperature permits an increase in ethanol and *1*-propanol transport whereas the transport of *2*-propanol and *1*-butanol is still severely hindered.

An increase in both water flux and selectivity with temperature is generally observed for ceramic membranes, which do not show swelling, confirming the importance of membrane swelling on the flux/selectivity behaviour of the ceramic-supported PVA membrane with temperature. Consistent with the trend for ceramic membranes [Verkerk *et al.*, 2001], an increase in separation factor in the following order is found: EtOH < *1*-PrOH < *2*-PrOH < *1*-BuOH. This is in contrast to the order normally found for the dehydration of alcohols using cross-linked PVA membranes in which the selectivity observed for *2*-PrOH is much higher than for *1*-BuOH [Burshe *et al.*, 1997]. More insight in the dehydration behaviour can be revealed when plotting water and alcohol permeance as a function of temperature. In this way, the influence of the process conditions on the membrane performance is decoupled [Wijmans, 2003].

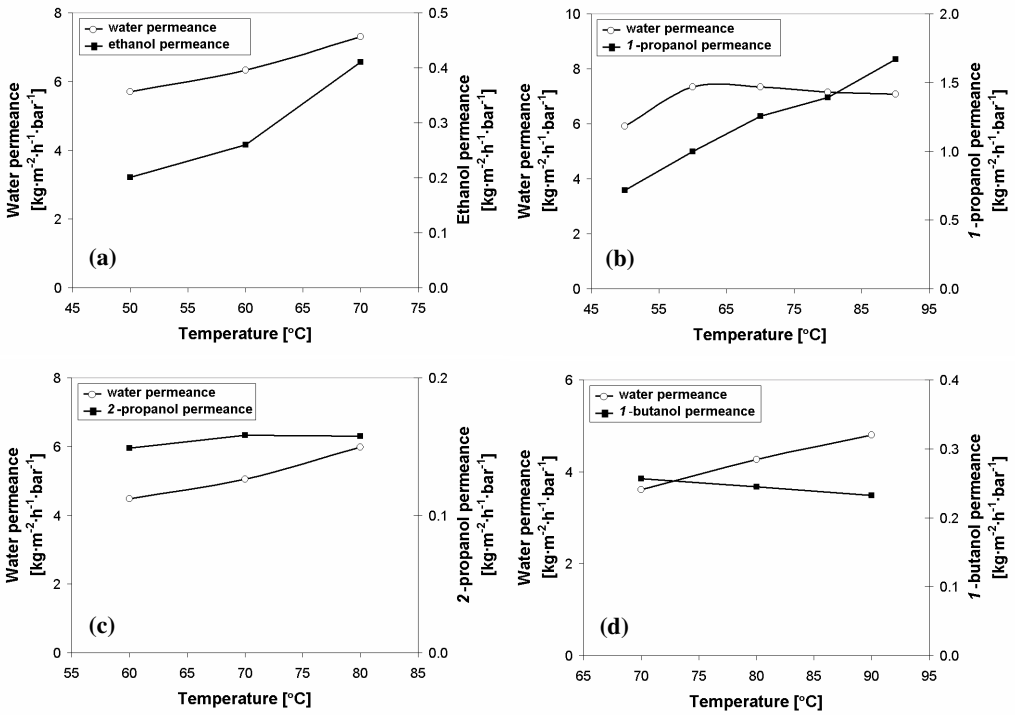

Figure 5.4 Water and alcohol permeance in the dehydration of aqueous alcohol mixtures, influence of temperature, membrane TNO-PVA-4a. (a) ethanol, 10 wt.% water; (b) *1*-propanol, 5 wt.% water; (c) *2*-propanol, 5 wt.% water; (d) *1*-butanol, 5 wt.% water.

From Figure 5.4a-d it can be seen that an increase in temperature results in an increase in water permeance for every alcohol/water system. This phenomenon may traditionally be explained by the increase in motion of the polymer chains and by the expansion of the free volume. In the dehydration of *1*-propanol, however, water permeance seems to be constant for temperatures higher than 50°C indicating a less pronounced effect of membrane swelling on the water transport at temperatures higher than 50°C. From Figure 5.4a-d it can be seen that the permeances of ethanol and *1*-propanol increase with temperature, whereas the *2*-propanol permeance remains nearly constant. The *1*-butanol permeance, however, decreases with an increase in temperature. In other words, the expansion of

the polymer chains and expansion of the free volume with temperature permits an increase in ethanol and *1*-propanol transport with an increase in temperature whereas the transport of *2*-propanol and *1*-butanol is still severely hindered. Similar to the water permeance, the first observation can be explained by the expansion of the polymer chains with an increase in temperature causing the ethanol and *1*-propanol transport to increase. For *2*-propanol and *1*-butanol, however, this means that the effect of the polymer chain expansion on the alcohol diffusivity has to be marginal. For *1*-butanol, this effect is completely cancelled out by the decrease in solubility in the membrane as illustrated by the decrease in permeance with an increase in temperature.

A plausible explanation for the different transport behaviour of the alcohols with an increase in temperature may be a severely limited swelling of the selective layer combined with the molecular cross-section of the alcohol [Huang and Jarvis, 1970]. Especially at the interface between the selective and the intermediate layer, the movement of PVA chains might be constrained because the surface of the intermediate layer is very smooth and contains pores roughly one order of magnitude smaller than the Flory radius of the PVA. For the alcohol with the largest molecular cross-section the influence of this effect on the alcohol permeance will be the largest leading to different transport behaviour.

5.3.2.3 Effect of feed water concentration on pervaporation

Dehydration experiments using various alcohols were performed at feed water concentrations ranging from 4.7 to 18.5 wt.%. In Figure 5.5a-d, water flux and separation factor are depicted as a function of the feed water concentration.

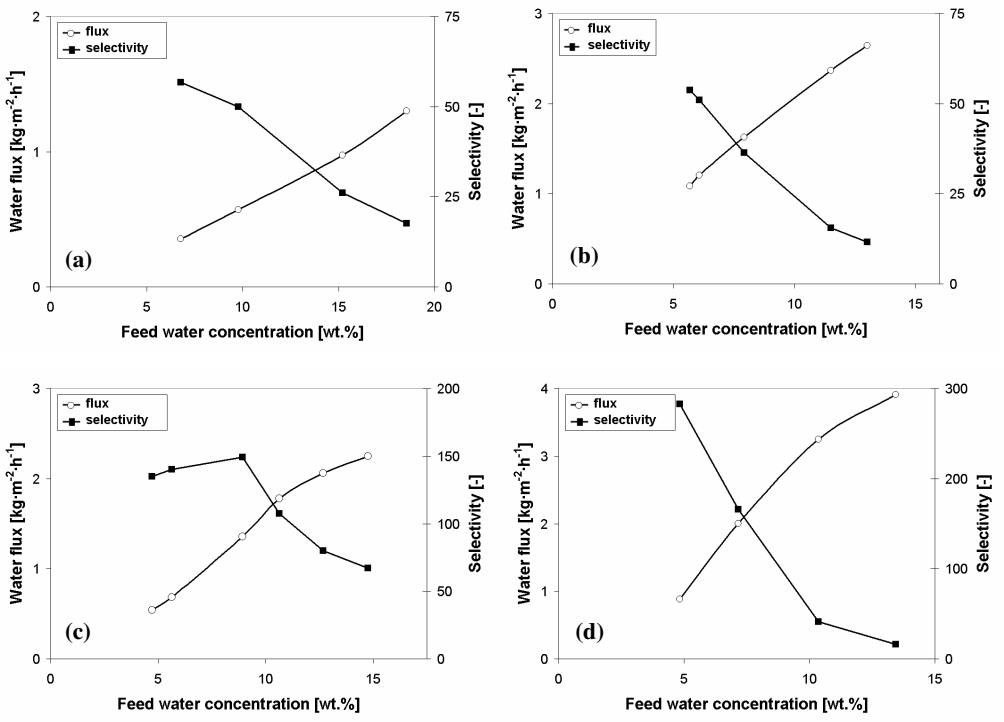

Figure 5.5 Water flux and selectivity in the dehydration of aqueous alcohol mixtures, influence of feed water concentration, membrane TNO-PVA-4a. (a) ethanol, $T = 60°C$; (b) *1*-propanol, $T = 70°C$; (c) *2*-propanol, $T = 70°C$; (d) *1*-butanol, $T = 70°C$.

From Figure 5.5a-d it can be seen that an increase in feed water concentration results in an increase in the water flux for every alcohol/water system. The relationship between water flux or permeance and feed water concentration can be explained by the interaction between the polymer molecules in the membrane and the permeating molecules

causing the membrane to swell. A higher feed water concentration corresponds to a larger extent of water sorption in, and consequently swelling of, the hydrophilic PVA layer. As a result, the mobility of the water in the PVA increases with water concentration causing the water flux to increase. For ethanol, *1*-propanol and *1*-butanol, the traditional trade-off between increased water flux and a decrease in selectivity is observed. The degree of swelling, due to the plasticizing effect of water on the polymer membrane, and the existence of a coupled transport can explain the increase in alcohol transport with an increase in feed water concentration [Guo *et al.*, 2004]. Most interestingly, in the dehydration of *2*-propanol, process selectivity increases with an increase in feed water concentration between 4 and 9 wt.% whereas it decreases at higher water concentrations. Possibly, the alcohol permeance through the membrane is greatly affected by the amount of water molecules in contact with the selective layer of the membrane at water concentrations higher than 9 wt.% causing the membrane to swell drastically. Consequently, more alcohol molecules can pass through the membrane and selectivity decreases. More insight in this behaviour can be revealed when plotting the water and alcohol permeance as a function of the feed water concentration. The results can be seen in Figure 5.6.

From Figure 5.6a-d it can be seen that an increase in feed water concentration results in an increase in the water and alcohol permeance for all alcohol/water systems. For *2*-propanol, however, the permeance seems to be constant up to a water concentration of 9 wt.% after which it increases at higher water concentrations. The marginal effect of the increase of feed water concentration (< 9 wt.%) on the alcohol permeance indicates that *2*-propanol remains severely hindered in spite off the partial plasticization of the membrane. However, the alcohol permeance increases at higher water concentrations, possibly due to swelling of the selective layer of the membrane. Also in the dehydration of *1*-butanol, the alcohol permeance suddenly increases at a feed water concentration higher than 9 wt.%.

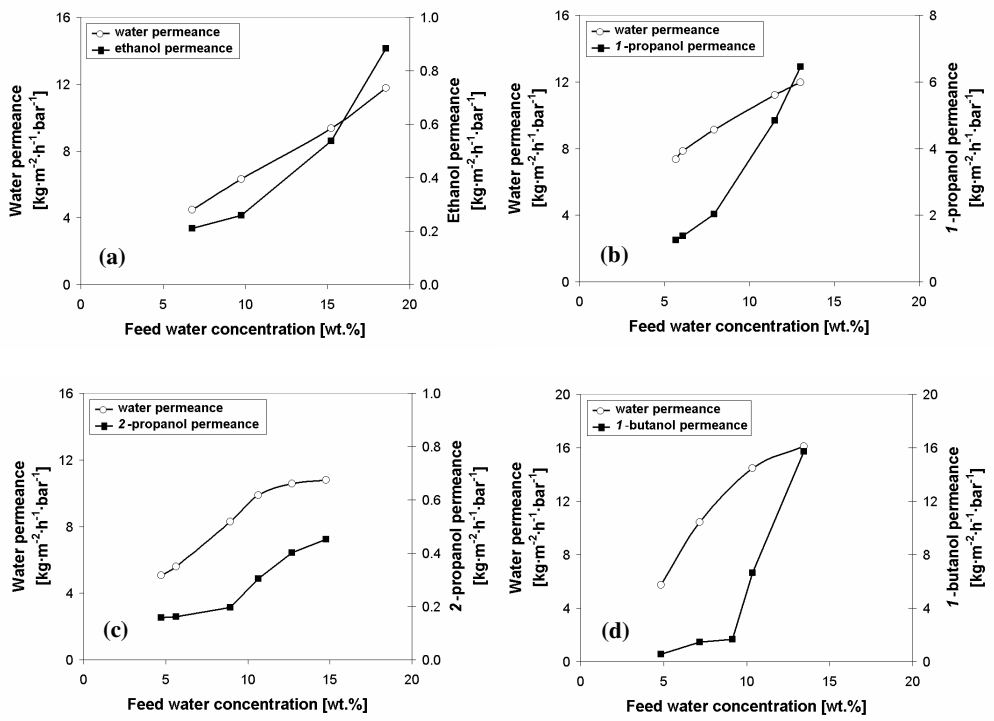

Figure 5.6 Water and alcohol permeance in the dehydration of aqueous alcohol mixtures, influence of feed water concentration, membrane TNO-PVA-4a. (a) ethanol, $T = 60°C$; (b) *1*-propanol, $T = 70°C$; (c) *2*-propanol, $T = 70°C$; (d) *1*-butanol, $T = 70°C$.

However, from Figure 5.6b and d it can clearly be seen that alcohol permeance in the dehydration of *1*-propanol and *1*-butanol is drastically higher as compared to the other alcohol permeance data. Taken into account that all measurements are performed using the same membrane over a period of four months and that the dehydration experiments of *1*-propanol and *1*-butanol are performed last, it is likely that the membrane performance is declined although the separation performance is still reasonable. Therefore, the dehydration experiments of *1*-butanol as a function of temperature and feed water concentration are repeated using membrane TNO-PVA-2b. The results can be seen in Figures 5.7 and 5.8. From these figures it can clearly be seen that for the dehydration of

1-butanol using membrane TNO-PVA-2b now also both water flux and separation factor increase with increasing feed water concentration.

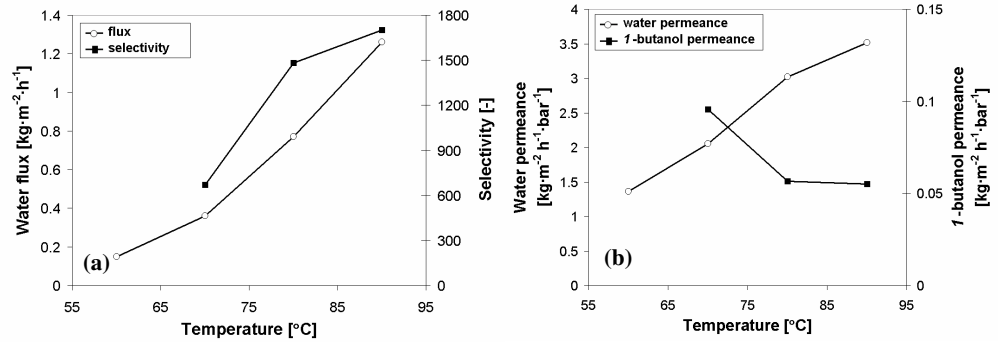

Figure 5.7 Dehydration of 94.5 (± 0.5) wt.% *1*-butanol, influence of retentate temperature, Membrane TNO-PVA-2b. (a) water flux and selectivity; (b) water and alcohol permeance.

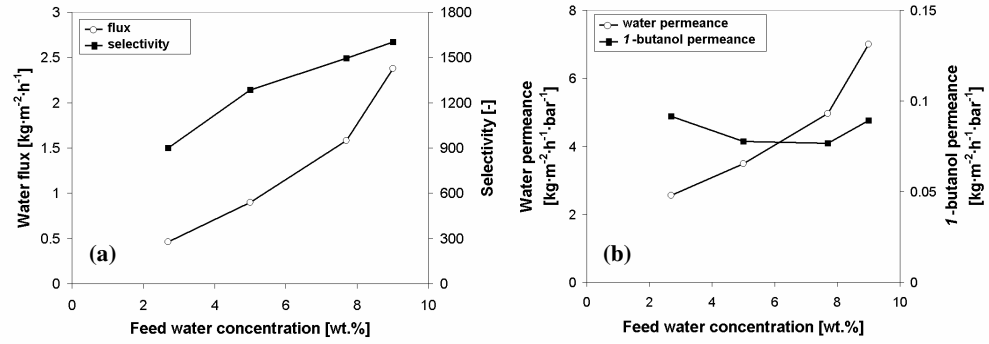

Figure 5.8 Dehydration of *1*-butanol, influence of feed water concentration, T = 80°C, membrane TNO-PVA-2b. (a) water flux and selectivity; (b) water and alcohol permeance.

5.3.2.4 Comparison of the dehydration of different alcohols

Water fluxes obtained in the dehydration of different alcohols as a function of temperature and feed water concentration can be compared as a function of the driving force over the membrane. Figure 5.9 shows the

water flux as a function of the driving force obtained at various temperatures and feed water concentrations for the dehydration of different alcohols.

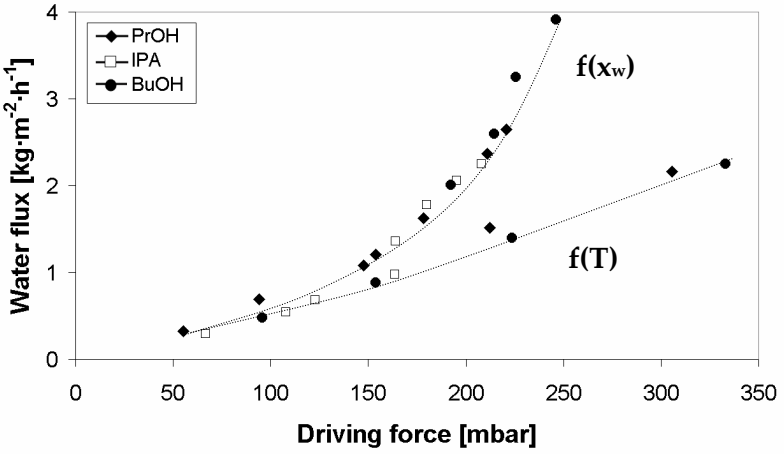

Figure 5.9 Dehydration of various alcohols, influence of driving force on the water flux as generated by either an increase in temperature or feed water concentration, membrane TNO-PVA-4a.

Given the congregation of the points in the figure, it is obvious that the transport of water through the membrane is not significantly affected by the type of alcohol that is used [Qiao *et al.*, 2005]. The water flux increases linearly with an increase in the driving force generated by an increase in temperature. For an increase in feed water concentration, however, the water flux increases exponentially with an increase in driving force. Thus, the swelling of the hydrophilic PVA membrane is more susceptible to an increase in water concentration compared to an increase in temperature due to the strong plasticising effect of water. This is also confirmed by the strong decrease in selectivity with an increase in feed water concentration as compared to the increase in feed temperature.

5.3.3 Membrane stability

5.3.3.1 Long-term stability

The long-term stability of the membrane has been examined over a period of six months in the dehydration of ethanol, *1*-propanol, *2*-propanol and *1*-butanol as described in the preceding paragraphs. Figure 5.10 shows the pervaporation performance of membrane TNO-PVA-4a in the dehydration of *1*-butanol in the beginning and at the end of the long-term performance study.

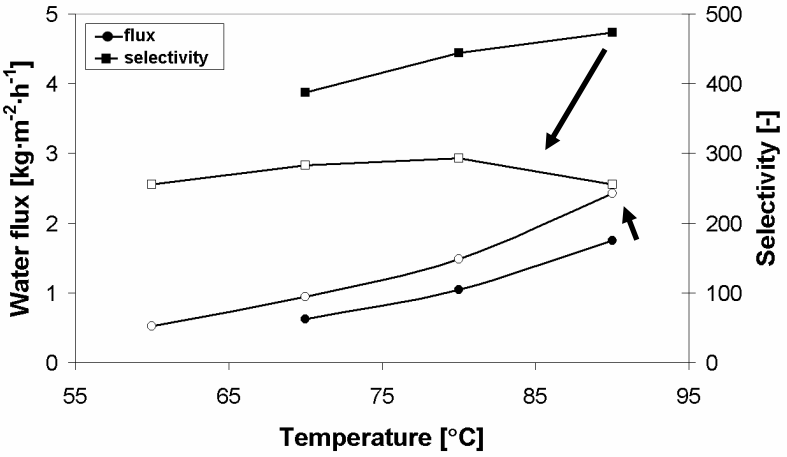

Figure 5.10 Dehydration of 94.5 (± 0.5) wt.% *1*-butanol, influence of process time, T = 80°C, membrane TNO-PVA-4a; closed symbols: fresh membrane; open symbols: after six months of operation.

From Figure 5.10 it can clearly be seen that the membrane performance is declined although the separation performance is still reasonable. Somewhat higher water fluxes have been obtained whereas the selectivity is substantially lower. Also the selectivity behaviour as a function of temperature is altered indicating a considerable increase in alcohol permeation. To investigate if the declined performance is caused by a decrease in the structural stability of the membrane layers, the separate layers have been investigated with SEM. Figure 5.11 and 5.12 show SEM pictures taken from the membrane after six months of operation.

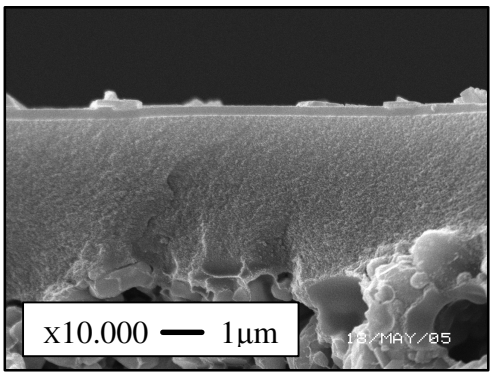

Figure 5.11 SEM-picture of the cross-section of the membrane showing the three separate membrane layers, membrane TNO-PVA-4a, pictures are taken after six months of operation.

It can be seen from Figure 5.11 that the three separate membrane layers have remained intact and are still strongly adhered to each other. This gives no indication that the decrease in performance is caused by defects in the membrane layers or a decreased adherence of the γ-Al_2O_3 - PVA boundary layer. Furthermore, no clear indication of the formation of meso-pores or other severe damage at the surface could be found. It is more likely that higher fluxes and permeances are caused by a decrease in cross-linking of the PVA-chains over time, due to removal of maleic acid.

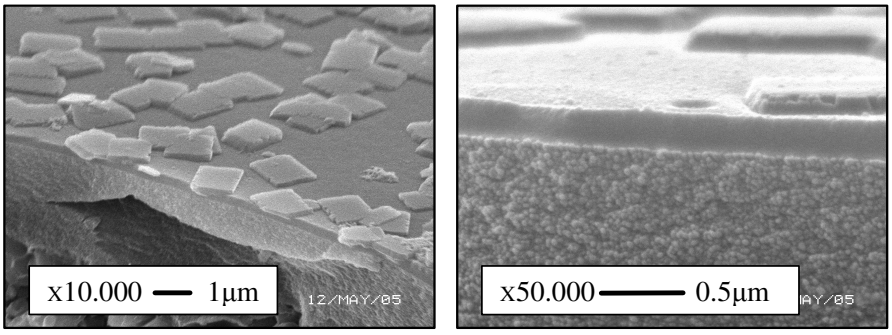

Figure 5.12 SEM-pictures of the cross-section of the PVA water selective layer on the intermediate γ-Al_2O_3 layers, membrane TNO-PVA-4a, pictures are taken after six months of operation.

From Figure 5.12 it can be seen that small crystalline contaminations are present on the membrane surface after six months of operation. The length and width of these contaminations are around 2 and 1 µm, respectively. The thickness is around 0.2 µm. EDX analysis indicates that the contaminations mainly consist of calcium carbonate, most likely originating from the water which is added to the alcohol/water mixture in order to keep the water concentration constant. Although demineralised water has been used, traces of salts are still present and, due to the large quantities of water that need to be added, it is likely that the salt concentration increases sufficiently to cause precipitation on top of the membrane. Campaniello *et al.* have also observed rectangular and egg-shaped white particles on top of the selective layer of a methylated silica membrane after pervaporation at elevated temperatures for 20 days [Campaniello *et al.*, 2004]. Although they have not analysed the composition of these contaminations, they were presumed to consist of dense silica originating from the silica layer.

5.3.3.2 Temperature stability

The thermal stability of the membrane has been examined in the dehydration of aqueous *1*-butanol at a temperature of 100°C. The water flux and selectivity as a function of the process time are shown in Figure 5.13.

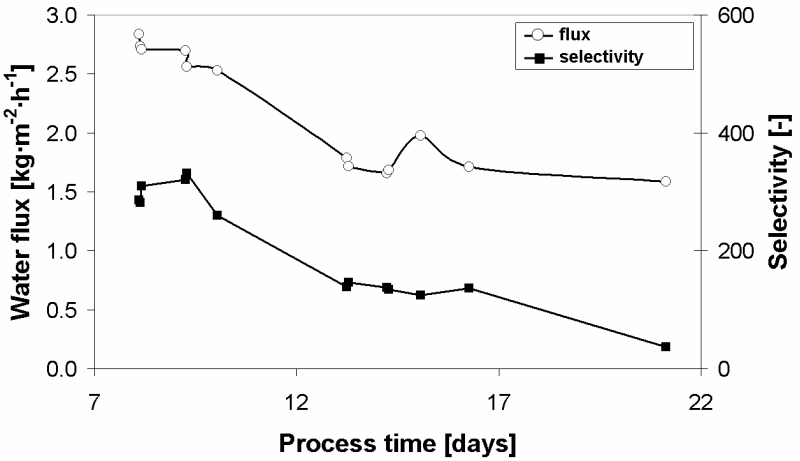

Figure 5.13 Dehydration of 94.5 (± 0.5) wt.% *1*-butanol, influence of process time, T = 100°C, membrane TNO-PVA-4b.

From Figure 5.13 it can clearly be seen that the membrane performance gradually decreases over a period of three weeks. As an example, the selectivity drops from a value of 300 to 25 in two weeks time. This in contrast to the behaviour observed at a temperature at 80°C, at which the membrane performance remains stable over a period of two weeks (see Figure 5.2). As a consequence, we conclude that the application window for these newly developed composite polymer/ceramic membranes is limited to 95°C.

5.3.3.3 Reversibility of the decrease in membrane performance

The reversibility of the decrease in membrane performance has been investigated by repeating the dehydration experiments as a function of temperature. These experiments have been performed subsequent to dehydration at 100°C, after membrane stabilisation at a temperature of 70°C. Figure 5.14 shows the initial performance membrane as a function of temperature together with the membrane performance obtained after pervaporation at 100°C.

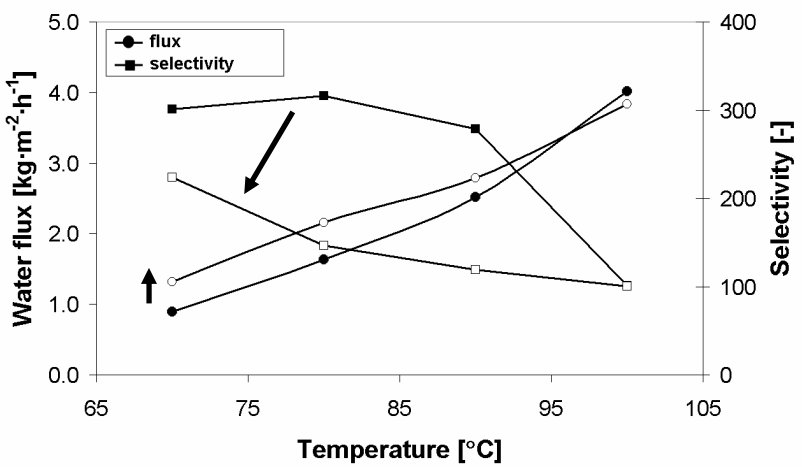

Figure 5.14 Dehydration of 95.0 (± 0.5) wt.% *1*-butanol, influence of temperature, membrane TNO-PVA-4c; closed symbols: fresh membrane; open symbols: after first temperature increase.

From Figure 5.14 it can be seen that the membrane performance is irreversibly declined after dehydration at 100°C. Slightly higher water fluxes have been obtained whereas the selectivity is substantially lower. Additionally, the simultaneous increase in both flux and selectivity at the increase in feed temperature from 70°C to 80°C is absent in the second dehydration experiments indicating an increase in alcohol permeation. This implies that the membrane has been irreversibly damaged probably due to a decrease of cross-linking of the polymer selective layer.

5.4 Conclusions

Thin high-flux and highly selective cross-linked PVA water selective layers has been prepared on top of an α-Al_2O_3 hollow fibre substrate. An intermediate γ-Al_2O_3 layer has been positioned on top of the substrates, in order to provide a surface sufficiently smooth for the ultra-thin PVA layer. Membranes have been analysed by SEM and pervaporation experiments. The thickness of the PVA top layer is in the order of 0.3 - 0.8 μm, and no substantial infiltration of PVA into the intermediate γ-Al_2O_3 layer is observed.

In the dehydration of *1*-butanol (80°C, 5 wt.% water) the membranes exhibit a high water flux (0.8 - 2.6 $kg \cdot m^{-2} \cdot h^{-1}$), combined with a high separation factor (500 - 10.000). The values for the flux and separation factor exceed typical values obtained for cross-linked PVA membranes on polymeric supports. With increasing temperature or feed water concentration, both flux and selectivity of the membrane in the dehydration of *2*-propanol and *1*-butanol increase simultaneously. This remarkable behaviour is in contrast to the trade-off generally observed for polymer membranes, *i.e.*, an increase in flux is typically combined with a decrease in separation factor. A possible explanation for this behaviour is a low degree of three dimensional swelling in the vicinity of the γ-Al_2O_3 - PVA interface. For the dehydration of ethanol and *1*-propanol the traditional trade-off between an increase in flux and a decrease in selectivity is observed.

The long-term and temperature stability of the membrane has been examined over a period of six months up to temperatures of 100°C. The membrane performance gradually decreases over a period of six months at

a temperature of 80°C. At a temperature of 100°C, the decline in performance is accelerated. SEM analysis gives no indication that the decrease in performance is caused by defects in the membrane layers or a decreased adherence of the γ-Al_2O_3 - PVA boundary layer. It is more likely that higher fluxes and permeances are caused by a decrease in cross-linking of the PVA-chains due to removal of maleic acid. As a consequence, we conclude that the application window for these newly developed composite polymer/ceramic membranes is limited to 95°C.

The performance of the composite hollow fibre membranes, combined with the possibility of simple support regeneration, makes them interesting candidates for a variety of applications. Additional studies are needed to assess whether the remarkable performance observed in this study is also observed for other combinations of selective polymer materials and mesoporous ceramic intermediate layers.

Acknowledgements

This work was performed in a cooperative project of the Centre for Separation Technology and was financially supported by TNO and NOVEM. We would like to thank Zeger Vroon from TNO-TPD for the preparation of the intermediate γ-Al_2O_3 support layers, and Niki Stroeks from TNO-IND for the preparation of the PVA selective layers.

Nomenclature

BuOH	butanol	
EtOH	ethanol	
MeOH	methanol	
N_i	flux of component *i*	[kg·m^{-2}·h^{-1}]
p_i^*	partial equilibrium vapour pressure [Pa]	
p_i^0	vapour pressure of pure component *i*	[Pa]
PrOH	propanol	
P_i	permeance of component *i*	[kg·m^{-2}·h^{-1}·bar^{-1}]

t	time	[h]
T	temperature	[°C]
x_i	molar fraction retentate	[mol·mol^{-1}]
y_i	molar fraction permeate	[mol·mol^{-1}]

Greek letters

α	separation factor	[-]
γ_i	activity coefficient	[-]

Subscripts

i	component i
0	initial
p	permeate
pr	process
r	retentate
t	final

References

Burshe, M.C., Sawant, S.B., Joshi, J.G., Pangarkar, V.G., Sorption and permeation of binary water-alcohol systems through PVA membranes crosslinked with multifunctional crosslinking agents, *Sep. Purif. Technol.*, 12 (1997) 145-156.

Campaniello, J., Engelen, C.W.R., Haije, W.G., Pex, P.P.A.C., Vente, J.F., Long-term pervaporation performance of microporous methylated silica membranes, *Chem. Commun.*, 7 (2004) 834-835.

Chen, F.R., Chen, H.F., Pervaporation separation of ethylene glycol-water mixtures using crosslinked PVA-PES composite membranes. Part I. Effects of membrane preparation conditions on pervaporation performances, *J. Membr. Sci.*, 109 (1996) 247-256.

Cuperus, F.P., van Gemert, R.W., Dehydration using ceramic silica pervaporation membranes - the influence of hydrodynamic conditions, *Sep. Purif. Technol.*, 27 (2002) 225-229.

Gallego-Lizon, T., Edwards, E., Lobiundo, G., Freitos dos Santos, L., Dehydration of water/*t*-butanol mixtures by pervaporation: comparative study of commercially available polymeric, microporous silica and zeolite membranes, *J. Membr. Sci.*, 197 (2002) 309-319.

Gmehling, J., Onken, U., DeChema Chemistry Data Series. Vapor-Liquid Equilibrium Data Collection, Vol. 1, Pt. 1: Aqueous-Organic Systems, 1977.

Guo, W.F., Chung, T-S., Matsuura, T., Pervaporation study on the dehydration of aqueous butanol solutions: a comparison of flux vs. permeance, separation factor vs. selectivity, *J. Membr. Sci.*, 245 (2004) 199-210.

Ho, W. S. W., Sirkar, K.K., Membrane Handbook, Chapman & Hall, New York, 1992.

Huang, R.Y.M., Jarvis, N.R., Separation of liquid mixtures by using polymer membranes. II Permeation of aqueous alcohol solutions through cellophane and poly(vinyl alcohol), *J. Appl. Pol. Sci.*, 14 (1970) 2341-2356.

Morigami, Y., Kondo, M., Abe, J., Kita, H., Okamota, K., The first large-scale pervaporation plant using tubular-type module with zeolite NaA membrane, *Sep. Purif. Technol.*, 25 (2001) 251-260.

Nam, S. Y., Chun, H.J., Lee, Y.M., Pervaporation separation of water-isopropanol mixture using carboxymethylated poly(vinyl alcohol) composite membranes, *J. Appl. Pol. Sci.*, 72 (1999) 241-249.

Peters, T.A., Fontalvo, J., Vorstman, M.A.G., Benes, N.E., van Dam, R.A., Vroon, Z.A.E.P., van Soest-Vercammen, E.L.J., Keurentjes, J.T.F., Hollow Fibre Microporous Silica Membranes for Gas Separation and Pervaporation; Synthesis, Performance and Stability, *J. Membr. Sci.*, 248 (2005) 73-80.

Qiao, X., Chung, T-S, Guo, W.F., Matsuura, T., Teoh, M.M., Dehydration of isopropanol and its comparison with dehydration of butanol isomers

from thermodynamic and molecular aspects, *J. Membr. Sci.*, 252 (2005) 37-49.

Rezac, M.E., Koros, W.J., Preparation of polymer-ceramic composite membranes with thin defect-free separating layers, *J. Appl. Pol. Sci.*, 46 (1992) 1927-1938.

Schehlmann, M. S., Wiedemann, E., Lichtenthaler, R. N., Pervaporation and vapor permeation at the azeotropic point or in the vicinity of the LLE boundary phases of organic/aqueous mixtures, *J. Membr. Sci.*, 107 (1995) 277-282.

Song, K.M., Hong, W.H., Dehydration of ethanol and isopropanol using tubular type cellulose acetate membrane with ceramic support in pervaporation process, *J. Membr. Sci.*, 123 (1997) 27-33.

van Veen, H.M., van Delft, Y.C., Engelen, C.W.R., Pex, P.P.A.C., Dewatering of organics by pervaporation with silica membranes, *Sep. Purif. Technol.*, 22 and 23 (2001) 361-366.

Verkerk, A.W., van Male, P., Vorstman, M.A.G., Keurentjes, J.T.F., Properties of high flux ceramic pervaporation membranes for dehydration of alcohol/water mixtures, *Sep. Purif. Technol.*, 22-23 (2001) 689-695.

Wang, X-P., Feng, Y-F., Shen, Z-Q., Pervaporation properties of a three-layer structure composite membrane, *J. Appl. Pol. Sci.*, 75 (2000) 740-745.

Wesslein, M., Heintz, A., Lichtenthaler, R. N., Pervaporation of liquid mixtures through poly(vinyl alcohol) (PVA) membranes. I. Study of water containing binary systems with complete and partial miscibility, *J. Membr. Sci.*, 51 (1990) 169-179.

Wijmans, J.G., Process performance = membrane properties + operating conditions, *J. Membr. Sci.*, 220 (2003) 1-3.

Yeom, C.K., Lee, S.H., Lee, J.M., Pervaporative permeations of homologous series of alcohol aqueous mixtures through a hydrophilic membrane, *J. Appl. Pol. Sci.*, 79 (2001) 703-713.

Yoshida, W., Cohen, Y., Ceramic-supported polymer membranes for pervaporation of binary organic/organic mixtures, *J. Membr. Sci.*, 213 (2003) 145-157.

Chapter 6

Preparation of zeolite-coated pervaporation membranes

Pervaporation is a promising option to enhance conversion of reversible condensation reactions, generating water as a by-product. In this work, composite catalytic membranes for pervaporation-assisted esterification processes are prepared. Catalytic zeolite H-USY layers have been deposited on silica membranes by dip-coating using TEOS and Ludox AS40 as binder material. Membrane pre-treatment and the addition of binder to the dip-coat suspension appear to be crucial in the process. Tuning of catalytic layer thickness is possible by varying the number of dip-coat steps. This procedure avoids failure of the coating due to the high stresses, which can occur in thicker coatings during firing. In the pervaporation-assisted esterification reaction the H-USY-coated catalytic pervaporation membrane was able to couple catalytic activity and water removal. The catalytic activity is comparable to the activity of the bulk zeolite catalyst. The collected permeate consists mainly of water and the loss of acid, alcohol and ester through the membrane is negligible. The performance of the membrane reactor is mainly limited by reaction kinetics and can be improved by using a more active catalyst.

This chapter is based on: Peters, T.A., van der Tuin, J., Houssin, C., Vorstman, M.A.G., Benes, N.E., Vroon, Z.A.E.P., Holmen A., Keurentjes, J.T.F., *Preparation of zeolite-coated pervaporation membranes for the integration of reaction and separation*, Catal. Today, 104 (2005) 288-295.

6.1 Introduction

Pervaporation is a promising option to enhance conversion of reversible condensation reactions, generating water as a by-product. Pervaporation is attractive because the energy consumption is low, the reaction can be carried out at the optimal temperature, and the separation efficiency in pervaporation is not determined by the relative volatility as in reactive distillation [Benedict *et al.*, 2003]. In most pervaporation-coupled esterification studies presented so far, the membranes used are catalytically inactive [Benedict *et al.*, 2003; Domingues *et al.*, 1999; Keurentjes *et al.*, 1994; Krupiczka and Koszorz, 1999; Liu *et al.*, 2001; Zhu *et al.*, 1996]. Several authors [David *et al.*, 1992; Bagnell *et al.*, 1993; Bernal *et al.*, 2002; Nguyen *et al.*, 2003], however, used membranes with catalytic activity to carry out esterifications of different alcohols. They showed that equilibrium displacement could be enhanced if the membrane selective layer itself provides the catalytic function. In these studies, however, the membranes were neither very catalytically active nor highly selective to water because one single layer provided both the selective and the catalytic function. Therefore, it has been suggested to use a composite catalytic membrane to be able to optimise both layers independently [Nguyen *et al.*, 2003; Peters *et al.*, 2004]. The principle of an esterification reaction in a composite catalytic membrane reactor is schematically shown in Figure 6.1.

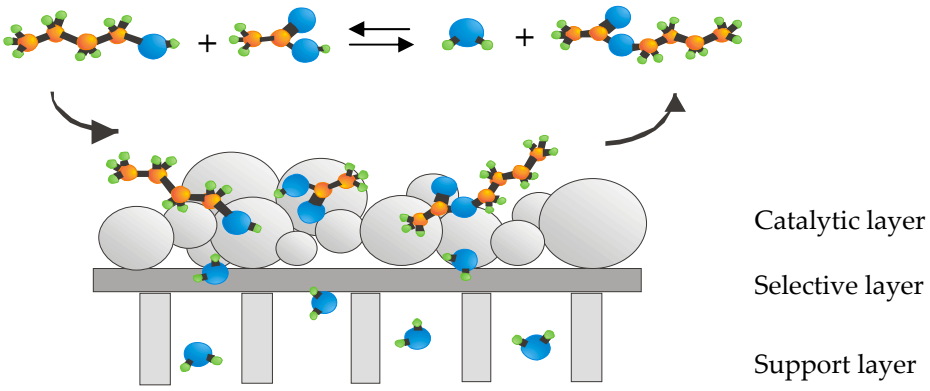

Figure 6.1 Esterification reaction in a composite catalytic membrane reactor.

The acid and the alcohol molecules diffuse into the catalytic layer where they are converted to an ester and water. The formed ester molecule diffuses back towards the bulk liquid whereas water is removed in-situ through the membrane due to the close integration of reaction and separation. Consequently, hydrolysis of the formed ester is reduced and the attained conversion will be increased compared to the inert membrane reactor David *et al.*, 1992; Bagnell *et al.*, 1993; Bernal *et al.*, 2002]. Additionally, heterogeneous catalysts might be used more efficiently due to the thinness of the catalytic layer present on the membrane support [Vergunst *et al.*, 2001]. Other advantages are that no catalyst neutralization or recovery is needed.

The present study focuses on the preparation of composite catalytic pervaporation membranes. The esterification reaction between acetic acid and butanol was taken as a model reaction. First the activity of various catalysts with respect to the esterification reaction was measured. Subsequently, composite catalytic membranes were prepared by applying a zeolite coating on top of ceramic silica membranes. The goal is to attain a strong and tuneable attachment of zeolite crystals on top of the selective microporous silica layer. Finally, the performance of the composite catalytic membrane as a combined reactor and separator in the esterification reaction was examined.

Zeolite coatings have been used as catalyst in various reactions like condensation, acylation and dehydrogenation reactions [Beers *et al.*, 2001a; Beers *et al.*, 2001b; Jansen *et al.*, 1997; Lai *et al.*, 2003; Nijhuis *et al.*, 2002; Vergunst *et al.*, 2001]. Zeolite coating is usually done through a crystallization step where the membrane is soaked in a zeolite crystallization mixture [Jansen *et al.*, 1997]. This method gives a strong attachment and possibly an oriented zeolite layer. However, zeolite crystallization takes place in highly alkaline aluminosilicate solutions. In the present case, direct zeolite crystallization was not possible because the microporous silica layer is not stable under these conditions. As a consequence, a dip-coat method was used. The membrane is immersed at a certain speed in a suspension of zeolite crystals that contains binder material followed by evaporation of the solvent by drying and calcination. Without this binder the deposited crystals will only bind to the surface by

"van der Waals" forces. In the dip-coat technique the resulting catalyst loading is satisfactory and easy controllable. This is important because in the preparation of composite catalytic membranes an optimum in catalytic layer thickness exists [Peters *et al.*, 2004]. Furthermore, it is not necessary to develop a special zeolite synthesis formulation for coating applications, so an already optimized and catalytically active zeolite can directly be applied.

6.2 Experimental

6.2.1 Activity of catalysts

The activity of various zeolites was measured in the esterification of acetic acid and butanol. The zeolites investigated were H-ZSM5 and H-USY and were obtained from Zeolyst Int. (Valley Forge, USA). The average particle size was 1 μm as measured by Scanning Electron Microscopy (SEM). Zeolite H-ZSM5 and H-USY, denoted as H-USY-x, where x represents the silica to alumina ratio, were used after calcination in an air stream for 8 hours at 500°C. For comparison with the zeolite catalysts also sulphated zirconium oxide was studied. A commercial sulphated zirconium oxide sample was acquired from Mel Chemicals (Manchester, UK) and was used after calcination in an air stream for 6 hours at 550°C.

The catalyst activity was studied in a batch reflux system. A three-necked flask equipped with a condenser and stirrer was charged with acetic acid (0.66 mol) and pre-activated catalyst. Then, the system was heated up to the reaction temperature after which pre-heated alcohol (0.66 mol) was added. The reaction temperature was maintained by means of a thermostatic water bath in which the reactor was immersed. For kinetic measurements, samples were taken periodically and analysed by a gas chromatograph equipped with a flame ionisation detector and a thermal conductivity detector. All catalysts were employed under similar reaction conditions. The reaction was performed at a temperature of 75°C. GC analysis confirmed that no by-products were formed. The reaction rate constants were evaluated from the measured time dependent concentration curves using the differential method. The non-linear least-squares regression technique was used to minimise the sum of the square differences on the reaction rate for acetic acid.

6.2.2 Coating and testing of the pervaporation membranes

Ceramic pervaporation hollow fibre membranes (TNO-TPD, The Netherlands) were used. The inner and outer diameter of the membranes is 2.0 mm and 3.2 mm, respectively. The length of the membranes is 20 cm. They consist of γ-alumina layers supported on a porous α-alumina tubular membrane. The permselective layer on the outside of the support is a thin (70 nm) layer made of microporous amorphous silica [18]. In the dehydration of *n*-butanol these membranes have proved to combine a high water flux with a good selectivity [Peters *et al.*, 2005].

Standard binder solution.

A silica binder solution was prepared as follows: TEOS (Merck, >98%) was mixed with ethanol and water. A small amount of nitric acid (65 wt.% in water) as a silicate oligomerisation catalyst was added and the resulting mixture was heated at 60°C for 3h under continuous stirring. The reaction mixture had a molar ratio TEOS/ethanol/water/HNO_3 of 1/3.8/6.4/0.085. Commercial colloidal silica (Ludox AS-40, Aldrich) has also been used as a binder solution.

Zeolite dip-coat suspensions.

The dip-coat solutions were prepared by mixing H-USY crystals and ethanol. Dealuminated zeolite H-USY with a Si/Al ratio of 40 was selected for the coating experiments. The Na_2O content was 0.05 wt.% and the surface area 650 $m^2 \cdot g^{-1}$. The amount of zeolite crystals was varied between 5 wt.% and 26 wt.%. The suspensions were sonicated at room temperature for 1h prior to use. 10 wt.% of standard binder solution was added to the zeolite dip-coat solution to enhance particle deposition and layer strength.

Dip-coat process.

Membranes were first immersed (16 $mm \cdot s^{-1}$) in the binder solution for 2 min and removed from the binder solution at the same speed. Next, membranes were dipped into a zeolite suspension for 2 min (longer times did not significantly change the final loading) at a speed of 16 $mm \cdot s^{-1}$. Typically, the zeolite dip-coat procedure started 1 min after the pre-treatment. Subsequently, the membranes were dried in air at 60°C for 2h and calcined for 16h in air at 500°C with a heating rate of 100 $K \cdot h^{-1}$.

Characterization.

The loading of zeolite crystals on the membrane surface was determined by the weight increase during the dip-coat process. The adhesion of zeolite crystals was tested by an ultrasonic bath treatment for 1h followed by scanning electron microscopy (SEM) to evaluate the amount of crystals remaining at the surface. SEM pictures were taken using a JEOL JSM-5600 with an acceleration voltage of 15 kV. Dry coated membrane samples were gold-coated prior to scanning.

Catalytic test

The activity of the zeolite-coated pervaporation membrane was measured in the esterification reaction between acetic acid and butanol under the same reaction conditions as mentioned above in the catalyst screening experiments. The membrane was placed in a stainless steel module module using Kalrez® O-rings. Effective membrane area used was 17 cm^2. The set-up used is depicted in Figure 6.2.

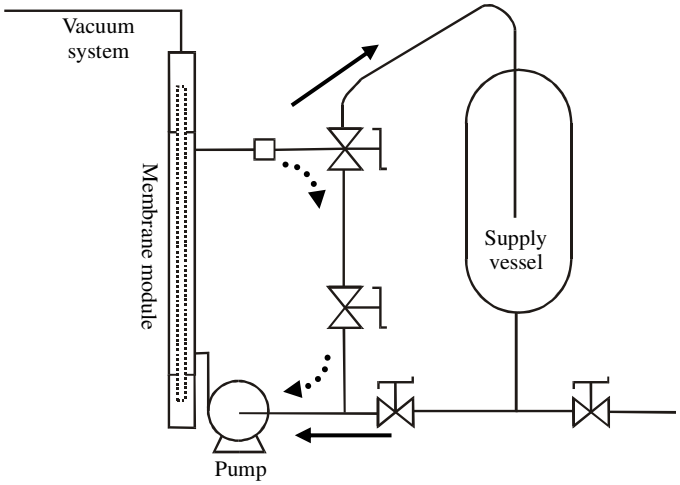

Figure 6.2 Set-up used in the catalytic tests and the pervaporation-esterification coupling.

The supply vessel was charged with a certain amount of acetic acid. Then, the system was heated up to the reaction temperature (T=75°C) after which the pre-heated equimolar amount of alcohol was added. The

reaction temperature was maintained by means of a thermostatic water bath in which the system was immersed. The liquid reaction mixture was recirculated through the membrane module by means of the pump (valves are in position 1) at a liquid flow rate of 40 $l \cdot h^{-1}$, which corresponds to a liquid superficial velocity exceeding 2 $m \cdot s^{-1}$ in order to eliminate polarization effects. On the permeate side a vacuum was maintained (10 mbar) by a cascade of a liquid nitrogen cold trap and a vacuum pump. After recirculation through the membrane module, the flow towards the supply vessel was stopped, decreasing the reactor volume to 30 ml, and the liquid was only flowing through the membrane module containing the catalytic membrane (valves are in position 2).

6.3 Results

6.3.1 Activity of heterogeneous catalysts

All experiments showed first-order behaviour in acetic acid and butanol concentration. The activity of the catalysts is expressed in terms of the second-order reaction rate constant normalised for the catalyst weight. As the reaction also proceeds without adding a catalyst, the first-order reaction rate constant of this reaction is also given. The results are shown in Table 6.1.

Table 6.1 Activity of the different catalysts in the esterification reaction between acetic acid and butanol, T=75°C.

catalyst	k [$m^3 \cdot mol^{-1} \cdot s^{-1}$]	k [$m^3 \cdot mol^{-1} \cdot g_{cat}^{-1} \cdot s^{-1}$]	T_c [°C]
No catalyst	$1.33 \cdot 10^{-9}$	-	-
H-USY-20	-	$9.82 \cdot 10^{-10}$	500
H-ZSM5-12.5	-	$5.91 \cdot 10^{-11}$	500
ZrO_2	-	$8.74 \cdot 10^{-9}$	550

Large-pore zeolites, like X and Y-type zeolites have proven to be efficient catalysts for esterification reactions [Corma *et al.*, 1989; Namba *et al.*, 1985]. Zeolite catalytic properties like pore size, acid strength distribution and hydrophobicity can be designed by preparing zeolites with different crystalline structure, acid exchange level and framework

Si/Al ratio. For example, with increasing Si/Al ratios, the zeolite surface becomes more hydrophobic and, therefore, has more affinity for the reactants, whereas the number of acid sites decreases. Hence, an optimum Si/Al ratio may exist. Figure 6.3 shows the influence of the zeolite Si/Al ratio for H-USY on the zeolite activity in the esterification reaction between acetic acid and butanol. The highest activity for the H-USY zeolite activity was found at a Si/Al ratio of around 20. This agrees with the value obtained by Corma et al. [1989] for the esterification of carboxylic acids in the presence of HY zeolites. H-ZSM5 had the lowest activity of the catalysts tested suggesting that the esterification is internally diffusion-limited due to the medium sized H-ZSM5 zeolite pores [Namba *et al.*, 1985]. Thus, most of the conversion occurs on the external surface of the crystallites.

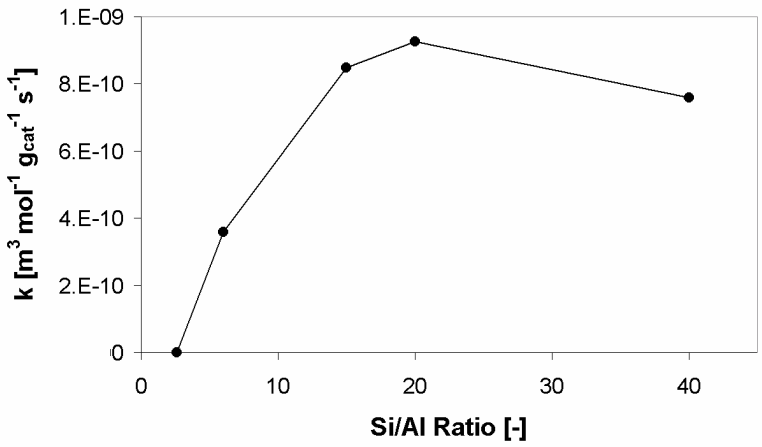

Figure 6.3 Effect of the H-USY Si/Al ratio on the reaction rate constant, T=75°C.

The activity and stability of sulphated zirconia towards the esterification reaction highly depends on the catalyst pre-treatment. At increasing calcination temperature, the crystallinity of the sulphated zirconia increases, whereas the surface area (see Table 6.1) and the amount of surface sulphur species decreases [Hu *et al.*, 2000]. Hence, an optimum in reactivity as a function of calcination temperature may exist. This optimum was found at a calcination temperature of 550°C. This agrees with the optimum calcination temperature obtained by Hino et al. [1981] for the

esterification reaction of acetic acid and ethanol in the presence of sulphated zirconia. From Table 6.1 it can be seen that the weight based activity of sulphated zirconia exceeded the activity of the two zeolites tested. However, due to water adsorption on the active sites or loss of surface sulphur sites, the activity of sulphated zirconia gradually decreased. Additionally, for the regeneration of this type of catalysts multiple steps are needed whereas for regeneration of zeolites only calcination in air has to be performed [Hino and Arata, 1981]. Therefore, H-USY zeolite is considered to be the most suitable catalyst to be applied as the catalytic layer in a catalytic membrane reactor.

6.3.2 Coating of the ceramic pervaporation membranes

6.3.2.1 Ludox AS-40 as binder

Commercial reactive colloidal silica nanoparticles such as Ludox AS-40 (40 wt.% suspension of colloidal silica in water) are commonly used as binder to enhance zeolite crystal attachment on aluminosilicate substrates [Beers *et al.*, 2001a; Beers *et al.*, 2001b; Jansen *et al.*, 1997; Nijhuis *et al.*, 2002]. From Figure 6.4 it can be seen that after pre-treatment of the membrane surface in a Ludox AS-40 solution, zeolite attachment was increased dramatically.

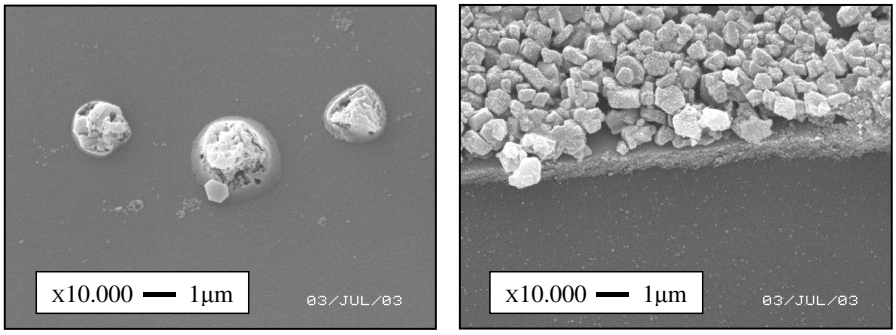

Figure 6.4 SEM pictures of a H-USY zeolite-coated membrane (top view), prepared with a 20 wt.% H-USY mixture in ethanol. (a) without pre-treatment; (b) with pre-treatment in a Ludox AS-40 binder solution.

Discontinuous zeolite coverage is clearly observed. However, the most interesting feature is that a Ludox layer is required to enable zeolite crystals to be attached to the surface. Figure 6.4b shows a Ludox layer of approximately 0.5 μm between the zeolite crystals and the selective silica layer of the membrane. Where there are no AS-40 particles (or very few) virtually no attachment is observed. This signifies how important pre-treatment of the membrane surface is for zeolite adhesion. The difficult attachment could be ascribed to the fact that the original membrane surface probably does not contain enough reactive sites to induce chemical attachment or does not exhibit enough surface roughness to induce physical attachment. Unfortunately, a full coverage could not be achieved and the zeolite layer was unstable under ultrasonic treatment. Therefore, oligomeric silica particles were considered as binder to enhance zeolite attachment and zeolite layer strength. Such a binder should not form a thick layer unlike the above-mentioned results, which could be detrimental to permeation. Additionally, an improved membrane coverage is expected as the reactivity of TEOS is higher compared to Ludox AS-40.

6.3.2.2 Oligomeric silica as binder

Figure 6.5 shows a zeolite-coated membrane obtained from a 20 wt.% zeolite dip-coat solution after pre-treatment in a 10 wt.% TEOS binder solution. It can be seen that a crack-free zeolite layer was obtained. The coverage is improved as compared to the membrane pre-treated in a Ludox AS-40 binder solution.

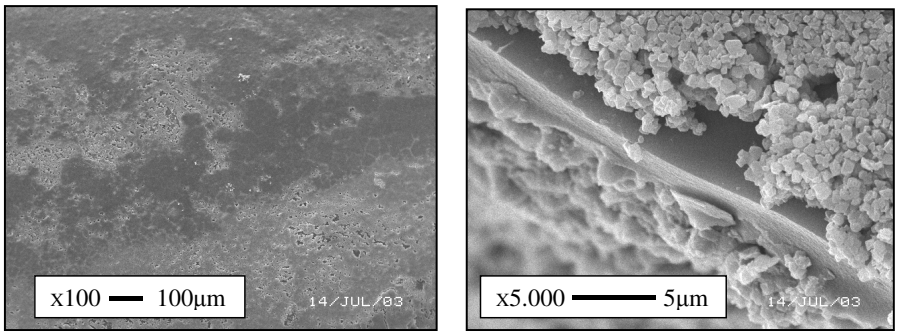

Figure 6.5 SEM pictures of a H-USY zeolite-coated membrane, prepared with a 20 wt.% H-USY mixture in ethanol pre-treated in a TEOS solution. (a) top view; (b) side view.

Coating a membrane once in a coating mixture of 20 wt.% H-USY resulted in a zeolite layer thickness of around 2 μm after calcination as seen by SEM, later confirmed using a profilometer. The amount of zeolite deposited on the membrane can be predicted from the solution film thickness that should remain on the surface upon withdrawal from the zeolite solution; on the basis of viscosity, surface tension, density, and the speed of withdrawal, the resulting zeolite layer thickness for a single withdrawal should be 3 μm [Lacy *et al.*, 1999]. This prediction agrees well with our experimental results. A significant amount of zeolite remains on the surface after 1 h of sonication, which indicates firm attachment of the zeolite layer. In order to increase zeolite layer strength, 10 wt.% of binder was added to the dip-coat solution. The influence of this binder on the zeolite layer is clearly visible from Figure 6.6. Due to the presence of binder in the dip-coat solution, separate zeolite particles in the zeolite layer are intergrown and the resulting zeolite layer is strengthened.

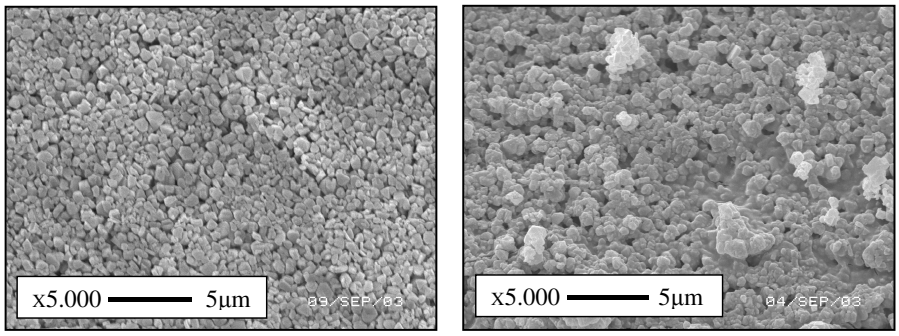

Figure 6.6 SEM pictures of a H-USY zeolite-coated membrane, prepared with a 20 wt.% H-USY mixture in ethanol pre-treated in a TEOS solution; (a) no binder in dip-coat solution; (b) 10 wt.% binder in dip-coat solution.

Varying the zeolite concentration in the coating mixture between 3 and 20 wt.% did not seem to affect the final layer thickness substantially. In more concentrated mixtures the zeolite layer thickness increased dramatically. In these thick layers, however, cracks appeared during drying and the layer was easily removed during the ultrasonic treatment. Therefore, in order to increase the layer thickness, the dipping procedure

was repeated four times. This deposition method avoids failure of the coating due to the high stresses, which can form in thicker coatings during drying or firing. A calcination step has been applied after every dip-coat experiment. The results are presented in Figure 6.7. From Figure 6.7b it can be observed that the zeolite layer thickness is approximately 10 μm (5 X 2 μm). The coverage is uniform as shown in Figure 6.7a. Hence, tuning of the zeolite coating thickness is possible by varying the number of dip-coat steps.

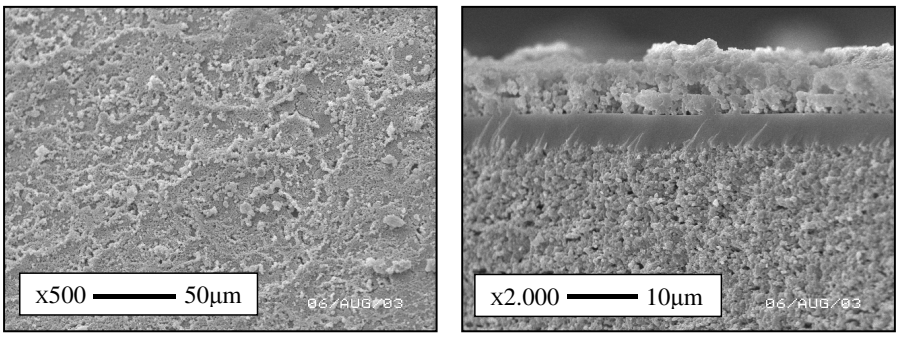

Figure 6.7 SEM pictures of a H-USY zeolite-coated membrane, prepared with a 20 wt.% H-USY mixture in ethanol pre-treated in a TEOS solution, procedure repeated four times. (a) top view; (b) side view.

6.3.3 Pervaporation-esterification coupling

The catalytic function of the H-USY-coated pervaporation membrane combined with its selective features was tested in the esterification reaction between acetic acid and butanol. For this, a membrane is selected which is dip-coated ten times resulting in a layer thickness of around 40 μm. Zeolite coverages up to 10 $g \cdot m^{-2}$ of membrane area, which translates to reactor loadings of zeolite up to 80 $kg \cdot m^{-3}$ of reactor volume were obtained. The activity of the coated membrane as compared to the activity obtained for the bulk zeolite catalyst. In both reactions the (initial) observed rate constants and intrinsic rate constants per gram of zeolite are in the same order of magnitude. The coated membrane exhibits an activity of $9.2 \cdot 10^{-10}$ $m^3 \cdot mol^{-1} \cdot s^{-1} \cdot g_{cat}^{-1}$, which is only 7 % lower than the value given in Table 6.1. Most likely, inhibition of external acid sites by the TEOS binder is

the explanation for the somewhat lower activity [Kunkeler *et al.*, 1997]. However, due to the relatively low amount of catalyst compared to the area-to-volume ratio of the experimental set-up (<100 $m^2 \cdot m^{-3}$, instead of 1000 $m^2 \cdot m^{-3}$ in a practical membrane module), a substantial conversion could not be reached within a reasonable time scale (typical 80 mg of catalyst-coated on a membrane with a length of 20 cm and a reactor volume of 30 ml). Therefore, it was chosen to use a feed at equilibrium conversion. This feed simulates the outlet stream from a conventional reactor, with an equimolar feed mixture at equilibrium conversion. The results are shown in Figures 6.8 to 6.10.

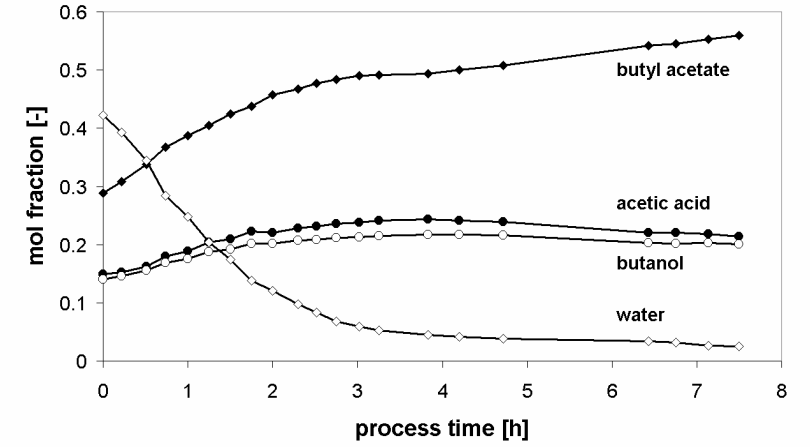

Figure 6.8 Mol fractions in the composite catalytic membrane assisted esterification of acetic acid and butanol.

From Figure 6.8 it can be seen that initial water removal from the reactor is high, which shows the selective function of the membrane. After three hours the excess of water in the reactor is removed suggesting that the performance of the membrane reactor is mainly limited by the reaction kinetics. From this stage, the water production due to reaction equals the water removal from reaction and thus, the water fraction is constant. In contrast to other studies [Bernal *et al.*, 2002; David *et al.*, 1992], the collected permeate consists mainly of water indicating the beneficial effect of the dual-layer structure. Thus, reactant and product loss through the

membrane are negligible as can be seen from Figure 6.9. The total flux through the membrane decreases in time mainly due to the decreasing water fraction in the reactor.

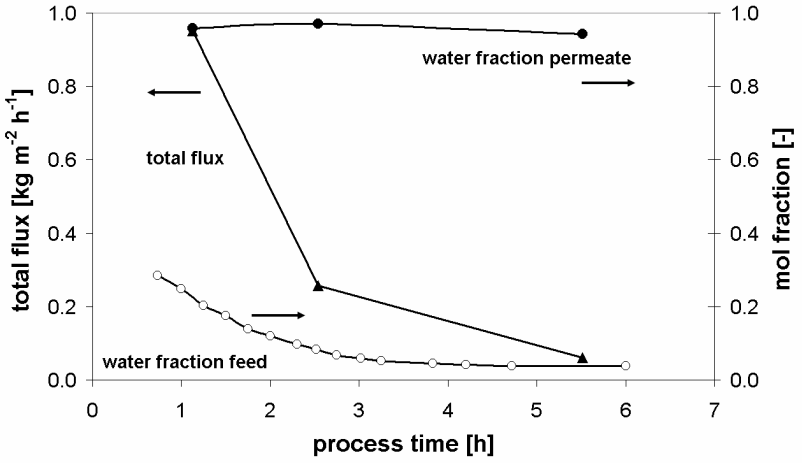

Figure 6.9 Permeate and feed water concentration and total flux through the membrane.

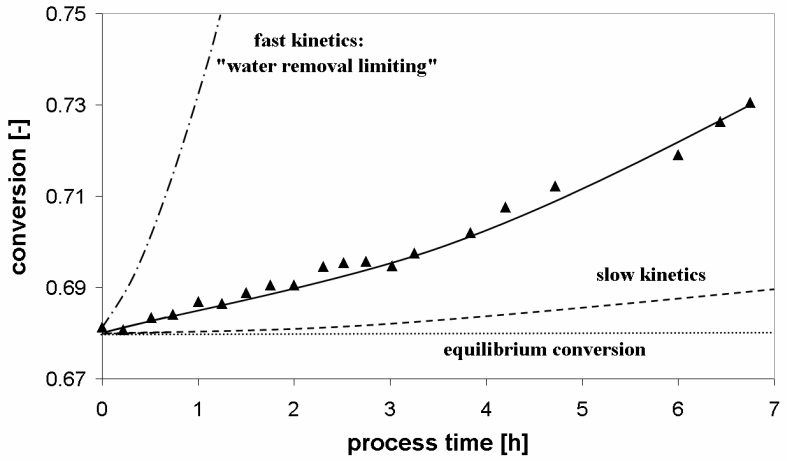

Figure 6.10 Conversion of acetic acid in the composite catalytic membrane assisted esterification of acetic acid and butanol (◎), T=75°C.

Figure 6.10 shows the conversion plotted against time for a catalytic membrane reactor. The simulated curves present two extreme cases: the system is limited by either reaction kinetics or by water removal. For the simulations regarding the water removal limited case, the reaction rate constant is chosen such that further increase did not alter the conversion behaviour. For the case that the reaction kinetics are limiting, the curve is obtained using the reaction rate constant for the uncatalysed reaction given in Table 6.1 assuming first-order reaction kinetics for both the reactants [Peters *et al.*, 2004]. Figure 6.10 it can be seen that the reached conversion of the catalytic membrane-assisted esterification reaction clearly exceeds thermodynamic equilibrium. It can also be seen that the performance of the catalytic membrane is indeed limited by kinetics and that the reached conversion can be improved substantially by using a more active catalyst. Furthermore, one should realize that applied area-to-volume ratio and catalyst amount are easily controllable by applying multiple membranes in one single module and consequently it is conceivable that an improved performance can easily be realized.

6.4 Conclusions

Composite catalytically active membranes can be used to enhance conversion of esterification reactions as the reaction and separation function are coupled very efficiently. An additional advantage is that both the selective layer and the catalytic layer can be optimised independently. In this work, composite catalytic membranes are prepared by a dip-coating technique. Catalytic zeolite H-USY layers have been deposited on silica membranes using TEOS as well as Ludox AS40 as binder. Membrane pre-treatment and the addition of binder to the dip-coat suspension appear to be crucial in the dip-coat process. Varying the zeolite concentration in the coating mixture between 3 and 20 wt.% did not seem to affect the final layer thickness. Tuning of catalytic layer thickness is possible by varying the number of dip-coat steps. This procedure helps to avoid failure of the coating due to high stresses that can occur in thicker coatings during drying and firing. In the pervaporation-assisted esterification reaction the catalytic membrane was able to couple catalytic activity and water removal. The catalytic activity of the H-USY-coated catalytic pervaporation

membrane was comparable to the activity of the bulk zeolite catalyst. The collected permeate consists mainly of water and thus, acid, alcohol and ester loss through the membrane are negligible. The performance of the system can be improved by using a more active catalyst.

Acknowledgements

This work was performed in a cooperative project of the Centre for Separation Technology and was financially supported by TNO and NOVEM. We would like to thank Henk Woestenberg for taking the SEM pictures.

Nomenclature

k_{obs}	observed reaction rate constant	$[m^3 \cdot mol^{-1} \cdot s^{-1}]$
k_r	rate constant normalized for catalyst amount	$[m^3 \cdot mol^{-1} \cdot g_{cat}^{-1} \cdot s^{-1}]$
t	time	[h]
T	temperature	[°C]
X	conversion	[-]

References

Bagnall, L., Cavell, K., Hodges, A.M., Mau, A.W., Seen, A.J., The use of catalytically active pervaporation membranes in esterification reactions to simultaneously increase product yield, membrane permselectivity and flux, *J. Membr. Sci.*, 85 (1993) 291-299.

Beers, A.E.W., Spruijt, R.A., Nijhuis, T.A., Kapteijn, F., Moulijn, J.A., Esterification in a structured catalytic reactor with counter-current water removal, *Catal. Today*, 66 (2001) 175-181.

Beers, A.E.W., Spruijt, R.A., Nijhuis, T.A., Kapteijn, F., Moulijn, J.A., Zeolite coated structures for the acylation of aromatics, *Micr. Mes. Mater.*, 48 (2001) 279-284.

Benedict, D.J., Parulekar, S.J., Tsai, S-P, Esterification of Lactic Acid and Ethanol with/without Pervaporation, *Ind. Eng. Chem. Res.*, 42 (2003) 2282-2291.

Bernal, M.P., Coronas, J., Menéndez, M., Santamaría, J., Coupling of reaction and separation at the microscopic level: esterification processes in a H-ZSM-5 membrane reactor, *Chem. Eng. Sci.*, 57 (2002) 1557-1562.

Corma, A., Garcia, H., Iborra, S., Primo, J., Modified faujasite zeolites as catalysts in organic reactions: Esterification of carboxylic acids in the presence of HY zeolites, *J of Catal.*, 120 (1989) 78-87.

David, M.O., Nguyen, T.Q., Neel, J., Pervaporation membranes endowed with catalytic properties, based on polymer blends, *J. Membr. Sci.*, 73 (1992) 129-141.

Domingues, L., Recasens, F., Larrayoz, M., Studies of a pervaporation reactor: Kinetics and equilibrium shift in benzyl alcohol acetylation, *Chem. Eng. Sci.*, 54 (1999) 1461-1465.

Hino, M., Arata, K., Synthesis of esters from acetic acid with methanol, ethanol, propanol, butanol, and isobutyl alcohol catalyzed by solid superacid, *Chem. Lett.*, (1981) 1671-1672.

Hu, J., Wei, C., Qiu, F., Xu, Z., Chen, Q., Preparation of a new type solid acid SO_4^{2-}/Fe_2O_3-ZrO_2-SiO_2 and its application in the esterification of acetic acid and butanol, *J. Nat. Gas Chem.*, 9 (2000) 212-216.

Jansen, J.C., Koegler, J.H., Calis, H.P.A., van den Bleek, C.M., Kapteijn, F., Moulijn, J.A., Geus, E.R., van der Puil, N., Zeolitic coatings and their potential use in catalysis, *Micr. Mes. Mater.*, 21 (1998) 213-226.

Keurentjes, J.T.F., Janssen, G.H.R., Gorissen, J.J., The esterification of tartaric acid with ethanol: kinetics and shifting the equilibrium by means of pervaporation, *Chem. Eng. Sci.*, 49 (1994) 4681-4689.

Krupiczka, R., Koszorz, Z., Activity-based model of the hybrid process of an esterification reaction coupled with pervaporation, *Sep. Pur. Technol.*, 16 (1999) 55-59.

Kunkeler, P.J., Moeskops, D., van Bekkum, H., Zeolite Beta: characterization and passivation of the external surface acidity, *Micr. Mater.*, 11 (1997) 313-323.

Lacy, W.B., Olsen, L.G., Harris, J.M., Quantitative SERS measurements on dielectric-overcoated silver-island films by solution-deposition control of surface concentrations, *Anal. Chem.*, 71 (1999) 2564-2570.

Lai, S.M., Martin-Aranda, R., Yeung, K.L., Knoevenagel condensation reaction in a membrane microreactor, *Chem Commun.*, 2 (2003) 218-219.

Liu, Q.L., Zhang, Z., Chen, H.F., Study on the coupling of esterification with pervaporation, *J. Membr. Sci.*, 182 (2001) 173-181.

Namba, S., Wakushima, Y., Shimizu, T., Yashima, T., Catalytic application of hydrophobic properties of high-silica zeolites. II. Esterification of acetic acid with butanols, *Stud. Surf. Sci. Cat.*, 20 (1985) 205-211.

Nguyen, Q.T., M'Bareck, C.O., David, M.O., Métayer, M., Alexandre, S., Ion-exchange membranes made of semi-interpenetrating polymer networks, used for pervaporation-assisted esterification and ion transport, *Mat. Res. Innovat.*, 7 (2003) 212-219.

Nijhuis, T.A., Beers, A.E.W., Kapteijn, F., Moulijn, J.A., Water removal by reactive stripping for a solid-acid catalyzed esterification in a monolithic reactor, *Chem. Eng. Sci.*, 57 (2002) 1627-1632.

Peters, T.A., Fontalvo, J., Vorstman, M.A.G., Keurentjes, J.T.F., Design rules for catalytic hollow fibre membranes for condensation reactions, *Trans. IChemE. Part A, Chem. Eng. Res. Des.*, 82 (2004) 220-228.

Peters, T.A., Fontalvo, J., Vorstman, M.A.G., Benes, N.E., van Dam, R.A., Vroon, Z.A.E.P., van Soest-Vercammen, E.L.J., Keurentjes, J.T.F., Hollow fibre microporous silica membranes for gas separation and pervaporation: synthesis, performance and stability, *J. Membr. Sci.*, 248 (2005) 73-80.

Vergunst, T., Kapteijn, F., Moulijn, J.A., Optimization of geometric properties of a monolithic catalyst for the selective hydrogenation of phenylacetylene, *Ind. Eng. Chem. Res.*, 40 (2001) 2801-2809.

Zhu, Y., Minet, R.G., Tsotsis, T.T., A continuous pervaporation membrane reactor for the study of esterification reactions using a composite polymeric/ceramic membrane, *Chem. Eng. Sci.*, 51 (1996) 4103-4113.

Chapter 7

Preparation of Amberlyst-coated pervaporation membranes

Catalytic Amberlyst 15 layers have been deposited on composite ceramic/PVA membranes by the dip-coat technique using Aculyn as a rheology modifier. Tuning of the catalytic layer thickness is possible by varying the number of dip-coat steps. A "dried-mud like" Amberlyst 15 layer is formed, which is stable during both pervaporation and reaction experiments. The contribution of the catalytic layer to the overall mass transport resistance is found to be negligible. In the pervaporation-assisted esterification reaction between acetic acid and butanol the catalytic membrane is able to couple catalytic activity and water removal. The catalytic activity of the Amberlyst-coated pervaporation membrane equals the activity of the unsupported catalyst. Due to the high activity of the Amberlyst catalyst, the performance of the Amberlyst-coated membrane is limited by the water removal rate. This in contrast to zeolite-coated pervaporation membranes, for which performance is limited by the catalytic activity.

7.1 Introduction

Pervaporation is a promising option to enhance the conversion of reversible condensation reactions, generating water as a by-product. Several authors have shown that the equilibrium displacement is enhanced by means of catalytically active membranes [David *et al.*, 1992; Bagnell *et al.*, 1993; Bernal *et al.*, 2002; Nguyen *et al.*, 2003]. The integration of the selective and catalytic function into one single layer, however, demands contradicting material properties. For example, to achieve high separation selectivity the diffusion of products inside the material should be low, whereas efficient use of the catalytic properties requires the diffusion of products to be high. The conflicting demands on materials properties can be avoided by accommodating the selective and catalytic features in two different distinct layers, which are in close physical contact. This approach allows independent optimization of the selective and the catalytic properties.

Previously, we have prepared zeolite-coated silica membranes by means of the dip-coat technique to integrate reaction and separation [Peters *et al.*, 2005a]. However, due to the low activity of the H-USY zeolite catalyst the performance of the composite membrane is limited by the reaction kinetics. Hence, the conversion can be improved substantially by using a more active catalyst. Ion-exchange resins, like Amberlyst 15 are the most common heterogeneous catalysts used and have proven to be effective in liquid phase esterification reactions [Yadav and Mehta, 1994; Xu and Chuang, 1996; Chen et al., 1999; Liu and Tan, 2001; Yadav and Thathagar, 2002; Peters *et al*., 2006] and have previously been used as catalytic coating in the hydration of alkenes [Ueda *et al.*, 2003]. The weight-based activity of Amberlyst 15 in the esterification of acetic acid and butanol is roughly ten times higher compared to the activity of the H-USY zeolite. Consequently, the performance of the composite membrane can greatly be improved by using Amberlyst 15 as the catalyst instead of HY-zeolite.

The present study focuses on the preparation of Amberlyst-coated catalytic pervaporation membranes. First, composite catalytic membranes have been prepared by applying an Amberlyst coating on top of composite ceramic/polymer membranes by means of a dip-coat technique. Using this

versatile technique, the catalyst loading is easily controllable [Beers *et al.*, 2003]. This is important because in the preparation of composite catalytic membranes an optimum in catalytic layer thickness exists [Peters *et al.*, 2004]. The performance of the composite catalytic membrane as a combined reactor and separator in the esterification reaction between acetic acid and butanol has been examined. Additionally, the effect of the catalytic layer thickness on the membrane performance is examined.

7.2 Experimental

7.2.1 Activity of catalysts

The activity of Amberlyst 15 was measured in the esterification of acetic acid and butanol in a batch reflux system. Amberlyst 15 was obtained from Rohm and Haas (Germany) and was dried for 24 hours at 90°C prior to use. A three-necked flask equipped with a condenser and stirrer was charged with a certain amount of acid and pre-activated catalyst. Then, the system was heated up to the reaction temperature after which the pre-heated alcohol was added. The reaction temperature was maintained by means of a thermostatic water bath in which the reactor was immersed. For kinetic measurements, samples were taken periodically and analysed by a gas chromatograph equipped with both a flame ionisation detector and a thermal conductivity detector. All catalysts were employed under similar reaction conditions. The reaction was performed at a temperature of 75°C. GC analysis confirmed that no by-products were formed.

7.2.2 Coating and testing of the pervaporation membranes

Composite ceramic/polymer pervaporation hollow fibre membranes (TNO, The Netherlands) were used. The supports consist of an α-Al_2O_3 hollow fibre substrate and an intermediate γ-Al_2O_3 layer [Peters *et al.*, 2005b]. The outer diameter and the length of the membranes are 3.2 mm and 20 cm, respectively. The intermediate γ-Al_2O_3 layers were modified by dip-coating in a 0.75 wt.% PVA (Mowiol 56/98, Clariant) solution. The preparation method is discussed in more detail by Peters *et al.* [Peters *et al.*, 2006b] and in Chapter 5.

Dip-coat suspensions

The dip-coat solutions were prepared by mixing ball-milled Amberlyst 15 and water. Via sieving, Amberlyst 15 powder with a particle size smaller than 56 μm was selected for the coating experiments. Aculyn®22 (acrylates/stearath-20 methacrylate copolymer) was added to the dip-coat solution to enhance particle deposition and layer strength. Aculyn is a rheology modifier, which hydrophobic parts associate with particles present in the solution. When the pH exceeds 7, Aculyn thickens and stabilises the suspension instantly. The composition of the dip-coat solution is given in Table 7.1. After mixing and subsequent stirring, the pH of the dip-coat solution was set to 8 using sodium hydroxide. The suspensions were sonicated at room temperature for 1h prior to use.

Table 7.1 Composition Amberlyst 15 dip-coat solution.

Component	Amount [g]	Composition [wt.%]
Water	51.8	93.4
Amberlyst 15	2.72	4.9
Aculyn	0.95	1.7

Dip-coat process

Membranes were first immersed (16 mm·s^{-1}) in water to wet the PVA membrane surface. After drying for two minutes, the membranes were immersed (16 mm·s^{-1}) in the catalyst suspension for 2 min and removed from the suspension at the same speed. Subsequently, the membranes were dried in air at 90°C for 2h. Afterwards, the membranes were treated with sulphuric acid (10 wt.%) to regenerate the catalytic coating. After washing with demi-water to remove the excess of sulphuric acid, the membranes were again dried in air at 90°C for 2h.

Characterization

The loading of Amberlyst particles on the membrane surface was determined by the weight increase during the dip-coat process. Scanning electron microscopy (SEM) pictures were taken using a JEOL JSM-5600 with an acceleration voltage of 15 kV. The air-dried composite membranes were cryogenically fractured in liquid nitrogen and gold-coated prior to scanning.

Pervaporation

Dehydration experiments of *1*-butanol (pro-analyse, Merck, Darmstadt, Germany) were carried out in a common pervaporation set-up (Figure 7.1) [Verkerk *et al.*, 2001] at a temperature of 80°C and a feed water concentration of 5.0 wt.%.

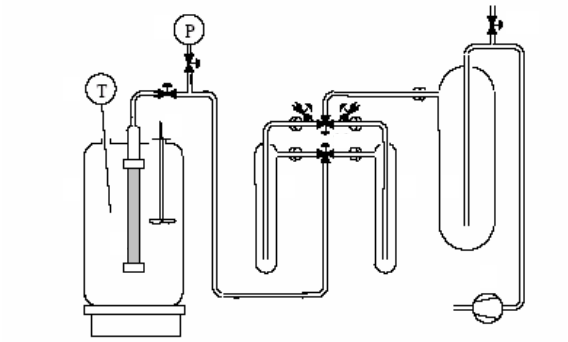

Figure 7.1 Set-up used for the pervaporation experiments.

At the permeate side a vacuum was maintained (10 mbar) by a cascade of a liquid nitrogen cold trap and a vacuum pump. The feed was supplied to the membrane by simply submerging the membrane in a large vessel containing the alcohol/water mixture. Sufficient stirring (3 pitched-blade stirrers mounted on a single axis, 1300 rpm) of the bulk mixture was used to avoid polarisation effects at the outside of the membrane. A further increase in stirrer speed did not alter the membrane performance. The retentate composition was analysed using Karl-Fischer titration, while the permeate composition was analysed using gas chromatography.

The performance of a membrane is usually expressed in terms of the water flux and separation factor. The latter is defined as:

$$\alpha = \frac{y_{H2O} / x_{H2O}}{y_j / x_j} \tag{7.1}$$

where y and x are the molar fractions in the permeate and retentate, respectively.

Pervaporation-esterification coupling

The activity of the catalyst-coated pervaporation membrane was measured in the esterification reaction between acetic acid and butanol under the same reaction conditions as mentioned above in the catalyst screening experiments. The set-up used is depicted in Figure 7.2.

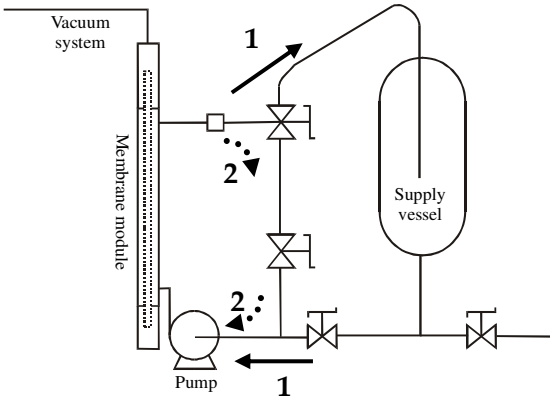

Figure 7.2 Set-up used in the catalytic tests and the pervaporation-esterification coupling.

The supply vessel was charged with a certain amount of acetic acid. Then, the system was heated up to the reaction temperature after which the pre-heated alcohol was added. The reaction temperature was maintained by means of a thermostatic water bath in which the system was immersed. The liquid reaction mixture was recirculated through the membrane module by means of a pump (valves are in position 1). After recirculation through the membrane module, the flow towards the supply vessel was stopped, decreasing the reactor volume to 35 mL, and the liquid was only flowing through the membrane module containing the catalytic membrane (valves are in position 2).

7.3 Results

7.3.1 Amberlyst 15 activity

The activity of Amberlyst 15 in the esterification reaction between acetic acid and butanol is evaluated at 75°C. In addition, the effect of milling and Aculyn addition on the Amberlyst activity is investigated.

Table 7.2 Activity of Amberlyst 15 in the esterification reaction between acetic acid and butanol, T=75°C.

Catalyst	Shape	k [$m^3 \cdot mol^{-1} \cdot s^{-1}$]	k [$m^3 \cdot mol^{-1} \cdot g_{cat}^{-1} \cdot s^{-1}$]
No catalyst	-	$1.33 \cdot 10^{-9}$	-
Amberlyst 15	beads	-	$1.6 \cdot 10^{-8}$
Amberlyst 15	powder	-	$1.8 \cdot 10^{-8}$
Amberlyst 15 – treated with Aculyn	powder	-	$1.74 \cdot 10^{-8}$

From Table 7.2 it can be seen that the activity of the powderous Amberlyst 15 is higher than the Amberlyst 15 beads. This can be explained by a slight contribution of internal mass transfer limitations in the bead-shaped Amberlyst particles.

Upon addition of Aculyn the pH of the dip-coat solution remains virtually unchanged (pH ~ 2). After drying also the Amberlyst activity appears not to be altered significantly by the addition of Aculyn. However, increase of the pH of the solution, to adjust the rheology, has a disastrous effect on the Amberlyst activity. After drying of the final Aculyn containing dip-coat solution, the Amberlyst catalyst no longer shows any activity. Therefore, the membranes have been treated with sulphuric acid after the deposition of the catalytic layer to regenerate the active sites in the catalyst.

7.3.2 Amberlyst coating

The dip-coating of Amberlyst 15 on composite ceramic/PVA membranes has been evaluated. Figure 7.3 shows an Amberlyst-coated PVA membrane obtained from a 5 wt.% Amberlyst dip-coat solution.

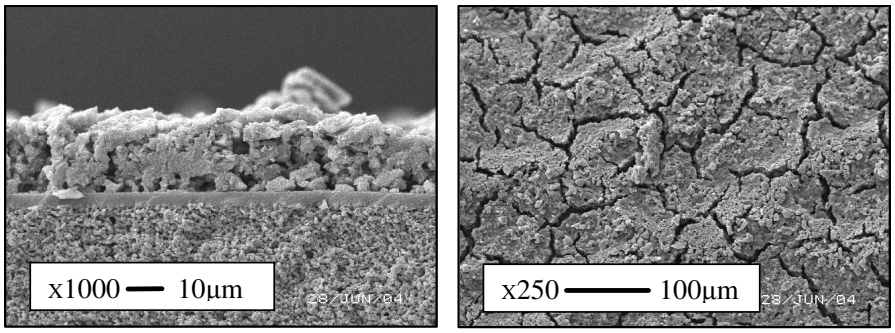

Figure 7.3 SEM pictures of an Amberlyst-coated PVA membrane, prepared with a 5 wt.% Amberlyst suspension in water, membrane TNO-PVA-3a. (a) top view; (b) side view.

It can be seen that an Amberlyst 15 layer with a thickness of around 25 µm (~40 mg) is obtained corresponding to a catalyst loading of 20 $g \cdot m^{-2}$. To increase the catalyst loading on the membrane surface, multiple dip-coat steps have been performed. The amount of deposited Amberlyst 15 shows a linear relationship with the number of dip-coat steps, as can be seen in Figure 7.4. Consequently, the catalytic layer thickness, and hence the amount of catalyst, can be adjusted by varying the number of dip-coat steps.

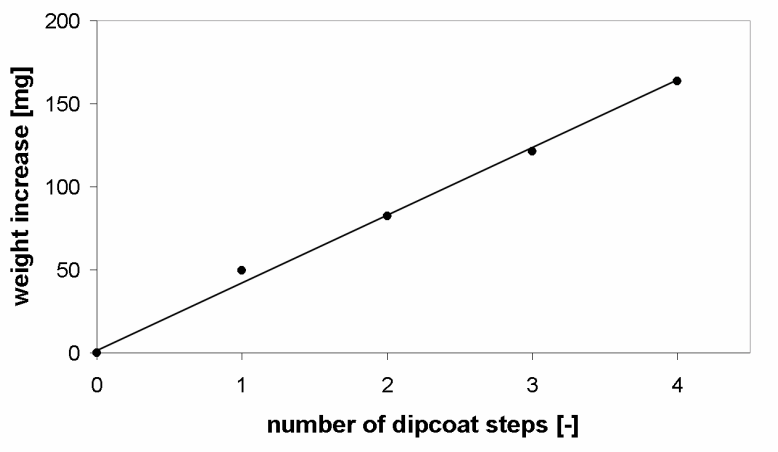

Figure 7.4 Number of deposited Amberlyst 15 as a function of the number of dip-coat steps, membrane TNO-PVA-3b.

7.3.3 Effect of the Amberlyst coating on the pervaporation performance

The effect of the Amberlyst 15 coating on the pervaporation performance of the composite ceramic/PVA membrane has been determined in the dehydration of *1*-butanol. The results are presented in Figure 7.5.

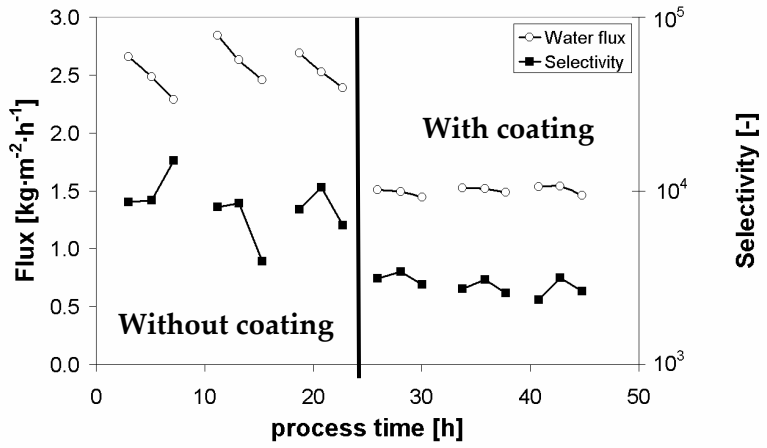

Figure 7.5 Effect of Amberlyst coating on membrane performance in the dehydration of *1*-butanol, 80°C, 5 wt.% water, membrane TNO-PVA-3a.

It can be seen that a stabilised flux, which is around 40% lower than the value before Amberlyst deposition, is obtained after deposition of an Amberlyst coating on top of the water selective layer of the membrane. As was seen previously [Peters *et al.*, 2006b] a similar flux decrease is also found in the start-up of a dehydration experiment (see Figure 5.2). This flux decrease is attributed to the decrease in swelling during the stabilisation period. Possibly, the additional layer on top of the membrane prevents swelling of the selective layer. Consequently, the initial water flux lies around the value for the stabilised flux. This assumption implies that the resistance to water transport in the catalytic layer would be negligible. The separation selectivity also seems to have decreased after membrane coating. However, it is likely that this decrease is due to the removal of the membrane from the experimental set-up, the dip-coat procedure, and the subsequent placement in the set-up. Figures 7.6 and 7.7 show SEM pictures taken from the composite membrane directly after coating and after the pervaporation measurements, respectively.

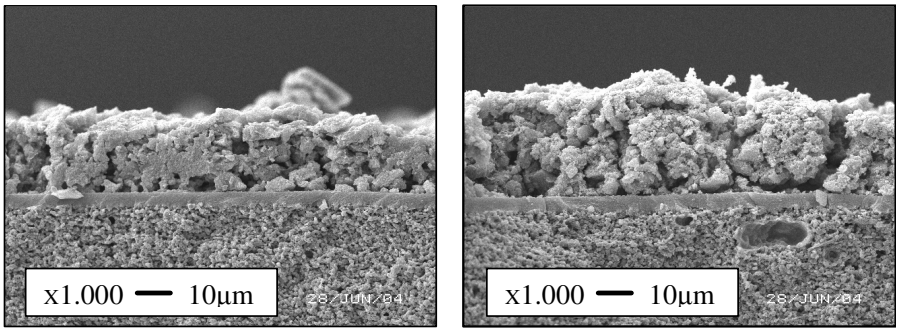

Figure 7.6 SEM pictures of an Amberlyst-coated membrane (a) side view; (b) side view after 20 hours of pervaporation; membrane TNO-PVA-3a.

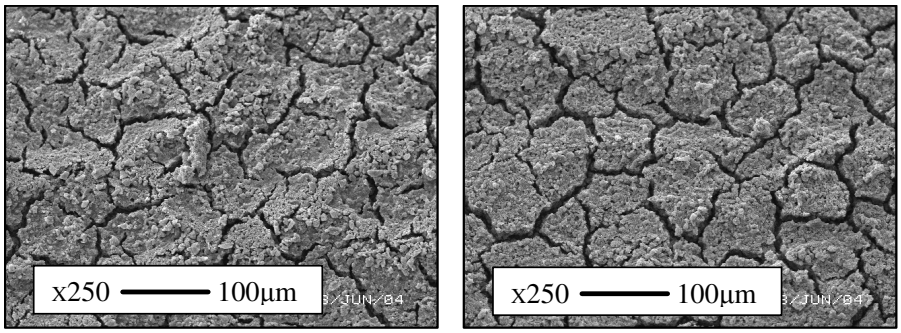

Figure 7.7 SEM pictures of an Amberlyst-coated membrane (a) top view; (b) top view after 20 hours of pervaporation; membrane TNO-PVA-3a.

From Figure 7.6 it can be seen that an Amberlyst 15 coating of around 25 µm is present on top of the membrane. The structural stability is excellent as the layer is intact after 30 hours of pervaporation although a "dried-mud like" Amberlyst 15 layer is formed (see Figure 7.7).

7.3.4 Pervaporation-esterification coupling

The catalytic function of the Amberlyst-coated pervaporation membrane combined with its selective features has been tested in the esterification reaction between acetic acid and butanol. For this, a membrane is selected which is coated with a catalytic layer thickness of 95 µm (see Figure 7.10b) corresponding to a total amount of around 200 mg. Amberlyst coverages up to 100 $g \cdot m^{-2}$ of membrane area, which translates to reactor loadings of Amberlyst up to 400 $kg \cdot m^{-3}$ of reactor volume, are obtained.

Using an equimolar stream of acetic acid and butanol, a substantial conversion could be reached within a reasonable time using the Amberlyst-coated membrane. The results are shown in Figures 7.8 and 7.9.

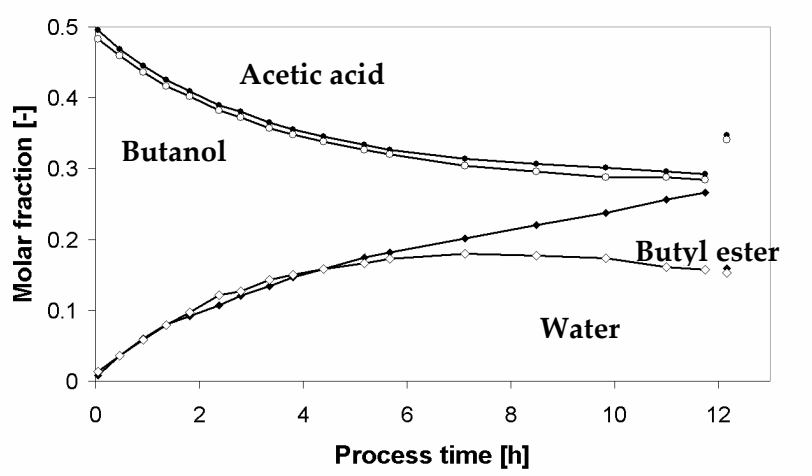

Figure 7.8 Mol fractions in the composite catalytic membrane assisted esterification of acetic acid and butanol at 75°C, membrane TNO-PVA-3b.

From Figure 7.8 it can be seen that the initial reaction rate is high whereas the water removal rate is low. Consequently, the acetic acid and butanol fraction decrease, while the water and ester fraction increase during the course of the reaction. After five hours the water fraction starts to deviate from the ester fraction, which shows the selective function of the membrane. The water fraction in the reactor reaches a maximum after a process time of seven hours when the rate of water formation equals the water removal rate. The performance of the composite membrane reactor, however, seems to be limited by the water removal rate because a substantial amount of water remains present in the reactor. This is confirmed in Figure 7.9, in which the conversion of the catalytic membrane-assisted esterification reaction is depicted as a function of process time. From this figure it can be seen that the slope of the conversion-time curve decreases in time, whereas for a kinetically controlled system the slope would be constant.

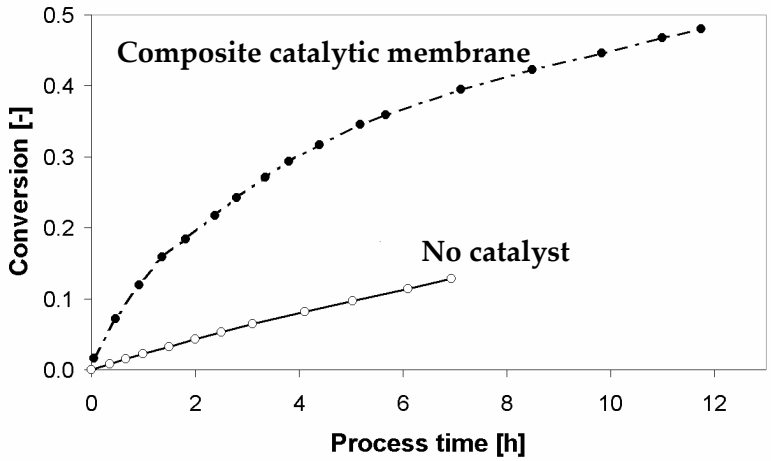

Figure 7.9 Conversion of acetic acid in the composite catalytic membrane assisted esterification of acetic acid and butanol at 75°C, membrane TNO-PVA-3b.

The reached conversion of the catalytic membrane-assisted esterification reaction, however, clearly exceeds the conversion reached for a membrane-assisted reaction in which no catalyst is present, showing the catalytic function of the composite membrane. The coated membrane exhibits an activity of $1.8 \cdot 10^{-8}$ $m^3 \cdot mol^{-1} \cdot s^{-1} \cdot g_{cat}^{-1}$, which is the same value as given in Table 7.1 for the unsupported powderous catalyst.

Figure 7.10 shows SEM pictures obtained from the membrane after 12 hours of reaction. From Figure 7.10b it can be seen that a catalytic layer with a thickness of around 95 μm is present on top of the composite ceramic/PVA membrane. The structural stability is excellent as the layer is intact after 12 hours of process although a "dried-mud like" Amberlyst 15 layer is formed as can be seen in Figure 7.10.

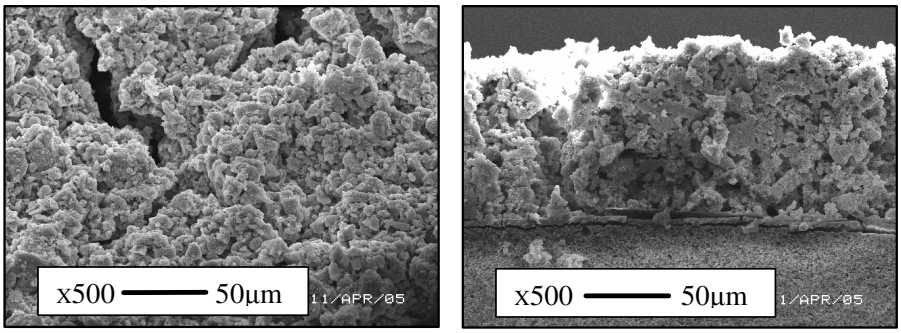

Figure 7.10 SEM pictures of the Amberlyst-coated membrane after 12 hours of reaction conditions, membrane TNO-PVA-3b. (a) top-view; (b) side-view;

Influence of the catalytic layer thickness

The catalytic function of the Amberlyst-coated pervaporation membrane combined with its selective features has been tested as a function of the catalytic layer thickness. For this, two membranes have been selected which have been coated with an Amberlyst layer of 70 and 95 µm, respectively. The characteristics of the Amberlyst-coated membranes are shown in Table 7.3 and Figure 7.11, respectively. Figure 7.12 show the water and butyl acetate fraction as a function of the process time for both membranes as obtained in the pervaporation-assisted esterification reaction.

Table 7.3 Properties of the catalytic membranes.

Membrane	Catalytic layer thickness [µm]	Amberlyst loading [mg]	Catalytic loading [g·m^{-2}]
TNO-PVA-4d	70	120	65
TNO-PVA-3b	95	180	105

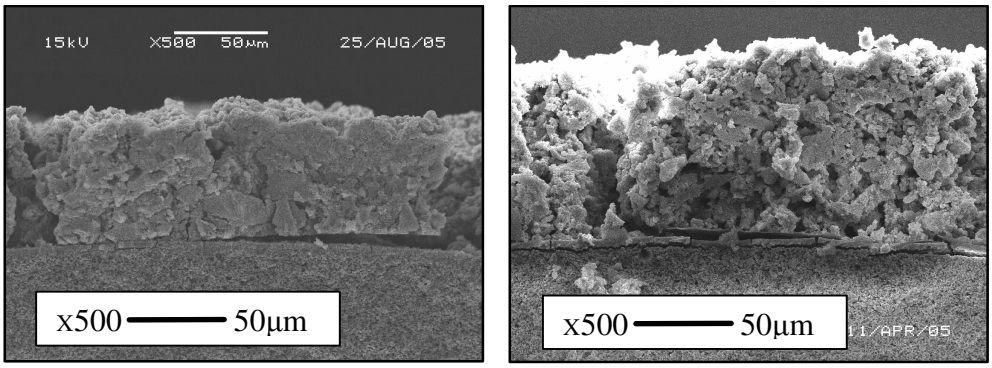

Figure 7.11 SEM pictures of the Amberlyst-coated membrane after 12 hours of reaction conditions. (a) membrane TNO-PVA-4d; (b) membrane TNO-PVA-3b.

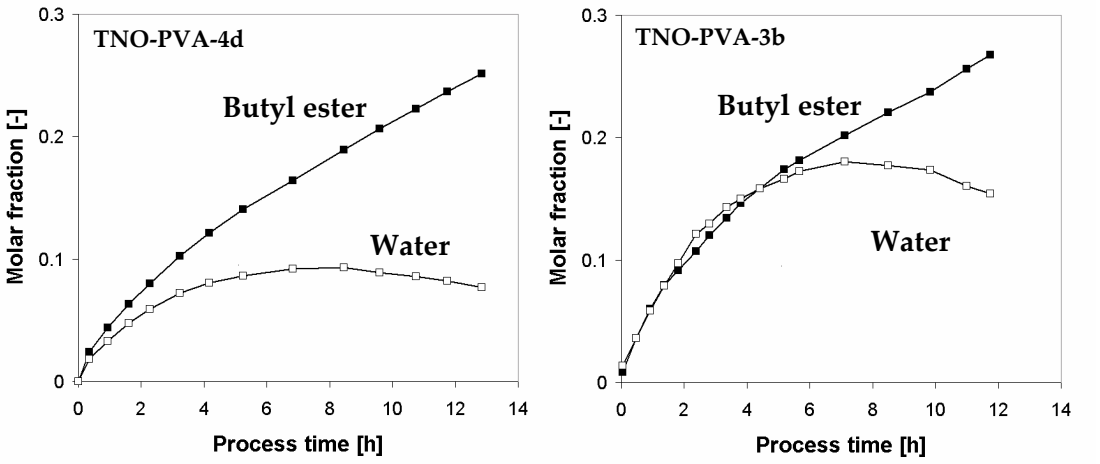

Figure 7.12 Water and ester fraction in the composite catalytic membrane assisted esterification of acetic acid and butanol at 75°C, (a) membrane TNO-PVA-4d; (b) membrane TNO-PVA-3b.

In the beginning of the process, the rate of chemical reaction is high, whereas water concentration is low. Consequently, water concentration gradually increases resulting in a higher water removal rate. At the same time the rate of chemical reaction, *i.e.*, the production rate of water, decreases. After a certain process time the water formation and removal

rate become equal and a maximum water concentration is observed. As can be seen from Figure 7.12, the increase in catalytic loading results in an increase in the maximum water fraction due to a higher reaction rate.

In Figure 7.13 the reached conversion obtained for membrane TNO-PVA-4d and TNO-PVA-3b is depicted as a function of the process time.

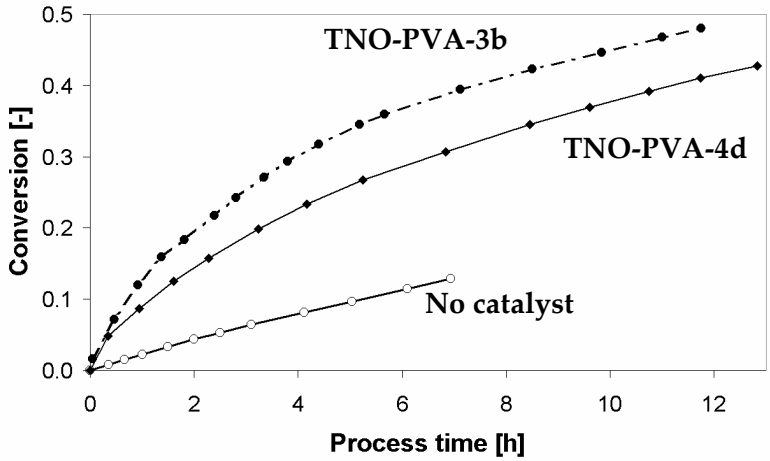

Figure 7.13 Conversion of acetic acid in the composite catalytic membrane assisted esterification of acetic acid and butanol at 75°C, membrane TNO-PVA-3b and TNO-PVA-4d.

For both membranes the reached conversion exceed the conversion reached for membrane-assisted reaction in which no catalyst is present. Although the water fraction in the reactor for membrane TNO-PVA-3b is higher as compared to membrane TNO-PVA-4d, the reached conversion is higher due to the higher catalytic loading. For membrane TNO-PVA-3b the average total flux and permeate water concentration is 0.09 $kg \cdot m^{-2} \cdot h^{-1}$ and 0.88, respectively. For membrane TNO-PVA-4d, however, the selectivity is much lower: the average total flux equals 0.19 $kg \cdot m^{-2} \cdot h^{-1}$ whereas the permeate water fraction is only 0.51. Although a catalytically active membrane is considered to be useful in promoting a desired chemical reaction even with a relatively poor intrinsic selectivity [Waldburger and Widmer, 1996], this means that relatively a large amount of acetic acid and

butanol is removed from the reaction mixture if the membrane used does not provide enough selectivity.

7.4 Conclusions

Composite catalytically active membranes can be used to enhance conversion of esterification reactions as the reaction and separation function are efficiently coupled. An additional advantage is that both the selective layer and the catalytic layer can be optimised independently. In this work, composite catalytic membranes have been prepared by dip-coating. Catalytic Amberlyst 15 layers have been deposited on composite ceramic/PVA membranes using Aculyn as rheology modifier. Tuning of catalytic layer thickness is possible by varying the number of dip-coat steps. Although a "dried-mud like" Amberlyst 15 layer is formed, the mechanical stability of the layer for both pervaporation and reaction experimental conditions appears to be sufficient. The resistance to water transport in the catalytic layer is found to be negligible.

In the pervaporation-assisted esterification reaction between acetic acid and butanol, the catalytic membrane is able to couple catalytic activity and water removal. After dip-coating and subsequent regeneration the high activity of the Amberlyst catalyst is re-established. In contrast to zeolite-coated pervaporation membranes, the performance of the Amberlyst-coated membrane is limited by the water removal rate.

Acknowledgements

This work was performed in a cooperative project of the Centre for Separation Technology and was financially supported by TNO and NOVEM.

Nomenclature

x_i	molar fraction retentate	[mol·mol^{-1}]
y_i	molar fraction permeate	[mol·mol^{-1}]
	Subscripts	
i	component i	

j component *j*

References

Bagnall, L., Cavell, K., Hodges, A.M., Mau, A.W., Seen, A.J., The use of catalytically active pervaporation membranes in esterification reactions to simultaneously increase product yield and permselectivity flux, *J. Membr. Sci.,* 85 (1993) 291-299.

David, M.O., Gref. R., Nguyen, T.Q., Neel, J., Pervaporation-esterification coupling. I. Basic kinetic model. *Trans. IChemE, Part A, Chem. Eng. Res. Des.*, 69 (1991) 335-340.

Beers, A.E.W., Nijhuis, T.A., Aalders, N., Kapteijn, F., Moulijn, J.A., BEA coating of structured supports – performance in acylation, *Appl. Catal. A*, 243 (2003) 237-250.

Bernal, M.P., Coronas, J., Menéndez, M., Santamaría, J., Coupling of reaction and separation at the microscopic level: esterification processes in a H-ZSM-5 membrane reactor, *Chem. Eng. Sci.,* 57 (2002) 1557-1562.

Chen, X., Xu, Z., Okuhara, T., Liquid phase esterification of acrylic acid with 1-butanol catalyzed by solid acid catalysts, *Appl. Catal. A*, 180 (1999) 261-269.

Liu, W.T., Tan, C.S., Liquid-phase esterification of propionic acid with n-butanol, *Ind. Eng. Chem. Res.*, 40 (2001) 3281-3286.

McKetta, J.J., Encyclopedia of chemical processing and design, Marcel Dekker, Vol 19 (1983).

Nguyen, Q.T., M'Bareck C.O., David, M.O., Métayer, M., Alexandre, S., Ion-exchange membranes made of semi-interpenetrating polymer networks, used for pervaporation-assisted esterification and ion transport, *Mat. Res. Innovat.,* 7 (2003) 212-219.

Peters, T.A., Fontalvo, J., Vorstman, M.A.G., Keurentjes, J.T.F., Design directions for composite catalytic hollow fibre membranes for condensation reactions, *Trans. IChemE, Part A, Chem. Eng. Res. Des.*, 82 (2004) 220-228.

Peters, T.A., van der Tuin, J., Houssin, C., Vorstman, M.A.G., Benes, N.E., Vroon, Z.A.E.P., Holmen, A., Keurentjes, J.T.F., Preparation of zeolite-

coated pervaporation membranes for the integration of reaction and separation, *Catal. Today*, 104 (2005a) 288-295.

Peters, T.A., Fontalvo, J., Vorstman, M.A.G., Benes, N.E., van Dam, R.A., Vroon, Z.A.E.P., van Soest-Vercammen, E.L.J., Keurentjes, J.T.F., Hollow fibre microporous silica membranes for gas separation and pervaporation: synthesis, performance and stability, *J. Membr. Sci.,* 248 (2005b) 73-80.

Peters, T.A., Benes, N.E., Holmen, A., Keurentjes, J.T.F., Comparison of commercial solid acid catalysts for the esterification of acetic acid with butanol, *Appl. Catal. A: General*, 297 (2006) 182-188.

Peters, T.A., Poeth, C.H.S., Benes, N.E., Buijs, H.C.W.M. Buijs, Vercauteren, F.F., Keurentjes, J.T.F., Ceramic-supported thin PVA pervaporation membranes combining high flux and high selectivity; contradicting the flux-selectivity paradigm, *J. Membr. Sci.,* (2006b) accepted.

Ueda, N., Matsubaou, K., Ikeda, K., Inoue, K., Yamamoto, S., Io, H., Organic polymer-coated cation-exchange resin-type catalysts and their use in hydration of olefins, Japanse Patent, JP 11076830 (1999).

Verkerk, A.W., van Male, P., Vorstman, M.A.G., Keurentjes, J.T.F., Properties of high flux ceramic pervaporation membranes for dehydration of alcohol/water mixtures, *Sep. Pur. Technol.*, 22-23 (2001) 689-695.

Waldburger, R.M., Widmer, F., Membrane reactors in chemical production processes and the application to the pervaporation-assisted esterification, *Chem. Eng. Technol.*, 19 (1996) 117-126.

Yadav, G.D., Mehta, P.H., Heterogeneous Catalysis in esterification Reactions: Preparation of phenethyl acetate and cyclohexyl acetate by using a variety of solid acidic catalysts, *Ind. Eng. Chem. Res.*, 33 (1994) 2198-2208.

Yadav, G.D., Thathagar, M.B., Esterification of maleic acid with ethanol over cation-exchange resin catalysts, *React. Funct. Polym.*, 52 (2002) 99-110.

Xu, Z.P., Chuang, K.T., Kinetics of acetic acid esterification over ion exchange catalysts, *Can. J. Chem. Eng*., 74 (1996) 493-500.

Chapter 8

Preliminary process design for catalytic pervaporation membrane-assisted esterification reactions

In this chapter, conventional production processes for esterification reactions are discussed. Subsequently, conceptual process configurations for hybrid pervaporation assisted esterification processes are presented. For two of these configurations preliminary large scale reactor evaluations are carried out using experimental data, *e.g.*, membrane permeability and catalyst activity. In a pervaporation plug flow reactor a thin layer of Amberlyst coated onto the membrane surface is sufficient to reach high conversions. However, for this configuration equilibrium conversion is obtained already in the beginning of the process and consequently a large part of the catalyst-coated membrane area is used inefficiently. As an alternative, an equilibrium mixture from which the majority of water is removed can be fed to the catalytic membrane module. In this way the coupling of water production and removal can be tuned more easily.

This chapter is partially based on: Peters, T.A., Benes, N.E., Keurentjes, J.T.F., *Zeolite-coated ceramic pervaporation membranes; pervaporation-esterification coupling and reactor evaluation*, Ind. Eng. Chem. Res., 44 (2005) 9490-9496.

8.1 Introduction

Esterification reactions represent a significant group of reactions commonly found in the chemical industry. Esterifications are typical examples of reactions, which are controlled by thermodynamic equilibrium. As a result, these reactions are faced with problems in product purification. The general steps for esterification processes include the reaction, removal of excess alcohol by distillation, catalyst neutralisation, drying, filtration to remove salts, steam treatment for deodorisation, decolourisation by active carbon, and final filtration [McKetta, 1983].

8.1.1 Conventional processes

A large number of industrial esterification processes have been developed. Esterifications are generally carried out using a homogeneous catalyst and the reaction mixture is re-fluxed until all the water has been removed [Holtmann, 1999]. The method to achieve complete conversion depends on the boiling point of the components and whether the units are operated batch-wise or continuously. Basically, three possibilities exist [McKetta, 1983].

(1) the boiling point of the ester is lower than that of water. In this case, the ester can be distilled off together with the alcohol. This method is for example used to produce methyl acetate, which forms an azeotrope with methanol; (2) ester and water can be distilled off together, usually as an azeotropic mixture. On condensation, the mixture separates into an ester and a water phase. To achieve complete separation, water or steam is often added to the reaction mixture. An example of this method is the production of butyl acetate; (3) the boiling point of the ester is higher than that of water. In this case, the water is distilled off, frequently as an azeotrope with the alcohol. If the alcohol/water mixture separates into two phases, the alcohol can be recycled into the reaction mixture. If water and alcohol do not separate, fresh alcohol has to be added to the reaction mixture continuously, or an additional separation step is required. This method is used in the production of non-volatile esters, such as phthalates, adipates and oleates.

As an illustration of the complexity of conventional production processes, the classical scheme for the continuous production of ethyl or propyl esters of low-volatility acids is shown in Figure 8.1.

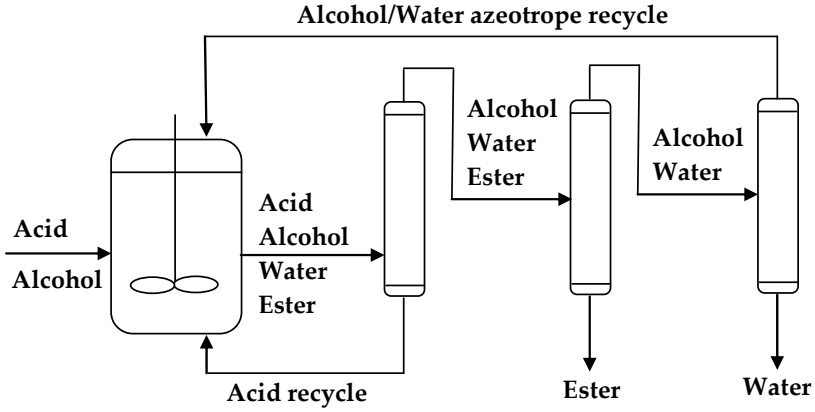

Figure 8.1 Classical scheme for the continuous production of ethyl/propyl esters of low-volatility acids.

Acid and alcohol are continuously fed into a reactor containing an excess of alcohol. The reaction mixture, containing alcohol, ester, water and some unreacted acid is taken from the reactor and is led over three distillation columns to remove the ester product and water as by-product. The unreacted alcohol is recycled back into the reactor. In the first column, the least-volatile component, unreacted acetic acid, is taken out as the bottom product and is recycled back to the reactor. Alcohol, water and the product ester are fed to a second column in which ester is removed as the bottom product. The overhead, water and alcohol, is fed to the third column in which water is removed and alcohol, in the form of a water/alcohol azeotrope is recycled back to the reactor.

A drawback of the conventional esterification processes is that a high concentration of water is permanently present in the reactor requiring a large excess of alcohol to drive the reaction. Additionally, the recovered ester is contaminated with quantities of water, causing product hydrolysis that decreases its purity, quality and usability for many applications. Furthermore, distillation is a high-energy demanding operation, which is

not recommended when dealing with temperature sensitive chemicals. Moreover, the necessity of an entrainer to separate the alcohol/water mixture requires the additional effort to clean and recycle this auxiliary agent. In this perspective, pervaporation has attracted attention as an alternative to conventional esterification processes.

8.1.2 Pervaporation

Pervaporation is a promising separation technique for the selective removal of water from liquid mixtures. Currently, about one hundred pervaporation units are operating worldwide, most of them dehydrating solvents, such as ethanol and 2-propanol. Now that pervaporation has been proven in end-of-pipe solutions, attention is turning to separations closer to the chemical reaction step [Wynn, 2001]. In most applications, pervaporation is not used as a stand-alone process but is combined with a second technique, for example a chemical reactor or a distillation column in a so-called hybrid process [Lipnizki *et al.*, 1999; van Hoof *et al.*, 2003]. These integrated processes allow lower equipment and energy cost in comparison to stand-alone processes [Sommer, 2002].

In pervaporation-esterification coupling, one side of a membrane is exposed to the liquid phase, while at the other side of the membrane vacuum is maintained. Water permeates preferentially through the membrane and evaporates, which drives the esterification reaction to the ester-side. Pervaporation reactors are attractive because the reaction can be carried out at the desired temperature, and the separation efficiency in pervaporation is not determined by the relative volatility as in reactive distillation [Benedict *et al.*, 2003]. Additionally, in pervaporation only the heat of vaporisation of the permeating component has to be supplied. Therefore, pervaporation is in many cases a more energy-efficient alternative for distillation, in which reboiling is responsible for ~75% of the total energy requirement. A techno-economical feasibility study has shown that the energy required in pervaporation decreases to only 16% of the total energy use in extractive distillation (per ton product) [van Veen, 2001]. In total, the production costs for esters by an esterification process based upon pervaporation are 30% lower than in the distillation process. Additionally, it has been proven that the costs of the required membrane modules are only a small part of the total production costs [van Veen, 2001].

8.2 Pervaporation-esterification processes

8.2.1 Process configurations

In general, several possibilities exist to implement the pervaporation module in the hybrid pervaporation process [Dams and Krug, 1991; Lim *et al.*, 2002]. In Figure 8.2, conceptual process flow diagrams for the batch, semi-batch, semi-batch continuous and continuous pervaporation-assisted esterification process are presented.

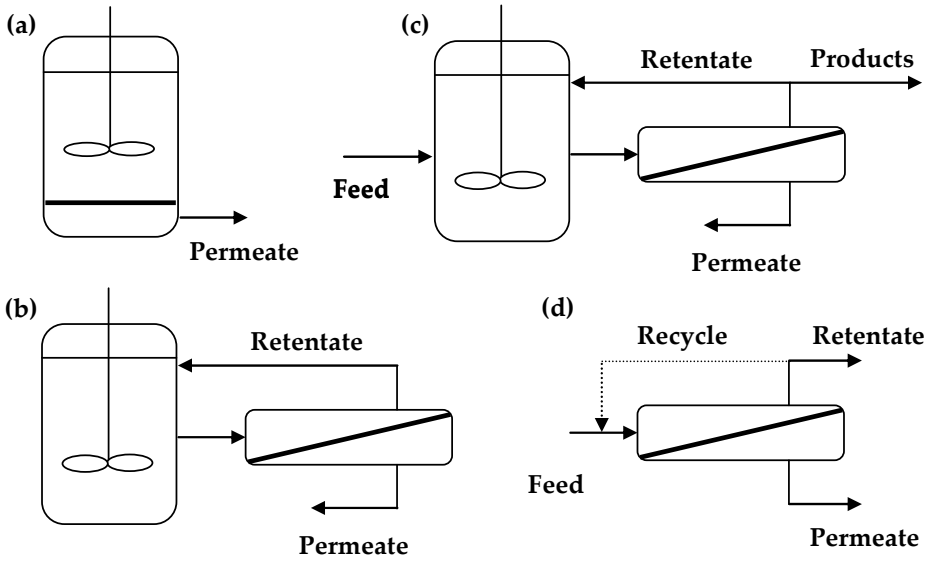

Figure 8.2 Conceptual process flow diagrams of pervaporation-assisted esterification processes. (a) batch pervaporation membrane reactor; (b) recycle batch pervaporation membrane reactor; (c) recycle continuous pervaporation membrane reactor; (d) plug-flow pervaporation membrane reactor.

The batch (Figure 8.2a) and the recycle batch (Figure 8.2b) pervaporation membrane reactor are the most commonly studied pervaporation membrane reactors [Lipnizki *et al.*, 1999]. In the batch pervaporation membrane reactor, a membrane is present in the stirred esterification reactor. In the recycle batch pervaporation membrane reactor the

membrane and the reactor are placed into two separate units, as shown in Figure 8.2b. In this process, the liquid reaction mixture from the esterification process is dehydrated in the membrane unit and recirculated to the reactor. This offers the advantage that the membrane area is decoupled from the reactor volume, which is an important consideration for low permeability membranes or for fast reactions. Additionally, it offers ease in membrane clean-up: two membrane modules can be employed, one in operation, while the other is in clean-up or regeneration. Moreover, in the case of membrane failure the chemical reactor can be maintained in operation in combination with a second membrane module.

Figure 8.2c shows the recycle continuous pervaporation membrane reactor. As compared to the recycle batch pervaporation membrane reactor (Figure 8.2b), a feed and a product stream are added to the configuration in order to produce products continuously. Continuous processes are usually employed for large volume products since these processes are less labour intensive. Batch processes are mainly advantageous when a variety of different products are produced in relatively small volumes using the same equipment.

In the plug flow continuous configuration the membrane and the reactor are combined in a single unit (Figure 8.2d). Combining the membrane and reactor into one single unit may offer advantages of process efficiency, compactness and flexibility due to its modular design, and reduction of energy input and investment and operating costs. Concerns exist, however, about the durability of membrane materials in harsh esterification conditions. Usually a recycle stream of the retentate is a pre-requisite for the process, because in most cases a single pass is unable to provide both a high purity retentate and permeate, not even at optimised process conditions. For the proposed process design in Figure 8.2b and c, vapour permeation could be a preferable alternative compared to pervaporation because high boiling inorganic acids and impurities remain in the liquid phase and do not affect the sensitive membrane material. This could lead to a longer life-time of the membrane, which is an important economic factor.

8.2.2 Operating parameters

For the performance of pervaporation-coupled esterification processes, the ratio of water production over water removal is found to be the key factor. The operating parameters affecting this ratio can be divided into three groups [Kemmere and Keurentjes, 2001].

- Operating parameters which affect the esterification reaction kinetics directly, *e.g.*, catalyst concentration and molar ratio of reactants;
- Parameters which influence the pervaporation process directly, *e.g.*, ratio of membrane area to the reactor volume;
- Parameters which simultaneously influence the esterification reaction kinetics and the pervaporation process, *e.g.*, temperature.

Based on both experimental and theoretical studies it was concluded that the temperature has the strongest influence on the performance because it affects both the kinetics of the esterification reaction and the pervaporation performance [Waldburger and Widmer, 1996]. The second important operating parameter is the initial molar ratio. For the process design depicted in Figure 8.2b and d, it has been found that the optimal alcohol to acid initial ratio is approximately 1.8 in the case of the esterification between acetic acid and methanol using a PVA water selective membrane [Assabumrungrat *et al.*, 2003]. A higher initial ratio results in a decreased acid concentration and thus a decreased reaction rate. On the other hand, at a feed ratio lower than the optimal the effect of alcohol loss through the membrane limits the conversion. Considering the parameters influencing the pervaporation process directly, the ratio of membrane area to reactor volume is important for batch processes. For continuous processes the flow rate compared to the available membrane area should be considered as the determining factor.

In the present study, a preliminary large scale catalytic membrane reactor evaluation is carried out based on the obtained experimental data for membrane permeability and catalyst activity. The composite catalytic membranes enable close and efficient integration of reaction and separation, while allowing independent optimisation of the catalytic and

separation function. Moreover, the catalyst coating might, to some extent, protect the membrane against mechanical damage.

Two process configurations are proposed. In the plug flow continuous configuration (configuration A, Figure 8.3), the membrane and the reactor are combined in a single unit. Usually a recycle stream of the retentate is required for the process, because in most cases a single pass provides insufficient retentate purity, even at optimised process conditions.

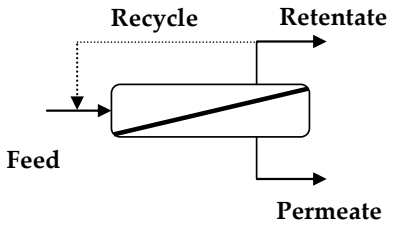

Figure 8.3 Conceptual process flow diagram for the plug-flow pervaporation membrane reactor.

Configuration B (Figure 8.4) consists of a reactor and two pervaporation modules. In this configuration, the liquid reaction mixture at equilibrium conversion from the esterification process is first dehydrated in the membrane unit to remove the excess of water. Subsequently, the mixture is lead through a module containing catalytic pervaporation membranes. In this configuration, the size of the catalytic membrane module can be reduced compared to configuration A because the volumetric feed is reduced (>25%) since the excess of water is removed. In the module containing the catalyst-coated membranes, the produced water is removed efficiently due to the close integration of reaction and separation.

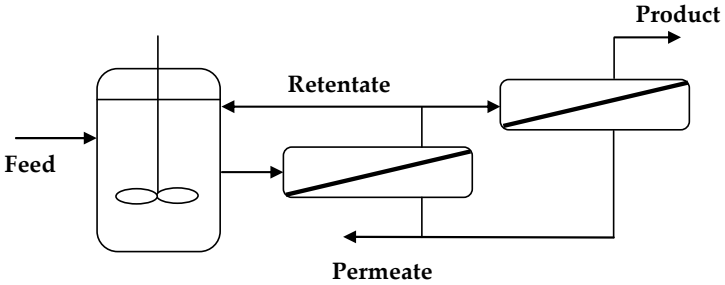

Figure 8.4 Conceptual process flow diagram containing two pervaporation modules.

8.3 Reactor evaluation

Due to the relatively low amount of catalyst compared to the area-to-volume ratio of the experimental laboratory set-up used in the experiments described in the previous chapters (<100 $m^2 \cdot m^{-3}$, instead of >2000 $m^2 \cdot m^{-3}$ in a practical membrane module) a substantial conversion could not be reached within a reasonable time scale. Therefore, in order to evaluate the performance of a larger scale practical membrane module, model simulations are performed. Additionally, the performance of a catalytic pervaporation membrane module is compared with the performance of a reactor in which the same loading of heterogeneous catalyst is simply dispersed in the bulk liquid.

Data used in the simulations, *e.g.*, membrane permeability and catalyst activity, are taken from the experiments described in the preceding chapters. The reactor dimensions are based on an annual production of 10.000 metric tons of butyl acetate. For configuration A, the feed consists of acetic acid and butanol in a stoichiometric ratio. For configuration B, the feed of the catalytic membrane module is an equilibrium mixture from which the majority of the water is removed. Along the length of the reactor water is removed continuously through the pervaporation membranes. The reactor is operated at 75°C and 1 bar. Based on a production rate of 1 $m^3 \cdot h^{-1}$ and a residence time of 6 hour, a reactor volume of 6 m^3 is required. This reactor volume corresponds to a catalyst loading up to 1300 kg. Using hollow fibre membranes with a diameter of 3 mm and a module void fraction of 0.2, a high membrane surface-area-to-volume ratio is obtained (4700 $m^2 \cdot m^{-3}$).

The reaction rate constant for the zeolite and Amberlyst-coated pervaporation membranes is estimated to be $9.2 \cdot 10^{-10}$ $m^3 \cdot mol^{-1} \cdot s^{-1} \cdot g_{cat}^{-1}$ and $1.8 \cdot 10^{-8}$ $m^3 \cdot mol^{-1} \cdot s^{-1} \cdot g_{cat}^{-1}$, respectively. In the calculations, the catalytic activity of the unsupported zeolite catalyst is taken 6.6% higher compared to the activity of the supported catalyst. As discussed in Chapter 7, the activity of the unsupported Amberlyst catalyst is equal to the activity of the supported catalyst. For both membranes, the membrane permeability is approximated to be $5.2 \cdot 10^{-7}$ $mol \cdot m^{-2} \cdot s^{-1} \cdot Pa^{-1}$.

Plug-flow pervaporation membrane reactor (Fig 8.3)

Figure 8.5 shows the conversion as a function of the catalytic layer thickness using the operating conditions previously mentioned obtained for zeolite-coated and Amberlyst-coated pervaporation membranes, respectively.

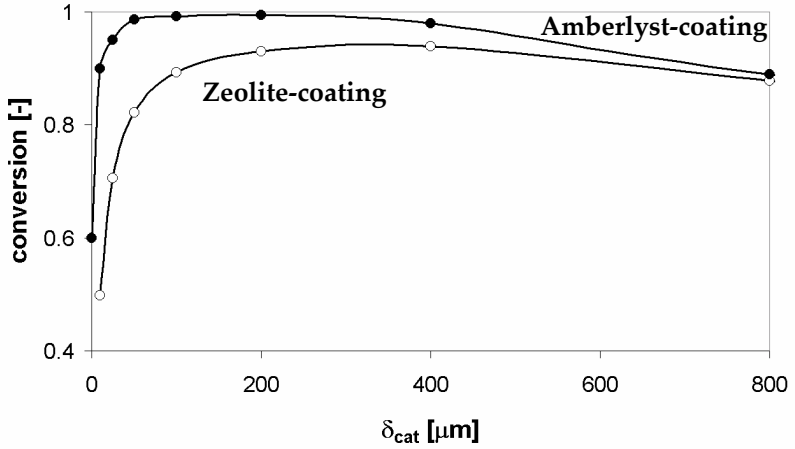

Figure 8.5 Effect of catalytic layer thickness on module performance; closed symbols.

From Figure 8.5 it can be seen that in a practical catalytic pervaporation membrane module, substantial conversions are reached within a reasonable timescale. The conversion obtained shows an optimum in conversion at a certain layer thickness, which value is a function of the reaction kinetics and membrane permeability [Peters *et al.*, 2004]. The increase in activity, by changing from zeolite-coated to Amberlyst-coated membranes, evidently results in an increase in conversion. In the case of the higher activity the diffusion of reactants inside the catalytic layer cannot keep up with the reaction rate, causing a decrease in the optimum catalytic layer thickness.

Because of the high catalytic activity of Amberlyst 15 as compared to H-USY zeolite coating, almost 100% conversion could be reached using Amberlyst-coated pervaporation membranes. However, equilibrium conversion is already reached in the initial stage of the process caused by

the fast reaction kinetics, due to the high catalytic activity and loading. As a result, the available membrane area is not sufficient to remove the water formed, leading to a significant increase in bulk water concentration. Consequently, a large part of the plug-flow membrane module is primarily used to remove the water formed in the initial stage of the reaction. In this perspective the performance of the catalytic membrane module might be enhanced by varying the spatial distribution of the different functionalities, *e.g.*, catalytic layer thickness along the length of the module [Lawrence *et al.*, 2005]. At the entrance of the module enough catalyst needs to be available in order to keep the reaction rate high whereas water removal is of less importance. In contrast, water removal has to be efficient at the exit of the reactor whereas the reaction rate, and thus the amount of catalyst, is less important. Hence, it would be advantageous to decrease the catalytic layer thickness along the length the module. To achieve the same effect, a sequence of modules having a different catalytic layer thickness can also be used. In this way the coupling of water production and removal can be tuned more easily. An extreme case for this approach is the configuration in which one single additional membrane module is implemented to remove the excess of water from an esterification mixture at equilibrium conversion. Consequently, the residence time in the catalytic membrane module can be reduced. In the following paragraph calculations based on this configuration are discussed.

Process flow diagram containing two pervaporation modules (Fig 8.4)

The second proposed configuration consists of a reactor and two pervaporation modules. In this configuration, the liquid reaction mixture from the esterification process is first dehydrated in a conventional pervaporation membrane unit to remove the excess of water. Subsequently, the mixture is lead through a module containing catalytic pervaporation membranes. Compared to the plug-flow pervaporation membrane reactor this implies that the feed of the catalytic membrane module is an equilibrium mixture from which the majority of the water is removed. Consequently, for configuration B selective water removal from the reaction mixture is critical whereas catalytic activity is of less importance. Figure 8.6 shows the effect of catalytic layer thickness and catalyst position on the performance of the catalytic pervaporation module.

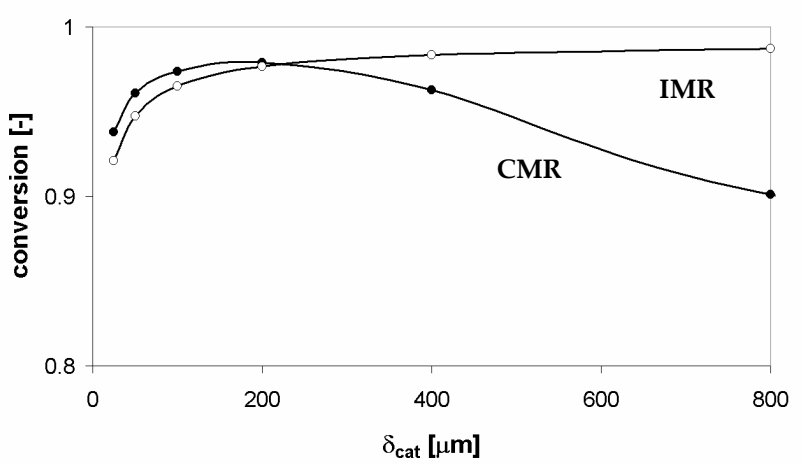

Figure 8.6 Effect of catalyst position and catalytic layer thickness on module performance; τ = 3 h; Feed: acetic acid; butanol; butyl acetate; water: 0.24; 0.24; 0.5; 0.02.

According to the performed reactor evaluation, Figure 8.6 suggests that the Amberlyst-coated membrane reactor, although only slightly, outperforms the reactor in which the catalyst is dispersed in the bulk liquid. Only for high catalytic loading the inert membrane reactor would perform better. However, from a practical point of view a high catalyst loading corresponds to an almost entirely filled void fraction between the membranes. As a consequence the module will behave as a packed bed membrane reactor, irrespective of the fact whether the catalyst is coated onto the membrane or dispersed in the liquid medium. Since transport limitations in the liquid phase are neglected, the performance of the inert membrane reactor is overestimated at high catalyst loadings. Hence, the process evaluation suggests that membranes coated with a thin Amberlyst layer can be an interesting option.

8.4 Conclusions

Composite catalytically active membranes can be used to enhance conversion of esterification reactions, as the reaction and separation functions are coupled very efficiently. An additional advantage of such

composite membranes is that both the selective layer and the catalytic layer can be optimized independently. Furthermore, the catalyst coating will, to some extent, protect the membrane against mechanical damage.

A preliminary reactor evaluation indicates that Amberlyst-coated membranes can be used to achieve high conversions, due to the high catalytic activity of Amberlyst. The reactor performance can be optimised by adjusting the catalytic layer thickness. Moreover, further optimisation can be achieved by varying the catalytic layer thickness over the length of the module. To achieve the same effect, a sequence of modules having a different catalytic layer thickness can also be used. In this way the coupling of water production and removal can be tuned more easily. A reactor evaluation has been carried out for an extreme situation, in which the feed to the final catalytic membrane reactor consists of a mixture at equilibrium, from which the excess of water is removed.

Acknowledgements

This work was performed in a cooperative project of the Centre for Separation Technology and was financially supported by TNO and NOVEM.

References

Assabumrungrat, S., Phongpatthanapanich, J., Praserthdam, P., Tagawa, T., Goto, S., Theoretical study on the synthesis of methyl acetate from methanol and acetic acid in pervaporation membrane reactors: effect of continuous-flow modes, *Chem. Eng. J.*, 95, (2003) 57-65.

Benedict, D.J., Parulekar, S.J., Tsai, S-P., Esterification of Lactic Acid and Ethanol with/without pervaporation, *Ind. Eng. Chem. Res.*, 42 (2003) 2282-2291.

Dams, A., Krug, J., Pervaporation-aided esterification – alternatives in plant extension for an existing chemical process, in: Bakish, R., (Ed.), *Proceedings of the Fifth International Conference on Pervaporation Processes in the Chemical Industry*, Bakish Material Corporation, Englewood, NJ, USA, (1991) 338-348.

Feng, X., Huang, R.Y.M., Studies of a membrane reactor: esterification facilitated by pervaporation, *Chem. Eng. Sci.*, 51 (1996) 4673-4679.

Holtmann, T., *Membranreaktoren zur Estersynthese*, Ph.D. thesis, Universität Dortmund, Shaker Verlag, Aachen, Germany, 2003.

van Hoof, V., van den Abeele, L., Buekenhoudt, A., Dotremont, C., Leysen, R., Economic comparison between azeotropic distillation and different hybrid systems combining distillation with pervaporation for the dehydration of isopropanol, *Sep. Pur. Technol.*, 37, (2004) 33-49.

Kemmere, M.F., Keurentjes, J.T.F., Industrial membrane reactors, in: Nunes, S.P., Peinemann, K.-V., (Eds.), *Membrane Technology*, Wiley-VCH, Weinheim, Germany (2001) 191-221.

Lawrence, P.S., Grünewald, M., Agar, D.W., Spatial distribution of functionalities in an adsorptive reactor at the particle level, *Catal. Today*, 105 (2005) 582-588.

Lim, S.Y., Park, B., Hung, F., Sahimi, M., Tsotsis, T.T., Design issues of pervaporation membrane reactors for esterification, *Chem. Eng. Sci.*, 57, (2002) 4933-4946.

Lipnizki, F., Field, R.W., Ten, P-K., Pervaporation-based hybrid process: a review of process design, applications and economics, *J. Membr. Sci.*, 153, (1999) 183-210.

Liu, K., Tong, Z., Liu, L., Feng, X., Separation of organic compounds from water by pervaporation in the production of *n*-butyl acetate via esterification by reactive distillation, *J. Membr. Sci.*, 256, (2005) 193-201.

McKetta, J.J., Encyclopedia of chemical processing and design, Marcel Dekker, Vol 19 (1983).

Peters, T.A., Fontalvo, J., Vorstman, M.A.G., Keurentjes, J.T.F., Design directions for composite catalytic hollow fibre membranes for condensation reactions, *Trans. IChemE, Part A, Chem. Eng. Res. Des.*, 82 (2004) 220-228.

Reid, E.E., 1952, Esterification, in *Unit Processes in Organic Synthesis*, 4th edition Groggins, P.H. (ed) (McGraw Hill, New York, USA) pp 596-642.

Sommer, S., *Pervaporation and vapour permeation with microporous inorganic membranes*, Ph.D. thesis, RWTH Aachen, Verlag Mainz, Germany, 2002.

van Veen, H.M., Reduction of energy consumption in the process industry by pervaporation with inorganic membranes: techno-economical feasibility study, *ECN-project report* (ECN-C--01-073) 2001.

Waldburger, R.M., Widmer, F., Membrane reactors in chemical production processes and the application to the pervaporation-assisted esterification, *Chem. Eng. Technol.*, 19 (1996) 117-126.

Wynn, N., Pervaporation comes of age, CEP magazine, 97 (2001) 66-72.

Chapter 9

Conclusions, recommendations and perspectives

In this thesis the preparation of composite catalytic pervaporation membranes and their application in condensation reactions has been investigated. These membranes enable close and efficient integration of reaction and separation, while allowing independent optimisation of the catalytic and separation functions. The present chapter summarises the conclusions and provides recommendations based on the findings of this work, ordered by chapter. Additionally, two possible future applications of the work presented in this thesis are discussed.

9.1 Conclusions and recommendations

In this thesis the preparation of composite catalytic pervaporation membranes for the integrated reaction and separation in condensation reactions has been investigated. First, a mathematical model has shown the added value of the composite membrane system compared to conventional reactor designs. Then, pervaporation membranes have been prepared by deposition of water selective microporous silica and cross-linked poly(vinyl)alcohol layers on the outer surface of hollow fibre ceramic substrates. The pervaporation performance of these membranes is extensively examined in the dehydration of various alcohols. Subsequently, catalytic pervaporation membranes have been developed by deposition of H-USY and Amberlyst 15 layers on silica and PVA membranes, respectively. Finally, the performance of the composite catalytic membranes as both separator and reactor has been examined in the esterification reaction between acetic acid and butanol.

Based on the findings of this work, the following conclusions and recommendations for future research can be given.

Pervaporation-esterification modelling

A mathematical model has shown the added value of the composite membrane/catalyst system compared to more usual reactor designs. Under the prevailing conditions, an optimum catalytic layer thickness has been found to be around 100 μm, which is practically feasible. At this optimum catalytic layer thickness, the performance of a catalytic membrane reactor might exceed the performance of an inert membrane reactor due to the close integration of reaction and separation. Using the model, catalytic membranes can be designed conveniently if both the reaction kinetic parameters and the membrane parameters are known.

Currently, several assumptions in the pervaporation-coupled esterification model have been made. For example, the membrane reactor is assumed to behave as an ideal isothermal plug-flow reactor. For a thorough analysis, the temperature drop along the length of the reactor, and axial diffusion in the catalytic layer need to be taken into account. Moreover, it is beneficial to adopt the Maxwell-Stefan approach for the description of diffusion in the catalytic layer, as this approach easily takes

into account drift fluxes caused by the water removal through the membrane. Additionally, the effect of the membrane selectivity on the reactor performance has to be considered. For membranes showing a moderate selectivity, it is more efficient to operate the reactor with a feed composition of the alcohol higher than the stoichiometric value due to the loss of reactant through the membrane [Assabumrungrat *et al.*, 2003].

Solid acid catalysis of esterification reactions

Esterification of acetic acid with butanol has been studied in a heterogeneous reaction system, using a variety of solid acid catalysts. The catalysts have been characterised using gas adsorption analysis (BET), X-ray diffraction (XRD), scanning electron microscopy (SEM) and the temperature-programmed decomposition (TPD) of adsorbed isopropylamine. The weight-based activity of the heterogeneous catalysts decreases in the following order: Smopex-101 > Amberlyst 15 > sulphated ZrO_2 > H-USY-20 > H-BETA-12.5 > H-MOR-45 > Nb_2O_5 > H-ZSM-5-12.5.

In the heterogeneous catalysis of esterifications using zeolites and sulphated zirconia, no clear relationship has been observed between the total amount of acid sites, measured with the temperature-programmed decomposition of isopropylamine, and the catalytic activity. In order to get more insight it is necessary to discriminate between Brønsted and Lewis acid sites, *e.g.*, using infrared spectroscopy on adsorbed ammonia or pyridine [Meloni *et al.*, 2001], or using solid state MAS NMR spectroscopy [Sutovich *et al.*, 1999]. In this way, it is also possible to obtain more insight in the esterification mechanism using heterogeneous catalysts [Koster *et al.*, 2001]. Moreover, the long-term stability of the heterogeneous catalysts in the esterification reaction needs to be examined further.

Hollow fibre silica membranes

Thin microporous silica membranes were prepared on the outer surface of hollow fibre ceramic substrates. In principle this enables relatively fast and inexpensive production of a large membrane surface area, combined with a low support resistance and a high membrane surface area / module volume ratio (> 1000 $m^2 \cdot m^{-3}$) compared to tubular membranes.

High He permeances ($1.1\text{-}2.9\cdot10^{-6}$ $mol\cdot m^{-2}\cdot s^{-1}\cdot Pa^{-1}$), high He/N_2 permselectivities (~ 100-1000) and an Arrhenius type temperature dependence of gas permeance indicate that the membranes are microporous and have a low number of defects. However, for pervaporation purposes the stability of the γ-alumina intermediate layer and the silica top layer remains an issue. More chemically resistant materials, like zirconia and titania have been applied on flat plate geometries in order to increase the membrane stability [van Gestel et al., 2002]. However, their application on hollow fibre supports is not straightforward and therefore all steps in the preparation method, *e.g.*, sol-gel synthesis, dip-coat procedure and sintering strategy need to be optimised for hollow fibre supports.

Composite ceramic-supported PVA pervaporation membranes

Thin, high-flux and highly selective cross-linked poly(vinyl)alcohol water selective layers have been prepared on top of hollow fibre ceramic supports. The thickness of the PVA top layer is in the order of 0.3 - 0.8 μm, and no substantial infiltration of PVA into the intermediate $\gamma\text{-}Al_2O_3$ layer is observed. In the dehydration of *1*-butanol (80°C, 5 wt.% water) the membranes exhibit a high water flux (0.8 - 2.6 $kg\cdot m^{-2}\cdot h^{-1}$), combined with a high separation factor (500 - 10.000). In the dehydration of *2*-propanol and *1*-butanol, a simultaneous increase in both water flux and separation factor is observed with increasing temperature or water concentration. A possible explanation for this behaviour is a low degree of three dimensional swelling in the vicinity of the $\gamma\text{-}Al_2O_3$ – PVA interface due to an enhanced structural stability.

The expensive ceramic support can easily be regenerated, *i.e.*, the organic layer can be removed either by washing the membrane with an appropriate solvent, or by thermal treatment. In contrast, full ceramic membranes have to be replaced and disposed of after contamination or damage. The application window for these newly developed composite polymer/ceramic membranes is limited to 95°C.

By optimisation of the parameters in the preparative route, *i.e.*, cross-linking agent and content, annealing temperature and time, and the properties of the ceramic support, the separation performance can be improved. Additionally, blending of poly(vinyl)alcohol with other

polymers, like poly(acrylic)acid [Burshe *et al.*, 1998], or incorporation of inorganic fillers, like tetraethoxysilane [Urigami *et al.*, 2002] or zirconia [Kim *et al.*, 2001] in the PVA selective layer can also enhance membrane performance.

In general, ceramic materials as a stable support structure for polymeric membranes could play an important role in enhancing membrane stability in all applications in which swelling of the polymeric selective membrane layer has to be minimised. As an example, the application of ceramic supports in the development of stable membranes for the removal of VOCs from waste water, and for the separation of organic/organic mixtures is demonstrated in paragraph 9.2.1.

Zeolite-coated pervaporation membranes

Catalytic pervaporation membranes have been developed by deposition of H-USY zeolite on top of ceramic silica membranes. Tuning of the catalytic layer thickness is possible by varying the number of dip-coat steps. In the pervaporation-assisted esterification reaction, the catalyst-coated pervaporation membrane is able to couple catalytic activity and water removal. However, the performance of the H-USY-coated membrane is mainly limited by reaction kinetics. Consequently, this type of catalytic pervaporation membranes might be applicable in the case where water removal from the reaction mixture becomes critical, *e.g.*, esterification mixtures with a high conversion or condensation reactions with a very low equilibrium conversion. In this perspective, the application of catalytic pervaporation membranes in the direct synthesis of dimethyl carbonate starting from methanol and carbon dioxide might greatly benefit from the integration of catalytic reaction and water removal due to the very low equilibrium conversion. This application is discussed more elaborately in paragraph 9.2.2.

Amberlyst-coated pervaporation membranes

Catalytic Amberlyst 15 layers have been deposited on composite ceramic/PVA membranes by a dip-coat technique using Aculyn as binder material. Due to the high activity of the Amberlyst catalyst, the performance of the Amberlyst-coated membrane is limited by the water

removal rate. This in contrast to zeolite-coated pervaporation membranes, which performance is limited by the catalytic activity.

A further improvement in reactor performance can be realised by optimisation of the catalytic layer in terms of thickness and, for example, porosity. In this way, the coupling between the water production and removal can be optimised. Aside from pervaporation-assisted esterifications, Amberlyst-coated pervaporation membranes could also be applied in the synthesis of diethylacetal, which is formed in the liquid phase by a reversible reaction between acetaldehyde and ethanol forming water as a by-product [Silva and Rodriquez, 2001]. In this perspective, a catalytic pervaporation membrane reactor can be an alternative for currently available technologies, *e.g.*, chromatographic and distillation techniques [Silva and Rodriquez, 2002].

Process design for catalytic pervaporation membrane-assisted esterification reactions

For the pervaporation-assisted esterification process, two process configurations based on catalytic pervaporation membrane modules are proposed. Preliminary large scale reactor evaluations are carried out based on the obtained experimental data, *e.g.*, membrane permeability and catalyst activity. A reactor evaluation proved that the outlet conversion for the catalytic pervaporation-assisted esterification reaction exceeds the conversion of a conventional inert pervaporation membrane reactor with the same loading of catalyst dispersed in the liquid bulk. This shows the added value of such a membrane system compared to conventional reactor designs. For a proper comparison with conventional existing production routes, *e.g.*, reactive distillation, more elaborate Aspen and FEMLAB calculations and a costs analysis need to be performed.

In the following section, two possible applications of the work presented in this thesis are explored. First, an extension of the application window for composite ceramic/polymer membranes is presented. Secondly, the possible use of water selective ceramic membranes under supercritical conditions is explored. As an example, the direct synthesis of dimethyl carbonate from methanol and carbon dioxide is taken.

9.2 Future perspectives

9.2.1 Composite ceramic/polymer membranes for organic separation

Currently, most commercial pervaporation processes involve the dehydration of alcohols and other organic solvents [Wynn, 2001]. In recent years, the potential use of pervaporation technology for the separation of organic mixtures and the removal of VOCs from waste water has attracted significant attention [Feng and Huang, 1997]. However, the use of commercially available polymeric membranes in the above mentioned applications has not attained widespread industrial acceptance, mainly due to degradation of the membrane in organic mixtures caused by swelling and a loss of membrane integrity [Jou *et al.*, 1997].

Many different membrane types, such as poly(dimethylsiloxane) (PDMS) [Ohshimia *et al.*, 2005], polyether-block-polyamides (PEBA) [Sheng, 1991; Ji *et al.*, 1994], poly(vinyl)acetate (PVAc) [Jou *et al.*, 1997], ethene-propene-diene terpolymer (EPDM) [Pereira *et al.*, 1998] and modified poly(phenylene oxide) [Doghieri *et al.*, 1994] have been examined for removal of VOCs from water by pervaporation. PDMS has proven to be the most promising material due to its hydrophobic and rubbery nature. However, it proves to be very difficult to prepare mechanically strong membranes from PDMS, because the mechanical strength of PDMS is notably poor [Ohshimia *et al.*, 2005].

In this perspective, the adaptation of ceramic materials as a stable support structure for polymeric membranes as presented in Chapter 5, could play an important role in enhancing the membrane stability in organic/organic separation by pervaporation. However, additional studies are needed to assess whether the remarkable performance observed in the dehydration of alcohols is also observed in the separation of organic/organic mixtures, and in the removal of VOCs from waste water. Additionally, membrane performance needs to be assessed for other combinations of selective polymer materials and mesoporous intermediate layers.

In addition to pervaporation, the polymer/inorganic composite membranes developed here may be used in other applications as well, such as nanofiltration and reverse osmosis. For non-aqueous nanofiltration in

particular, the prevention of membrane swelling is very important. In general, all applications in which swelling of the polymeric selective membrane layer upon contact with the feed becomes a problem can benefit from the adaptation of ceramic materials.

9.2.2 Direct synthesis of DMC from methanol and CO_2

The development of environmentally benign processes utilising carbon dioxide, which is a cheap and safe C_1 resource as well as a non-toxic reaction medium, has received much interest. One of the most attractive reactions is the direct synthesis of dimethyl carbonate (DMC) starting from carbon dioxide and methanol [Hou *et al.*, 2002]. However, the main problem for this reaction is the low equilibrium conversion. The direct synthesis of dimethyl carbonate starting from methanol and carbon dioxide can greatly benefit from water removal to increase the equilibrium conversion. Several studies have been performed to study the effect of water removal on the obtained conversion using molecular sieves [Choi *et al.*, 2002; Hou *et al.*, 2002], or using a series reaction using trimethyl orthoformate [Tomishige *et al.*, 1999] or dimethoxy-propane [Tomishige and Kunimori, 2002]. However, the use of inorganic dehydration agents proved not to be successful due to the reversibility of adsorption under reaction conditions, while the addition of trimethyl orthoformate or dimethoxy-propane was not suitable due to a decrease in DMC formation rate, and the formation of by-products [Tomishige and Kunimori, 2002].

An alternative for water removal by means of molecular sieves is the use of water selective membranes. Li *et al.*, have studied the membrane-enhanced formation of DMC using three types of mesoporous membranes. It was found that the conversion of methanol improved remarkably whereas the selectivity slightly increased [Li *et al.*, 2003]. However, the membranes showed substantial permeation of the reactants and, as a result, it was proposed to use carbon dioxide as a sweep flow containing methanol to compensate for the loss of methanol.

Microporous ceramic membranes are an alternative for the mesoporous membranes used by Li *et al.* [Li *et al.*, 2003]. Microporous inorganic membranes are envisioned as promising candidates for gas separation under harsh conditions and have been extensively used in gas separation and pervaporation [Peters *et al.*, 2005]. In the dehydration of alcohols, these

membranes appear to combine high selectivities with high permeabilities. Under supercritical conditions, however, silica membranes have only been used to separate small species, such as oils, micelles, and homogeneous catalysts, from carbon dioxide while maintaining supercritical conditions [van den Broeke *et al.*, 2001; Verkerk *et al.*, 2002; Goetheer *et al.*, 2003].

If microporous silica membranes would maintain their water selectivity under supercritical conditions, the direct formation of DMC would greatly benefit from this. This requires the membrane to be stable, permselective and to show a reasonable flux at increased temperatures and pressures. Present membranes, however, do not display enough stability [Verkerk, 2003]. Hence, new membranes have to be developed, with properties tailored for application under supercritical conditions. These materials should have a low adsorption of carbon dioxide and organic compounds, which block the membrane material. Potentially the most interesting membrane materials are sol-gel derived amorphous transition metal oxides containing heterogeneous transition metal bonds [Brinker and Scherer, 1990]. These materials show a high stability and the sol-gel synthesis allows tailoring of their properties.

9.3 Concluding remarks

In this thesis two new membrane concepts are introduced; ceramic-supported polymer membranes that show an improved performance compared to existing membranes, and catalytic membranes for which close integration of reaction and molecular separation offers advantages over conventional processes. Academic studies of these new concepts can be extended towards future applications, such as ceramic-supported hydrophobic polymers for organic removal, and other equilibrium reaction systems such as the direct formation of DMC from methanol and carbon dioxide. However, industrial acceptance of membrane processes in general is hampered by concerns about reliability. At this point, the challenge is to design and demonstrate reliable pilot scale membrane processes, based on the new concepts presented in this thesis.

References

Assabumrungrat, S., Phongpatthanapanich, J., Praserthdam, P., Tagawa, T., Goto, S., Theoretical study on the synthesis of methyl acetate from methanol and acetic acid in pervaporation membrane reactors: effect of continuous-flow modes, *Chem. Eng. J.*, 95 (2003) 57-65.

Brinker, C.J., Scherer, G.W., Sol-gel Science, The physics and chemistry of sol-gel processing, Acedemic Press Inc, San Diego, USA, 1990.

van den Broeke, L.J.P., Goetheer, E.L.V., Verkerk, A.W., de Wolf, E., Deelman, B., van Koten, G., Keurentjes, J.T.F., Homogeneous reactions in supercritical carbon dioxide using a catalyst immobilized by a microporous silica membrane, *Angew. Chem. Int. Ed.*, 40 (2001) 4473-4474.

Burshe, M.C., Sawant, S.B., Joshi, J.B., Pangarkar, V.G., Dehydration of ethylene glycol by pervaporation using hydrophilic IPNs of PVA, PAA and PAAM membranes, *Sep. Purif. Technol.*, 13 (1998) 47-56.

Choi, J-C., He, L-N., Yasuda, H., Sakakura, T., Selective and high yield synthesis of dimethyl carbonate directly from carbon dioxide and methanol, *Green Chemistry*, 4 (2002) 230-234.

Doghieri, F., Nardella, A., Sarti, G.C., Valentini, C., Pervaporation of methanol-MTBE mixtures through modified poly(phenylene oxide) membranes, *J. Membr. Sci.*, 91 (1994) 283-291.

Feng, X., Huang, R.Y.M., Liquid separation by membrane pervaporation: a review, *Ind. Eng. Chem. Res.*, 36 (1997) 1048-1066.

van Gestel, T., Vandecasteele, C., Buekenhoudt, A., Dotremont, C., Luyten, J., Leysen, R., van der Bruggen, B., Maes, G., Alumina and titania multilayer membranes for nanofiltration: preparation, characterization and chemical stability, *J. Membr. Sci.*, 207 (2002) 73-89.

Goetheer, E.L.V., Verkerk, A.W., van den Broeke, L.J.P., de Wolf, E., Deelman, B., van Koten, G., Keurentjes, J.T.F., Membrane reactor for homogeneous catalysis in supercritical carbon dioxide, *J. Catalysis*, 219 (2003) 126-133.

Hou, Z., Han, B., Liu, Z., Jiang, T., Yang, G., Synthesis of dimethyl carbonate using CO_2 and methanol: enhancing the conversion by controlling the phase behavior, *Green Chemistry*, 4 (2002) 467-471.

Jou, J-D., Yoshida, W., Cohen, Y., A novel ceramic-supported polymer membrane for pervaporation of dilute volatile organic compounds, *J. Membr. Sci.*, 162 (1999) 269-284.

Kim, K-J., Park, S-H., So, W-W., Moon, S-J., Pervaporation separation of aqueous organic mixtures through sulphated zirconia-poly(vinyl alcohol) membrane, *J. Appl. Pol. Sci.*, 79 (2001) 1450-1455.

Koster, R., van der Linden, B., Poels, E., Bliek, A., The mechanism of the gas-phase esterification of acetic acid and ethanol over MCM-41, *J. Catal.*, 204 (2001) 333-338.

Li, C-F., Zhong, S-H., Study on application of membrane reactor in direct synthesis of DMC from CO_2 and CH_3OH over Cu-KF/MgSiO catalyst, *Cat. Today*, 82 (2003) 83-90.

Liu, Q-L., Xiao, J., Silicalite-filled poly(siloxane imide) membranes for removal of VOCs from water by pervaporation, *J. Membr. Sci.*, 230 (2004) 121-129.

Meloni, D., Laforge, S., Martin, D., Guisnet, M., Rombi, E., Solinas, V., Acidic and catalytic properties of H-MCM-22 zeolites 1. characterization of the acidity by pyridine adsorption, *Appl. Catal. A: General*, 215 (2001) 55-66.

Ohshima, T., Kogami, Y., Miyata, T., Uragami, T., Pervaporation characteristics of cross-linked poly(dimethylsiloxane) membranes for removal of various volatile organic compounds from water, *J. Membr. Sci.*, 260 (2005) 156-163.

Pereira, C.C., Habert, A.C., Nobrega, R., Borges, C.P., New insights in the removal of diluted volatile organic compounds from dilute aqueous solution by pervaporation process, *J. Membr. Sci.*, 138 (1998) 227-235.

Peters, T.A., Fontalvo, J., Vorstman, M.A.G., Benes, N.E., van Dam, R.A., Vroon, Z.A.E.P., van Soest-Vercammen, E.L.J., Keurentjes, J.T.F., Hollow fibre microporous silica membranes for gas separation and pervaporation; synthesis, performance and stability, *J. Membr. Sci.*, 248 (2005) 73-80.

Sheng, J., Separation of dichloroethane-trichloroethylene mixtures by means of a membrane pervaporation process, *Desalination*, 80 (1991) 85-95.

Silva, V.M.T.M., Rodriquez, A.E., Synthesis of diethylacetal: thermodynamic and kinetic studies, *Chem. Eng. Sci.*, 56 (2001) 1255-1263.

Silva, V.M.T.M., Rodriquez, A.E., Dynamics of a fixed-bed adsorptive reactor for synthesis of diethylacetal, *AIChE J.*, 48 (2002) 625-634.

Sutovich, K.J., Peters, A.W., Rakiewicz, E.F., Wormsbecher, R.F., Mattingly, S.M., Mueller, K.T., Simultaneous Quantification of Brønsted- and Lewis-Acid Sites in a USY Zeolite, J. Catal., 183 (1999) 155-158.

Tomishige, K., Sakaihori, T., Ikeda, Y., Fujimoto, K., A novel method of direct synthesis of dimethyl carbonate from methanol and carbon dioxide catalyzed by zirconia, *Cat. Letters*, 58 (1999) 225-229.

Tomishige, K., Kunimori, K., Catalytic and direct synthesis of dimethyl carbonate starting from carbon dioxide using CeO_2-ZrO_2 solid solution heterogeneous catalyst: effect of H_2O removal from the reaction system, *Appl. Catal. A: General*, 237 (2002) 103-109.

Urigami, T., Okazaki, K., Matsugi, H., Miyata, T., Structure and permeation characteristics of an aqueous ethanol solution of organic-inorganic hybrid membranes composed of poly(vinyl alcohol) and tetraethoxysilane, *Macromolecules*, 35 (2002) 9156-9163.

Verkerk, A.W., Goetheer, E.L.V., van den Broeke, L.J.P., Keurentjes, J.T.F., Permeation of carbon dioxide through a microporous silica membrane at subcritical and supercritical conditions, *Langmuir*, 18 (2002) 6807-6812.

Verkerk, A.W., *Application of silica membranes in separations and hybrid reactor systems*, PhD thesis, Eindhoven University of Technology, Universiteitsdrukkerij, Technische Universiteit Eindhoven, Eindhoven, the Netherlands, 2003.

Wu, Y., Wang, S., Jin, M., Yang, X., Poly(acrylate-co-acrylic acid)/polysulfone composite membranes for pervaporation of volatile organic compounds from water, *Sep. Sci. Technol.*, 36 (2001) 3529-3540.

Wynn, N., Pervaporation comes of age, CEP magazine, 97 (2001) 66-72.

Dankwoord

Allereerst wil ik mijn promotor, Jos Keurentjes, bedanken. Bedankt Jos, voor de mogelijkheden die je me hebt gegeven tijdens mijn promotie. Tijdens mijn afstudeerperiode had je al snel door dat ik wel oren had naar een promotie, maar dan moest er wel de mogelijkheid voor me zijn om een gedeelte van het werk in Trondheim, Noorwegen uit te voeren. En zo geschiedde. Het leek er wel op alsof we er alles zo op hadden gepland, zo goed volgde alles op elkaar. Vijf maanden Eindhoven, negen maanden Trondheim, daarna bijna drie jaar Eindhoven en nu weer Oslo. Als ik vantevoren geweten had dat het zo zou gaan lopen dan had ik er meteen voor getekend.

Graag zou ik ook Nieck Benes willen bedanken voor de mogelijkheid die ik altijd had, of dacht te hebben, om zijn kantoor binnen te lopen met onduidelijkheden. Aan het einde van de promotie keek hij er al niet meer van op dat ik ondertussen alweer vijf minuten aan zijn tafel zat voordat hij me had opgemerkt. Ik moet je wel, of liever gezegd, sommige mede-promovendi, nogmaals duidelijk maken dat ik daar niet alleen maar zat met problemen, maar ook soms voor de gezelligheid.

De afgelopen vier jaren zouden sowieso niet zo aangenaam zijn geweest zonder de goede sfeer binnen de vakgroep. Het hoogtepunt van deze sfeer moet toch wel gezocht worden in Brazilie waar we op een uitermate gezellige en ontspannende studiereis zijn geweest. De AIChE meeting in San Francisco met uitstap naar Yosemite National Park mag hier natuurlijk ook niet vergeten worden. Bij deze zou ik iedereen, die bij heeft gedragen aan deze aangename werksfeer, willen bedanken. In het bijzonder, Marcus van Schilt, die als kamergenoot de afgelopen vijf jaar tevens mijn gepraat en muziek aan heeft moeten horen.

Uiteraard wil ik ook Marius Vorstman bedanken voor het begeleiden van mijn promotie gedurende de eerste anderhalf jaar. Je hebt samen met Javier Fontalvo, richting gegeven aan het onderzoek tijdens het altijd onduidelijke eerste jaar. Mede dankzij deze basis, is de rest van het project zo goed verlopen. Bedankt Marius en Javier.

Binnen TNO zou ik graag Esther van Soest-Vercammen, Zeger Vroon, Henk Buijs, Frank Vercauteren, Niki Stroeks, Renz van Ee en Roelant van Dam willen bedanken voor de discussies tijdens de projectbijeenkomsten,

het maken van membranen, maar vooral voor de goede samenwerking in het project. Dank ben ik ook verschuldigd aan Anders Holmen en Edd Blekkan voor de mogelijkheid die ik van jullie heb gehad om negen maanden in Trondheim door te brengen. Tusen takk.

Bedankt, Jeroen van der Tuin, Joost van de Venne, Christian Poeth en Rene Vermerris, zonder jullie had ik meer tijd moeten doorbrengen op het lab om alle data te verzamelen. Ik hoop dat jullie de afstudeerperiode ook leuk hebben gevonden. Ook wil ik Christophe Houssin bedanken voor de hulp tijdens het aanbrengen van zeolietlagen op membranen. Tevens wil ik de leescommissie, Jaap Schouten, Freek Kapteijn en Lester Kershenbaum, bedanken voor het becommentariëren van het proefschrift. Verder wil ik mijn familie en vrienden bedanken voor de steun de afgelopen jaren. Speciaal mijn ouders, zonder de mogelijkheid om te gaan studeren had ik hier nu niet gestaan. Aan het einde van dit dankwoord, zou ik graag Ingrid willen bedanken met wie ik nu samen een nieuwe periode in het leven inga. Je bent drie jaar geleden voor mij naar Eindhoven verhuisd. We hebben het daar erg naar ons zin gehad ondanks dat het niet altijd even gemakkelijk voor je is geweest. Ik hoop dat je je er toch thuis hebt gevoeld en dat we het net zo leuk gaan krijgen in ons nieuwe appartement in Oslo.

Thijs

Personal

Thijs Peters was born on the 6th of May 1978 in Breda in the south of the Netherlands. After finishing the secondary school "Mencia de Mendoza Lyceum" in 1996, he studied Chemical Engineering at the Eindhoven University of Technology. During his education he did a traineeship in Barcelona, Spain on the drying of polymer pellets. He also assisted in the practical course for first-year students at the Eindhoven University of Technology. His graduation project was performed at the Process Development Group, under the supervision of prof. dr. ir. J.T.F. Keurentjes and concerned the micellar catalysis of propylene. During his study he was member of the "Chemiewinkel Eindhoven", an environmental consultancy agency that advises private persons on questions about environmental pollution and environment related questions. After he graduated in August of 2001, he started as a Ph.D. student in the Process Development of prof. dr. ir. J.T.F. Keurentjes on the project called `development of catalytic pervaporation membranes for the integration of reaction and separation`. During his PhD project he worked for nine months in the Kinetics and Catalysis group of Anders Holmen in Trondheim, Norway. From the 1th of November 2005 he is employed by Sintef Materials and Chemistry in Oslo, Norway.

List of publications

Articles

Peters, T.A., Fontalvo, J., Vorstman, M.A.G., Keurentjes, J.T.F., Design directions for composite catalytic hollow fibre membranes for condensation reactions, *Trans. IChemE, Part A, Chem. Eng. Res. Des.*, 82 (2004) 220-228.

Peters, T.A., Fontalvo, J., Vorstman, M.A.G., Benes, N.E., van Dam, R.A., Vroon, Z.A.E.P., van Soest-Vercammen, E.L.J., Keurentjes, J.T.F., Hollow fibre microporous silica membranes for gas separation and pervaporation: synthesis, performance and stability, *J. Membr. Sci.,* 248 (2005) 73-80.

Peters, T.A., van der Tuin, J., Houssin, C., Vorstman, M.A.G., Benes, N.E., Vroon, Z.A.E.P., Holmen, A., Keurentjes, J.T.F., Preparation of zeolite-coated pervaporation membranes for the integration of reaction and separation, *Catal. Today*, 104 (2005) 288-295.

Peters, T.A., Benes, N.E., Keurentjes, J.T.F., Zeolite-coated ceramic pervaporation membranes; pervaporation-esterification coupling and reactor evaluation, *Ind. Eng. Chem. Res.*, 44 (2005) 9490-9496.

Peters, T.A., Benes, N.E., Holmen, A., Keurentjes, J.T.F., Comparison of commercial solid acid catalysts for the esterification of acetic acid with butanol, *Appl. Catal. A: General*, 297 (2006) 182-188.

Peters, T.A., Poeth, C.H.S., Benes, N.E., Buijs, H.C.W.M. Buijs, Vercauteren, F.F., Keurentjes, J.T.F., Ceramic-supported thin PVA pervaporation membranes combining high flux and high selectivity; contradicting the flux-selectivity paradigm, *J. Membr. Sci.,* (2005) accepted.

Peters, T.A., Benes, N.E., Keurentjes, J.T.F., Ceramic-supported thin PVA pervaporation membranes: long-term and temperature stability in the dehydration of alcohols, submitted.

Peters, T.A., Benes, N.E., Keurentjes, J.T.F., Amberlyst-coated pervaporation membranes: preparation and pervaporation-esterification coupling, submitted.

Patents

Buijs, H.C.W.M., Vercauteren, F.F., Peters, T.A., Benes, N.E., Keurentjes, J.T.F., van Soest-Vercammen, E.L.J., Composite membrane and its use in separation processes, Application No./Patent No. 05077144.3-., filed.

Refereed proceedings

Peters, T.A., Fontalvo, J., Vorstman, M.A.G., Keurentjes, J.T.F., Design rules for catalytic hollow fibre membrane modules for condensation reactions, in Proc. 3rd International Symposium on Multifunctional Reactors. (ISMR-3, August 27-30, 2003); Editors: L. Kershenbaum, Bath, United Kingdom, (2003) 16-20.

Peters, T.A., Fontalvo, J., Vorstman, M.A.G., Keurentjes, J.T.F., Catalytic pervaporation membrane reactors for the integrated reaction and separation in condensation reactions, in Proc. AIChE Annual Meeting 2003. (November 16-21, 2003); Editors: -, San Francisco, CA, United States of America, (2003).

Peters, T.A., Benes, N.E., Vroon, Z.A.E.P., Keurentjes, J.T.F., Development of catalytic pervaporation membranes for integration of reaction and separation, in Proc. 6th International Conference on Catalysis in Membrane Reactors. (ICCMR-6, July 6-9, 2004); Editors: R. Dittmeyer, Lahnstein, Germany, (2004) 201.

Peters, T.A., Vorstman, M.A.G., Benes, N.E., Keurentjes, J.T.F., Development of catalytic pervaporation membranes for integration of reaction and separation in condensation reactions, in Proc. Euromembrane 2004 (Sept 28 -Oct 1, 2004); Editors: J. Hapke, Ch. Na Ranong, D. Paul, K.-V. Peinemann, Hamburg, Germany, (2004) 339.

Vroon, Z.A.E.P., Dam van, R., Soest-Vercammen van, E.L.J., Peters, T.A., Benes, N.E., Keurentjes, J.T.F., Synthesis, performance and stability of sol-gel derived silica membranes onto hollow fibre ceramic membranes for pervaporation, in Proc. International Symposium on Inorganic and Environmental Materials 2004. (ISIEM 2004, October 18-21, 2004); Editors: -, Eindhoven, the Netherlands, (2004) 221.

Peters, T.A., Benes, N.E., Keurentjes, J.T.F., Development of catalytic pervaporation membranes for the integration of reaction and separation, 4th Netherlands Process technology Symposium (NPS4, October 26-27, 2004), Veldhoven, the Netherands.

Peters, T.A., Benes, N.E., Keurentjes, J.T.F., Development of catalytic pervaporation membranes for integration of reaction and separation, in Proc. 5th International Symposium on Catalysis in Multiphase Reactors &

4th International Symposium on Multifunctional Reactors. (Camure-5 & ISMR-4, June 15-18, 2005); Editors: J. Levec, A. Pintar, Portoroz, Slovenia, (2005) 139-140.

Peters, T.A., Benes, N.E., Keurentjes, J.T.F., Development of catalytic pervaporation membranes for integration of reaction and separation, in Proc. 2th International Symposium on Structured Catalysts and Reactors. (ISOSCAR-2, October 15-18, 2005), Editors: -, Delft, The Netherlands, (2005).

Peters, T.A., Benes, N.E., Buijs, H.C.W.M., Vercauteren, F.F., Keurentjes, J.T.F., Thin high flux ceramic-supported PVA membranes, in Proc. Worskhop ''Membranes in Solvent Filtration''. (March 23-24, 2006), Editors: -, Leuven, Belgium (2006).

Peters, T.A., Benes, N.E., Keurentjes, J.T.F., Thin high flux ceramic-supported PVA membranes, in Proc. Euromembrane 2006 (September 24-28, 2006); Editors: -, Taormina (Messina), Italy, (2006).